A practical guide to coding line-by-line trace gas absorption in Earth's atmosphere

Sergey Korkin , Andrew M. Sayer , Amir Ibrahim , Alexei Lyapustin

PII: S0022-4073(25)00007-X
DOI: https://doi.org/10.1016/j.jqsrt.2025.109345
Reference: JQSRT 109345

To appear in: *Journal of Quantitative Spectroscopy & Radiative Transfer*

Received date: 21 March 2024
Revised date: 23 October 2024
Accepted date: 6 January 2025

Please cite this article as: Sergey Korkin , Andrew M. Sayer , Amir Ibrahim , Alexei Lyapustin , A practical guide to coding line-by-line trace gas absorption in Earth's atmosphere, *Journal of Quantitative Spectroscopy & Radiative Transfer* (2025), doi: https://doi.org/10.1016/j.jqsrt.2025.109345

Highlights

- Despite the existence of numerous computer programs for absorption spectroscopy, the code development process is poorly covered in literature.
- Our paper shows how to create a code for line-by-line molecular absorption spectroscopy from scratch.
- We explain the process in three steps: a) simulation of absorption by a molecule using HITRAN database; b) simulation of absorption in a gas cell by a group of molecules; c) simulation of absorption in Earth atmosphere using MODTRAN profiles.
- The goals of the paper are the simplification of software development, documentation, and support, and ultimately the transfer of knowledge between generations of scientists.
- Our paper comes with an open-source code, in C-language, and numerical data for unit testing, thus insuring independent reproducibility of our results.

A practical guide to coding line-by-line trace gas absorption in Earth's atmosphere

Sergey Korkin [1,2,*], *Andrew M. Sayer* [1,2], *Amir Ibrahim* [2], and *Alexei Lyapustin* [2]

[1] University of Maryland Baltimore County, Baltimore, MD, USA

[2] NASA Goddard Space Flight Center, Greenbelt, MD, USA

[*]Corresponding author: sergey.v.korkin@nasa.gov

"*Talk is cheap. Show me the code.*"

– Linus Torvalds[1]

Abstract

We present two new open-source codes, in the C language, for simulation of the line-by-line molecular (gas) absorption in the solar spectral region with wavelengths up to ~2500 (*nm*). The first one, `gcell`, simulates absorption spectroscopy in a gas cell for a given length of the cell, temperature, and pressure. The second one, `aspect`, is for spectroscopy in Earth's atmosphere - a common need for remote sensing applications. Both use the HITRAN database for line shape (Voigt) modeling. `Aspect` adapts height variations of the thermodynamic parameters (profiles) from MODTRAN. Separate discussion of the gas cell and the atmospheric modes simplifies software development, documentation, and support, and ultimately the transfer of knowledge between generations of scientists. These are the main goals of the current paper. Despite the existence of numerous computer programs for absorption spectroscopy, the code development process is poorly covered in literature. As a result, it is difficult for a non-developer to confidently modify an existing code or create a new tool within a reasonable amount of time.

[1] https://en.wikiquote.org/wiki/Linus_Torvalds (see Sec. 2000-s: 2000-04)

Keywords

Atmosphere absorption spectroscopy, line-by-line, open-source, code development, radiative transfer (RT), Earth science.

Contents

1. Introduction

Absorption of radiation as a function of wavelength λ (widely used in Earth science in the solar spectral region of up to approximately 2,500 (*nm*)) or wavenumber ν ~ 1/ λ (more common in spectroscopy) by the atmosphere-surface system is a fundamental physical process that influences the Earth's radiation budget and, through that, drives its climate (*Luther* et al., 1988; *Kochanov* et al., 2019; *Pincus* et al., 2020). Molecules absorb radiation at only specific wavelengths corresponding to differences in energy between different possible quantum excitation states – that is, different rotational, vibrational, and electronic configurations. For an

isolated molecule, these lines are pure and "monochromatic"[2], though in practice (whether in a gas cell or Earth's atmosphere) the fact that molecules exist in groups, interacting with one another, and with different populations of excitation states, greatly complicates matters and leads to broadening and shifting of lines (*Elsasser*, 1942; *Goody & Yung*, 1989; *Liou*, 2002).

The gas spectroscopy started to systematically attract the attention of scientists in as early as XIX-th century. *Pouillet* (1838) and *Tyndall* (1859) reported on the influence of gaseous absorption on transfer of solar radiation through the atmosphere. *Foote* (1856) arguably was the first scientist to link the atmospheric heating rate (global warming) with CO_2 concentration. Later, *Arrhenius* (1896, 1897) continued this research. In the modern era, these pioneering works are continued by the Orbiting Carbon Observatory (OCO[3]), the Scanning Imaging Absorption Spectrometer for Atmospheric Chartography (SCIAMACHY[4]), the Greenhouse Gases Observing Satellite (GOSAT[5]), and other missions. Thus, the importance of the effect of atmospheric absorption was recognized about two centuries ago and since then has remained a focus of the atmospheric community.

Besides climate and weather, accurate simulation of absorption is necessary for satellite remote sensing of the ocean, land, and particles suspended in atmosphere (aerosols, water droplets, ice crystals). For these studies, certain optical (solar and thermal) and radio instruments, both passive (radiometers) and active (lidars, radars), typically measure in "atmospheric windows". The atmospheric windows are range of wavelengths (spectral bands) where absorption is low, but still not negligible. In these spectral bands the atmospheric absorption is not an object of study, but an obstacle. Accurate retrieval algorithms must take this absorption into account.

In the Earth atmosphere, the radiation is absorbed by particles (aerosols) and molecules of trace gases. Gas absorption is usually divided into two components. First, is the absorption in spectral lines of the molecules, which has a pronounced spectral pattern – the absorption power may vary by orders of magnitude even within a narrow spectral band – due to the aforementioned dependence on specific permitted rotational, vibrational, and electronic structure transitions. Second is the continuum absorption, which is smoother, and often that of water vapor is most

[2] Strictly speaking, "monochromatic" light wave is an idealization because the wave has originated at some point in time and space and will end its existence at a different point and moment of time.
[3] https://ocov2.jpl.nasa.gov/
[4] https://www.sciamachy.org/
[5] https://www.gosat.nies.go.jp/en/

important (*Clough* et al., 1989; *Shine* et al., 2012; *Mlawer* et al., 2012 & 2023). In practice parameters to fit observed gas absorption lines are determined empirically from laboratory measurements on a line-by-line (LBL) basis assuming some basic line absorption shape, and then the continuum is calculated as the difference between these measurements and LBL calculations. Then one fits this residual absorption – arising due to the complex interplay between molecules that is intractable to model purely theoretically - with models that are largely empirical. Further in this paper, we focus only on the first component – absorption by spectral lines – of atmospheric spectroscopy.

Apart from the water vapor continuum, mostly affecting wavelengths in the red and longer wavelengths, there are other gases manifesting spectrally smooth variations in the UV-Vis part. Ozone (O_3) is the most important absorber in this spectral range. The presence of this gas causes a drop in the atmospheric transmittance towards shorter wavelengths (e.g., see the second chart from the top of Fig. 2.13 in *Bohren & Clothiaux*, 2006), causing the need for atmospheric correction. Fortunately, *a*) most ozone is located high in the Earth atmosphere, and the ozone correction theoretical background is simply a direct transmittance, exponential with respect to (w.r.t.) absorption optical thickness, frequently noted in RT as τ, along the solar and view directions; *b*) the transmittance depends on the ozone absorption cross-sections, which possess moderate temperature and pressure dependence, measured in a laboratory at different concentrations, a limited set of thermodynamical conditions, and reported as look-up tables (*Hearn*, 1961; *Orphal* et al., 2016). Besides ozone, these smooth components of spectral absorption are measured for other important atmospheric trace gases (*Bogumil* et al., 2003). We do not include this "continuum-type" absorption in our paper.

Since the mentioned pioneering works in Earth science, as well as in astrophysics, the field of absorption in planetary atmospheres has been growing. Results of these studies are published in dedicated journals (e.g., Journal of Molecular Spectroscopy and Journal of Quantitative Spectroscopy and Radiative Transfer), monographs, chapters in books, and papers in journals not specialized in spectroscopy. Spaceborne spectrometers studying Earth and other planets, and countless laboratory measurements generate an avalanche of experimental data. Numerous datasets combine the data in a raw and processed format (e.g., after parametrization). Some of the datasets, like the widely used high-resolution transmission molecular absorption database

(HITRAN [6]), have become standards in science and industry (*McClatchey* et al. 1973; *Rothman* et al., 1978, 2005, 2010, 2021). Examples of other spectral databases include GEISA (*Delahaye* et al., 2020), which has been developed since the 1980s, CDMS (*Müller* et al., 2005), ASTER (*Baldridge* et al., 2009), to name a few. In this paper we use that part of the HITRAN database that models lines with the Voigt shape profile. We refer the reader to Sec. 4.4 below for references on the Voigt spectrum and to Sec. 4.5 for some legacy and recent references on the non-Voigt line shapes.

In this paper we also do not include one type of absorption with a smooth spectral dependence, which is included in HITRAN to a certain degree. This phenomenon is (inelastic) collision induced absorption – CIA (*Goody & Yung*, 1989: Sec.5.3.4 for O_2 and 5.5.3 for CO_2; *Richard* et al., 2012; *Karman* et al., 2019). This is not to be confused with (elastic) collisional broadening. During collision of molecules, some energy transitions forbidden for molecules at steady state may become possible, which leads to absorption of radiation at corresponding wavelengths. CIA is most important for O_2 and N_2 (*Karman* et al., 2018). The phenomenon manifests itself at high concentrations. It is parametrized in HITRAN as scaling factors (binary coefficients) and molecule concentrations, e.g. $K_{ab}(\nu) = k(\nu)/(n_a \cdot n_b)$. Here '*a*' and '*b*' denote two colliding molecules, '*n*' is concentration, '$k(\nu)$' is the absorption cross-section at a given wavenumber ν. The dependence of *n* on temperature *T* and pressure *p* leads to the same in the CIA coefficients.

Analysis and application of the collected data relies on numerical modeling. The models are basically computer programs. Once developed, they may be used for decades, which assures reliability (*Korkin* et al., 2022: see references in Sec.1). But over time they are left as black boxes. Contrary to the scientific background (theory), and documenting of the measurement process (technique), codes do not get enough attention. They either start as or often become poorly written software due to factors such as obscure coding practices (as these evolve over time), unclear structure, lack of documentation and unit testing. Input/output formats, runtime, or accuracy may no longer meet the requirements of new missions. New tools are needed to improve reprocessing of heritage missions, and to get the most out of upcoming Earth science missions such as NASA's Plankton, Aerosol, Cloud, ocean Ecosystem (PACE [7]: *Werdell* et al., 2019). The PACE Ocean Color Instrument (OCI) has a finer wavelength resolution than heritage

[6] https://hitran.org/
[7] https://pace.gsfc.nasa.gov/

NASA imagers, which demands flexible (for simulation of different and variable atmospheric constituents) and accurate (to avoid bias in retrievals) software tool for atmospheric spectroscopy.

As a result of the neglect of software it is hard or impossible, to confidently support (apply minor changes) or modify (significantly change) a "black box"[8] and/or a "spaghetti code"[9] within a reasonable amount of time - especially when the need is pressing. This problem has been recognized not only in planetary spectroscopy but in science in general (*Kendall* et al., 2008; *Sanders & Kelly*, 2008; *Segal & Morris*, 2008; *Easterbrook & Johns*, 2009; *LeVeque* et al., 2012; *Pipitone & Easterbrook*, 2012; *Kanewala & Bieman*, 2014; *Wilson* et al., 2014; *Heaton & Carver*, 2015; *Storer*, 2017; *Adorf* et al., 2018; *Hinsen*, 2019, *Dubey*, 2022). In Earth science, legacy tools currently used at many institutions are largely limited to heritage sensors (e.g. MODIS) and no longer supported as the developers have retired or passed away. Other tools exist (see Sec.2), but access or support are often unavailable. Lack of support makes it difficult to confidently change the code. The need to change the code arises from needs to: ***a)*** update atmospheric spectroscopy database as new information becomes available, e.g. new HITRAN release (*Zhu* et al., 2019); ***b)*** add new atmospheric profile, or add absorption by a new molecule or its isotopes; ***c)*** update with improved models of the spectral line shape, such as speed-dependent Voigt profile (see Sec.4.5).

Code is therefore the main topic of the paper. We use and refer to known equations, but only to support code documentation. We do not get into details of spectroscopy (although the reader is referred to various books and papers) and refer to equations and relevant parameters as they appear in the code. However, in the paper we do not discuss those "technical" parts relevant to the code only: declaration of variables, memory allocation/deallocation, printouts. The reader will see all that in the source that comes with the paper. In the text we focus on the tight coupling between an equation and its representation as an element of code. Thus, at any moment, the developer is focused on what is needed now.

For simplicity of coding, the paper introduces the process of development sequentially from simple to complicated. Sec.4 shows how to read the HITRAN database, briefly explains

[8] https://en.wikipedia.org/wiki/Black_box
[9] https://en.wikipedia.org/wiki/Spaghetti_code

necessary parameters, and shows relevant code for calculation of the relative (per molecule) absorption cross-section by a single line. We calculate the Voigt line shape in Sec.4.4 and list a few references for "beyond Voigt" models of spectral line shape in Sec.4.5. Sec.4.6 gives a few numbers to test calculation by a single line – unit testing. In Sec.5 we combine absorption from many spectral lines assumed independent. The line mixing effect (e.g., interference of broad lines) is ignored, however we provide references for further reading in Sec.5.2. For a given temperature, pressure, and length of the cell we calculate the absorption optical thickness of the gas (Sec.5.3). Such gas cells are used in laboratories and field measurements. Our C-code `gcell` aims to support measurements that use gas cells. Sec.5.4 gives some independently created data to test code `gcell`.

An atmosphere is basically a vertical stack of gas cells, each with some given temperature, pressure, and particle species number concentrations varying with height – profiles. In Sec.6 we combine the gas cell calculation with MODTRAN (*Berk* et al., 2014 & 2017) atmospheric profiles, described briefly in Sec.6.1. Later in Sec.6 we integrate the profiles over height in order to calculate τ between top-of-the-atmosphere (TOA) and user-defined level of height, paying particular attention to units of the amount of gas in the atmospheric column. An open-source C code for LBL simulation of the atmospheric spectroscopy, `aspect`, is the main product presented in the paper. Note that `aspect` is a revised and updated version of the LBL solver of the Spherical Harmonics Interpolation and Profile Correction (SHARM-IPC) tool (*Lyapustin*, 2003) for broad band RT. We show how to test `aspect` in Sec.6.6.

We endeavor to give the interested reader a chance to start using our codes as soon as possible. For that purpose, Sec. 3 is devoted to software. It explains how to install `gcell` and `aspect`, helps understand input, output, content of the header files, lists all files that come with the package and explains the purpose of each. The section shows structure of both codes (call graphs). As both codes overlap significantly in terms of source files used, we recommend readers understand `gcell` even if one needs to simulate absorption in the atmosphere. Information from Sec. 3 is sufficient to start using our codes.

One more topic that should be clarified from the very beginning is terminology. In what follows, the word "*line*" will refer to a spectral line of a molecule, while a line with ASCII symbols in the HITRAN database file will be called "*record*". We use the word "*profile*" when we talk about

the change of atmospheric parameters with height. For the dependence of absorption by a single line vs. wavenumber, which is often called "*line profile*", we use the word "*line shape*". We do not deal with scattering in this paper. As a result, we often drop the word "*absorption*" for τ. For the same reason, "*extinction*" and "*absorption*" are used synonymously here. "*Spectral dependence*" refers to variation of some parameter over wavenumber or wavelength, depending on the context. Speaking about software, we say "C-code" for simplicity. However, we use some features from C++, e.g. we allocate and deallocate memory using `new` and `delete` functions, hence one must use a compiler with C++ support.

In this project, we use C for the reasons of numerical efficiency, standardization, long-lasting history, and wide usage in science and engineering (*Press* et al., 1992 & 2007; *Oliveira & Stewart*, 2006; *Gottschling*, 2021). C can be easily wrapped in Python and the two follow the same column-major rule for allocation of matrices in memory; the original SHARM-IPC LBL tool, which we have refactored, was also developed in C. However, we do not expect much knowledge of C/C++ from the reader. Basically, our codes use 1D arrays, nested loops, and functions that may take scalars and arrays as input and output arguments. Tools like ChatGPT[10] quickly provide small, clear, compilable examples for all that.

In the following Sec.2, which we have not yet mentioned, we provide references to some already existing tools for gas spectroscopy. The list is long and by far incomplete. However, we argue that our tools `gcell` and `aspect` may also find their place among the existing ones and be useful for the community.

2. Many tools for atmospheric spectroscopy: why publish one more?

An enormous number of tools for numerical simulation of absorption spectroscopy has been created within the past ~50 years in order to meet a huge variety of practical needs. This is caused by different physical environments (Earth, stars, planets), observation geometries (laboratory, open air horizontal path, plane-parallel or spherical atmosphere), spectral resolutions (broad band, LBL), numerical techniques (real-time calculations, lookup tables - LUTs, principal component analysis - PCA, neural network – NN approaches), physical effects (spectral line absorption, continuum absorption, scattering by molecules and/or aerosols and clouds), desired

[10] https://chat.openai.com/

input (spectral database and atmospheric profiles) and output parameters (transmittance, radiance, flux, derivatives), target instrument design (air- vs. spaceborne, field of view, spectral response functions), and, last but not least, forms of software product (stand-alone tool, linked library, language, open-source or proprietary).

These and other needs are satisfied by the following RT tools[11], a complete list of which is likely impossible to compile[12]: 4A (*Scott & Chedin*, 1981), AER[13] set of RT models (e.g., LBLRTM in *Clough* et al., 2005), AMSUTRAN (*Turner* et al., 2019), ATREM (*Gao* et al., 1993; *Thompson* et al., 2015), BTRAM[14] (*Chapman* et al., 2010), FARMS (*Xie* et al., 2016), FASCODE (*Clough* et al., 1981), GENLN2 (*Edwards* et al., 1992), LINEPAK[15] (*Gordley* et al., 1994), KOPRA (*Stiller* et al., 2001), LOWTRAN (*Kneizys* et al., 1988), MCARaTS[16] (*Iwabuchi & Okamura*, 2017), MODTRAN (*Berk* et al., 2014 & 2017), MolecFit[17] (*Smette* et al., 2015), MOLIERE (*Urban* et al., 2004), MOSART (*Cornette* et al., 1994), PSG[18] (*Villanueva* et al., 2018), RADIS (*Pannier & Laux*, 2019), RFM (*Dudhia*, 2017), RRTM (*Mlawer* et al., 1997), RTTOV (*Saunders* et al., 1999), SpectraPlot[19] (*Goldenstein* et al., 2017), STREAMER & FLUXNET[20] (*Key & Schweiger*, 1998), TAPAS[21] (*Bertaux* et al., 2017), TAU[22] (*Hollis* et al., 2013 & 2014), VSTAR (*Bailey & Kedziora-Chudczer*, 2012), σ-IASI (*Amato* et al., 2002; *Carissimo* et al., 2005). Source code and user guides, in addition to publication(s), are available from corresponding websites (see footnotes). Some websites provide an online interface to run calculations (in particular NASA GSFC's PSG – Planetary Spectrum Generator). Graphics processing units (GPUs) are used for LBL calculations in *Collange* et al., (2008) – an example of modern hardware usage for known theory. This GPU paper explains the implementation at a high level, however, no details about the code itself are given.

[11] https://en.wikipedia.org/wiki/Atmospheric_radiative_transfer_codes
[12] We refer the reader to respective papers for definition of the acronyms.
[13] http://rtweb.aer.com/lblrtm.html
[14] https://blueskyspectroscopy.com/
[15] https://www.spectralcalc.com
[16] https://sites.google.com/site/mcarats/monte-carlo-atmospheric-radiative-transfer-simulator-mcarats
[17] https://www.uibk.ac.at/eso/software/molecfit.html.en
[18] https://psg.gsfc.nasa.gov/
[19] https://spectraplot.com/
[20] https://stratus.ssec.wisc.edu/fluxnet/
[21] http://cds-espri.ipsl.fr/tapas/
[22] http://www.ucl.ac.uk/exoplanets/

In order to account for absorption in atmospheric windows, comprehensive RT packages that focus on scattering of radiation, like ARTS[23] (*Buehler* et al., 2018), SASKTRAN[24] (*Bourassa* et al., 2008), SCIATRAN[25] (*Rozanov* et al., 2014), SHARM-IPC (*Lyapustin* et al., 2010), or libRadtran[26] (*Emde* et al., 2016) come with built-in and/or stand-alone tools for simulation of molecular absorption. PCA (*Liu* et al., 2016; *Yang* et al., 2016; *Havemann* et al., 2018) and AI/ML/NN techniques are also used, e.g. to reduce computational burden in broadband calculations and for other purposes (*Zhou* et al., 2021; *Kistenev* et al., 2022; *Prischepa* et al., 2023; *Chen* et al., 2024).

Input for LBL computations come from datasets containing spectral optical properties of molecules and defining models that describe how these optical properties change with temperature and pressure. HITRAN, updated roughly every four years, is arguably the oldest and most used spectroscopic database (*Rothman* et al., 1978 – earliest report in the HITRAN format, 1987 – the name HITRAN is introduced, 2005 & 2010 & 2021 – reviews of HITRAN). GEISA[27] (*Delahaye* et al., 2021), ABSCO (*Payne* et al., 2020), and SCIAMACHY molecular absorption spectra[28] (*Bogumil* et al., 2003) are other examples of databases for atmospheric applications; some references to IR, far IR, microwave, and submillimeter databases are listed in (*Gordon* et al., 2016). Appendix A in *Rothman* et al., (2008) explains how to convert the line intensities from the Jet Propulsion Laboratory (JPL, *Pickett* et al., 1998) and Cologne Database for Molecular Spectroscopy (CDMS: *Müller* et al., 2005) catalogs to that of HITRAN.

Our paper focuses on the terrestrial atmosphere and solar spectral region, up to the wavelength $\lambda \sim 2500$ (*nm*). For typical atmospheric conditions further in the paper we also rely on HITRAN for simulation of absorption by a spectral single line. The HITRAN Application Programming Interface (HAPI[29]: *Kochanov* et al., 2016) is an open-source Python package that can download LBL data from the HITRAN online database, HITRAN*online* (*Hill* et al., 2013 & 2016). The package is well documented in the above-mentioned papers, manual, and in a carefully written code. HAPI contains functions for calculation of absorption spectrum for a given temperature

[23] https://www.radiativetransfer.org/
[24] https://usask-arg.github.io/sasktran/
[25] https://www.iup.uni-bremen.de/sciatran
[26] www.libradtran.org
[27] https://geisa.aeris-data.fr/
[28] https://www.iup.uni-bremen.de/gruppen/molspec/
[29] https://hitran.org/hapi/

and pressure. Different line shape models are available, but height dependence of temperature and pressure are not built in. Therefore, HAPI is not convenient for atmospheric calculations on a large scale but can be used for validation of the gas cell calculations and absorption coefficient at a given height in atmosphere.

The mentioned non-exhaustive list of codes shows that some spectroscopic tools are new (use modern language, GPU, provide interface for online calculations), some are old, some are publicly available, but some are not. Corresponding papers and user guides describe theory behind the tools, input, and output, which is convenient for an end user. But as a drawback, such tools are often used as a "*black box*" which does not allow the user "*to better understand the physics of radiative transfer*", complicates research by obscuring "*intermediate variables*", and are imperfect for "*pedagogical purposes*" (*Schreier* et al., 2019: pp.2-3). A paper or a manual about a package does not necessarily mean a paper or a manual explaining how to create – hence confidently modify – the package. Further, a full radiative transfer package, like the one simulating spectral radiance in an atmosphere, is too powerful for a simple problem, like light absorption by a gas in a cell or along a horizontal path, and too complicated to learn how to use and develop from scratch. Big codes are not always a good fit for small needs. The user runs onto a bigger problem if there is a need to replace an absorption database in a third party developed code that supports, say, only HITRAN.

The "black box" software model prevents debugging, refactoring, long-lasting support, and transition of knowledge with the workforce – be those new hires, or experts coming from other fields. An example of the need for relatively simple refactoring is the update of the HITRAN database file format. In 2004, the file format changed from 100 characters per record (line in ASCII file) to 160 (*Rothman* et al., 2005: p.142). Sec.4.1 below shows that a knowledgeable user would spend a few minutes to make and test the necessary change. But even for the developer, the update of theoretical foundation for absorption by a single line (Sec.4.5) will require more time. The latter task is barely manageable by someone who does not understand the insights of the code. In addition to lack of time for in-depth studying of the existing code, the gap in knowledge may be caused by the way the existing open-source code is written.

The need for publication of codes was recognized in spectrometry in the 1960's (*Armstrong*, 1967). Despite that, our abovementioned literature analysis revealed a gap in discussing the

software development of the spectroscopic codes, as opposed to theoretical background. A rare example is the Generic Atmospheric Radiation LBL Infrared Code (GARLIC: *Schreier* et al., 2014), which is a Fortran 90/2008 re-implementation (refactoring) and extension of the Modular InfraRed Atmospheric Radiative Transfer (MIRART) Fortran 77/90 code (*Schreier & Boettger*, 2003). MIRART and GARLIC are programs for infrared-microwave atmospheric RT forward modeling and retrievals. GARLIC offers limb and nadir observation geometry, user-defined instrumental field-of-view and spectral response function, Jacobians, different spectral line shapes, optimized algorithms for LBL calculations of molecular cross sections, and other features useful for applications. Noteworthy, the developers paid attention to the software side of the scientific code (see Sec. 3: "Implementation - GARLIC" in their paper). They did not simply add new features into the previous version, MIRART, but invested time in refactoring: translation from Fortran 77/90 to Fortran 90/2008, with emphasis on modular structure, and validation of intermediate results (unit testing).

Overall, the MIRART-GARLIC family is an example of caring about software in addition to science: MIRART was first announced in 2000 (*Schreier & Schimpf*, 2001), this "transition phase" from MIRART to GARLIC took place in 2007, the GARLIC paper was published in 2014. In 2019, GARLIC was reimplemented again – this time as PYthon scripts for Computational Atmospheric Spectroscopy (Py4CAtS) in order to use numeric and scientific Python modules for computationally-intensive code sections (*Schreier* et al., 2019). Py4CAtS inherits and further extends the GARLIC capabilities, and it is publicly available[30].

Now we come to answer the question from the title of this section. Despite an avalanche of tools for atmospheric spectroscopy has already been reported in countless papers, and many of the tools offer publicly available codes, the process of development of a spectroscopic tool is poorly covered. In our paper, we discuss the development of a simple (compared to many others) code. But we show the process of the development from the very beginning in three modes: absorption by a single line ("basic"), absorption in a gas cell by a group of lines ("moderate"), and absorption in atmosphere that involves atmospheric profiles ("hard"). If the user needs to simulate absorption in a gas cell or along a horizontal path (no profiles), the "hard" part can be dropped. Through that, we wish not to overload the reader with unnecessary details. We used a

[30] https://atmos.eoc.dlr.de/tools/Py4CAtS/

similar approach in our previous paper on how to understand and write from scratch a program for numerical simulation of multiple scattering of sunlight in a plane-parallel atmosphere, commonly referred to as radiative transfer code (*Korkin* et al., 2022).

In a short, our goal is a simple tool explained at the code level. To meet the goal, we target developers first and users next. However, before one starts digging through the code development process, it is a good idea to prove that the offered code works. It is also practical to immediately show the complexity of the code, so that a potential developer would estimate the time needed for the job. Our next section explains the code structure and shows how to install and use it.

3. Code structure and usage

This section serves as a quick start guide. It explains a simple installation process, input, output, and structure of the code – see **Fig.1(*a, b*)**. After reading this section, the reader will be able to confidently use our codes for calculating of the LBL absorption optical thickness $\tau(\nu)$ in a gas cell or in the atmosphere, at the desired wavenumbers, ν (cm^{-1}). The wavenumber is literally the number of wavelengths fitting 1 (*cm*): ν (cm^{-1}) = 10^4 / λ (μm) = 10^7 / λ (nm).

In this section and onwards, we use the following notation. The `Courier` font is used for the software relevant text: elements of code, commands, file names, paths, input and output data. We use **`bold`** symbols for arrays, and *`italic`* for parameters (mostly defined in headers). Hence ***`bold italic`*** refers to an array defined in a header file. We use the C-notation to refer to an element `i` of an array: **`A`**`[i]`. As the reader will see, `gcell` and `aspect` uses 1D arrays only. We type the unit conversion constants in `grey`. In naming convention, we prefer `under_score` over `CamelCase`, despite the latter was found preferable for speed and accuracy of manipulating programs (*Binkley* et al., 2009).

The code has no preferences regarding the C-compiler and has been tested using GCC under Linux, and Intel C compiler integrated into Microsoft Visual Studio via oneAPI toolbox. Before compilation, it is necessary to check paths to the HITRAN database in the header `./src/paths.h` and update, if necessary, as explained in the next section. We also recommend the reader to get acquainted with the content of the headers before using, not to mention changing, the code.

The end-of-line marker in Windows ASCII file may cause "segmentation fault" error under Unix or a HITRAN data file is not read properly: output is populated with zeros and code prints out `nlines=0` despite visual inspection of the HITRAN file tells the opposite. An easy fix is to open and save all ASCII files (input and HITRAN database) under Unix. Although we made sure to perform this open-save operation for all ASCII files, and ran all tests on a Linux machine, we advise the user to try the fix again, should the error occur.

3.1 Header files

Code `aspect` uses three primary header files, `paths.h`, `const_param.h` and `hprofiles.h`, and one auxiliary header `cmplx.h`. The goal of the three is to localize all parameters, including paths to files with the HITRAN data, in just a few files. Using these files, updating or adding a new molecule, isotope, or changing the profile (in `aspect`) is straightforward. The first header is short. It contains paths to the HITRAN database, `*.par` and `TIPS` (Sec.4.2) files. The user must check these paths before compilation and update as needed.

The next header, `const_param.h`, contains values of physical constants (e.g., speed of light, standard temperature and pressure, the Planck constant, etc.), precomputed mathematical constants (e.g., π, square root of π, natural logarithm of 2, etc.), scale factors to convert units (e.g., `mbar_to_atm = 1.0/1013.25` converts pressure from millibars to atmospheres), file names (e.g., HITRAN `*.par` files with the line parameters, "q"-files for isotopes), parameters of isotopes for each molecule (e.g., number of isotopes per each molecule, abundance, molar mass, etc.), some accuracy parameters, e.g., `tau_min` is the smallest value of the total τ to be saved in the binary file - all smaller τ are ignored; `delta_nu = 25.0` means that contribution from all HITRAN lines within $\Delta\nu = 25$ (cm^{-1}) from the given frequency is significant. This 25 (cm^{-1}) is a standard cutoff in line shape models in the solar reflectance band (*Clough* et al., 1981: p.152; *Lyapustin*, 2003: p.870; *Shine* et al, 2012: p.542). Alternatively, the cutoff can be defined as a certain number of half-widths at half-maximums (HWHM). For example, HAPI uses 50 HWHMs as default cutoff value (*Kochanov* et al, 2016: p.25). One should check appropriate literature and update the parameter as necessary.

A peculiar parameter is `water_mass_density = 1.0` (g/cm^3) which is used to convert the water vapor columnar amount in *atm-cm* (Sec. 6.3) to the precipitated (liquid) water

equivalent in *cm* and at standard temperature. Of course, this scale factor of `1.0` could be dropped in calculations, at the expense of code readability.

The last header, `hprofiles.h`, contains extracts from MODTRAN: temperature, pressure, air density, and molecular concentration height profiles, for six standard atmospheric profiles and eight molecules. It also defines grid of heights, ***`zkm`*`[ ]`**. In Sec.6, we talk more about its content.

As a first step, the user is supposed to download the package `aspect_gcell` from the journal website[31] or from our GitHub repository[32]; unzip if necessary. Note that GitHub has a 25Mb limitation on file size. Because of that, we have zipped `./hitran/01_hitdb.par` and `./hitran/06_hitdb.par` (HITRAN data for H_2O and CH_4, respectively) before uploading. These must be unzipped into the same directory before use. We uploaded other HITRAN `*.par` files, including the one for a single O_2-record, without compression. We assume in subsequent that all files and folders are in `aspect_gcell` folder; all paths are defined relevant to it – see our GitHub repository for structure of folders and files. Once all paths have been confirmed, both programs are ready for compilation.

3.2 Installation, input, and output parameters

3.2.1 Gas cell mode

As software goes, `gcell` is a relatively simple, small code. **Table 1** shows files necessary to run the code; **Fig.1**(*a*) shows its structure. The HITRAN database and TIPS files for molecules #1-7 and 10 (HITRAN molecular numbering is discussed shortly in Sec. 4.1) come with the code in `./hitran/` and `./hitran/TIPS/`, respectively, but are not shown in the table and on the chart.

Table 1: Description of files for `gcell`. Makefiles and the `main(…)` program file come first in the list, followed by other source files, headers, input and output ASCII files. Location of each file in the distributive is shown assuming `./` is the directory where the package was extracted. Files used only for the gas cell code (and not `aspect`) are highlighted in gray.

File name and location	File purpose

[31] In this case, all source files are in the same directory; `make_directories.py` creates proper subdirectories.
[32] https://github.com/korkins/aspect_gcell/

General files	
`./makefile`	A makefile that runs both `makefile_g` (gas cell mode) and `makefile_a` (atmospheric mode)
`./makefile_g`	Make file for gas cell mode only.
C source files	
`./src/main_gcell.cpp`	Main program file. Calculates LUT with $\tau(\nu)$ for a gas cell and saves the LUT into a file.
`./src/count_lines.cpp`	Counts the number of records (lines in HITRAN file) within an interval $[\nu_{min} : \nu_{max}]$ in the HITRAN `*.par` file and returns the index for the first line, if found.
`./src/isotops.cpp`	Calculates TIPS ratio for the given temperature and returns parameters of all isotopes of the given molecule
`./src/ix1ix2.cpp`	For a given interval, it returns the first `ix1` and last `ix2` indices of array elements belonging to the interval; zero-offset for `ix` is assumed.
`./src/read_hitran160.cpp`	Reads the HITRAN data from a `*.par` file assuming 160-symbols long format
`./src/voigt/humlicek.cpp`	Calculation of the Voigt spectrum using *Humlíček* algorithm; borrowed from SHARM-IPC (*Lyapustin*, 2003)
`./src/voigt/cmplx.cpp`	Defines complex arithmetic operations for `humlicek.cpp`; borrowed from SHARM-IPC (*Lyapustin*, 2003)
Headers	
`./src/paths.h`	Defines paths to HITRAN database and TIPS files
`./src/const_param.h`	Defines physical and mathematical constants, HITRAN and TIPS file names.
`./src/voigt/cmplx.h`	Header for `humlicek.cpp` and `cmplx.cpp` files; borrowed from SHARM-IPC (*Lyapustin*, 2003)
Input and output ASCII files	
`./gcell-o2a.inp`	Test input for oxygen A-band scenario (Sec. 5.3.1).
`./gcell-ch4.inp`	Test input for methane scenario (Sec. 5.3.2).
`./check/gcell_o2_check.txt`	Output for `gcell-o2a.inp` for checking purpose

`./check/gcell_ch4_check.txt`	Output for `gcell-ch4.inp` for checking purpose
`./check/gcell_noinp_check.txt`	Output for `gcell` when run without input file

The `makefile` contains GCC commands, with flags, to compile all sources under Unix and link these into an executable. Running the `make` command starts compilation of `gcell` first, followed by `aspect`. This process takes a few seconds. Alternatively, the user may run `make -f makefile_g` to compile the gas cell mode only. Under Windows, the user simply creates a Visual Studio project, dumps the source files in it, and compiles in Debug or Release mode.

Once compiled, `gcell` can be checked by running this command without arguments (we assume a Unix environment hereafter; note `./` in the command below)

```
$ ./gcell
```

In this case, `gcell` tells the user that no input file is provided and the default O_2 A-band case will run. In ~0.1 seconds a file named `O2.txt` will appear in the `gcell` directory, containing two header lines explaining the content of the output file and an array with two columns. The top line contains a fill value (to keep the shape of the array) and the column number density *n* (*molec/cm*^{2}). Next come wavenumbers, ν (*cm*$^{-1}$), in the left column and corresponding optical thickness τ(ν) in the right one. This mode quickly tests the package – compare the content of `O2.txt` with `./check/gcell_noinp_check.txt`.

A user defined input comes from a text file with a fixed (in terms of sequence of input parameters) format:

```
molec_id  nu_usr_min  nu_usr_max  dnu  lcm  T_kelv  p_atm  fname
```

Parameters in the line (with data types), left to right are:

`molec_id` (`integer`) defines the gas species following HITRAN's notation: 1 (H_2O) – water vapor; 2 (CO_2) – carbon dioxide; 3 (O_3) – ozone; 4 (N_2O) – nitrous oxide; 5 (CO) – carbon monoxide; 6 (CH_4) – methane; 7 (O_2) – molecular oxygen; 10 (NO_2) – nitrogen dioxide. These are some species commonly used for passive remote sensing of Earth's atmosphere and surface from satellites in the visible and near-infrared portions of the solar

spectral range. However, the user should check for the importance of absorption by other species in their spectral region of interest.

`nu_usr_min`, `nu_usr_max`, `dnu` (`double`) define grid of wavenumbers, ν (cm^{-1}). The minimum (left) and maximum (right) points in the grid are `nu_usr_min` and `nu_usr_max`, respectively.

`lcm` (`double`) length of the gas cell in *cm*.

`T_kelv` (`double`) temperature in the gas cell in Kelvins (*K*).

`p_atm` (`double`) pressure in the gas cell in atmospheres (*atm*).

`fname (string`) defines output file name (optionally, with path – up to 256 symbols long).

Consider `gcell-ch4.inp` with the following content:

```
6  4081.901  4505.699  0.002  8.0  296.0  1.0  gcell-ch4.txt
```

One runs this case by typing[33]

```
$ ./gcell gcell-ch4.inp
```

[33] In MS Visual Studio, add the file via `Configuration Properties\Debugging\Command Arguments`

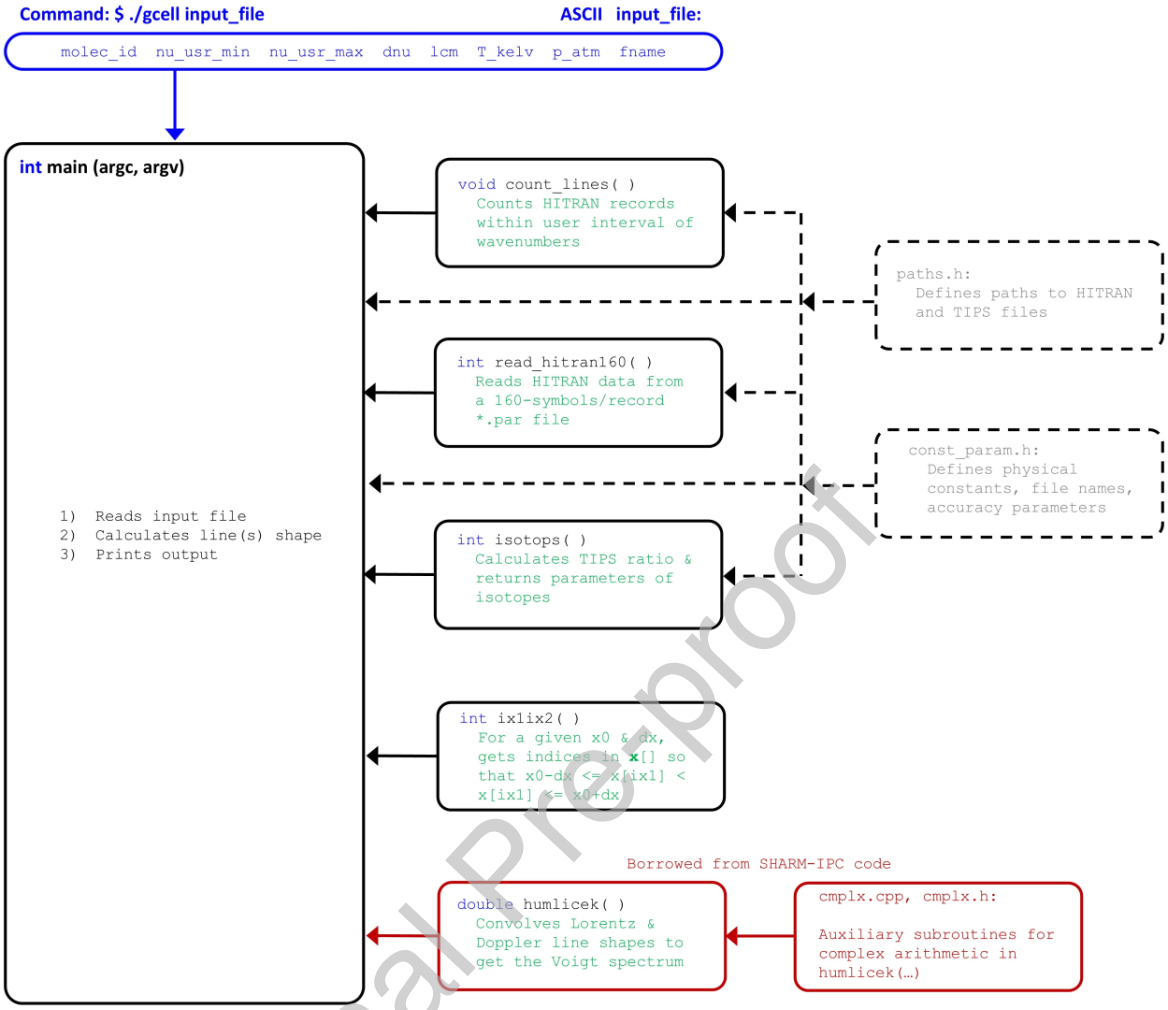

Fig.1(a): Structure of `gcell`. Subroutines are shown in the order they are called. Dashed lines correspond to header files.

It corresponds to simulation of methane, CH_4, which is HITRAN's molecule #6, across the [4081.901, 4505.699] (cm^{-1}) spectral band with step 0.002 (cm^{-1}) in an 8 (*cm*) long gas cell at temperature 296 (*K*) and pressure 1 (*atm*). According to the last parameter, the output file is `gcell-ch4.txt`.. If the input and the executable files are not in the same directory, a full path must be specified. As defined in `paths.h`, the full path length must not exceed 256 characters: `path_len_max = 256`.

We provide `gcell-ch4.inp` with the package. The corresponding output data, generated on our side, is located in `./check/gcell-ch4_check.txt`. We also provide an input file

`gcell-o2a.inp`. and the corresponding output in `./check/gcell-o2a_check.txt` for an oxygen A-band scenario.

Spaces and tabs in the input files are ignored. However, due to fixed format of the input, the input parameters are not optional. In the gas cell mode, we assume natural atmospheric abundances for isotopes (which HITRAN parameters already account for). Otherwise, one must rescale the abundances from HITRAN's default to those used *de facto*.

The gas cell assumes a single type of molecule. By changing one line of code, see Eq.(8) below, it is easy to account for a gas-air mixture. Thus, the gas cell mode can be used for simulation of absorption of molecules of the gas on a horizontal path in the air. In this case, the temperature and pressure remain constant, but one must modify input to account for the mixing ratio, and the "gas cell" will be long, e.g., `lcm = 100000.0` for a 1 (*km*)-long trace. With these few last comments made, we continue to the atmospheric mode – code `aspect`.

3.2.2 Atmospheric mode

The codes `aspect` and `gcell` share some source files. In addition to those from **Table 1** without grey highlighting, **Table 2** shows files that pertain exclusively to `aspect`. For example, `aspect` uses all the same headers as `gcell`, and one more, `hprofiles.h` – the only one listed in **Table 2**. **Fig. 2(*b*)** shows structure of `aspect`.

Table 2: Description of files for `aspect`. The content is like in **Table 1**, which non-highlighted files are also dependencies of `aspect`.

File name and location	File purpose
General files	
`./makefile_a`	A make file for atmospheric mode only.
C source files	
`./src/main_aspect.cpp`	Calculates LUT with spectral and height dependence of $\tau(\nu)$ and saves the LUT into a file.
`./src/hisotops.cpp`	For each isotope of a given molecule, calculates the TIPS ratio as a function of height, and returns the molar mass, abundance, and the number of isotopes.
`./src/intparab.cpp`	Approximates 3 points with a parabola and integrates it for a given interval, covered by the parabola.

`./src/kabs.cpp`	Calculates the spectral absorption cross-section per molecule.
`./src/simpson.cpp`	Numerically integrates a function using Simpson's rule[34].
`./src/tauabs25.cpp`	Integrates the extinction profile over height from TOA to a set of user-defined heights not exceeding z = 25 (*km*). For any altitude above this point, the function returns integral from TOA to 25 (*km*)
Headers	
`./src/hprofiles.h`	Contains MODTRAN profiles for temperature, pressure, air number density, relative concentration of the gas spices, and grid of heights.
Input and output ASCII data files	
`./aspect-ch4.inp`	Test input for a methane scenario; runtime ~1800 seconds (45823 relevant HITRAN-2020 lines).
`./aspect-o2a.inp`	Test input for the oxygen A-band scenario; runtime ~2 seconds (345 relevant HITRAN-2020 lines)
`./check/aspect_noinp_check.txt`	Output for `aspect` called without input file.
`./check/aspect_ch4_check.txt`	Output for `aspect-ch4.inp` for checking purpose
`./check/aspect_o2_dat_check.txt`	Output for `aspect-o2a.inp` containing metadata: initial point of the wavenumber interval $\nu 0$, step $d\nu$, number of points over ν, number of altitude points. This file also shows 2 Python commands for reading the binary files (see below).
Output binary data files	
`./check/aspect_o2_check.bin`	Output for `aspect-o2a.inp` with $\tau(\nu)$ as 32-bit floating point numbers as a function of height (lead dimension) and wavenumber.
`./check/aspect_O2_inu_check.bin`	Output for `aspect-o2a.inp` with the wavenumber grid expressed as a 32-bit integer index.

Once compiled, the following command is used to run `aspect` from the command line (like for `gcell`, we assume commands are typed in Unix environment)

[34] https://en.wikipedia.org/wiki/Simpson's_rule

```
$ ./aspect filename
```

The `filename` is an ASCII file with input parameters in the following format:

```
molec_id iatm column_amount nu_usr_min nu_usr_max dnu nzkm zkm[] fname fmt
```

Parameters, left to right are:

`molec_id` (`integer`) defines a molecule of gas following the HITRAN notation (see `gcell` discussion above)

`iatm` (`integer`) – defines atmospheric profile of temperature and pressure following MODTRAN: 1 – Tropical, 2 – Midlatitude Summer, 3 – Midlatitude Winter, 4 – Subarctic Summer, 5 – Subarctic Winter 6 – Standard US 1976 atmosphere (see Sec. 6.1);

`column_amount` (`double`) defines the atmospheric total column amount of the selected gas. For the water vapor, `molec_id = 1`, the column amount indicates centimeters of precipitated water (see Sec. 6.5). For all other molecules, the column amount is defined in parts per million in a volume (*ppmv*) . Negative value, e.g. -1.0, instructs `aspect` to borrow the column amount from MODTRAN (see Sec. 6.2).

`nu_usr_min`, `nu_usr_max`, `dnu` (`double`) define a grid of wavenumbers, ν (cm^{-1}). The minimum (left) and maximum (right) points in the grid are `nu_usr_min` and `nu_usr_max`, respectively. To include the maximum point, `aspect` calculates the number of points in the grid, `nnu`, by rounding the number of intervals towards the nearest greater integer using `ceil`

```
nnu = int(ceil((nu_usr_max - nu_usr_min)/dnu))+1
```

Note, higher `nnu` impose higher requirements on memory.

`nzkm` (`integer`) defines the number of heights at which the absorption optical depth will be calculated. The amount of memory required for calculations and the size of the output file depend on `nnu*nzkm`.

`zkm``[nzkm]` (`double`, array of `nzkm` elements) – defines array of heights, in kilometers (*km*), from the lowest to the highest one, w.r.t. the ground level, z = 0.0 (*km*). The output value at

the requested height **zkm**[iz] corresponds to τ from the MODTRAN's TOA level, z = 120 (*km*), to the given height.

fname (string) defines output file name (optionally, with path – up to 256 symbols long).

fmt (string of 3 characters) defines format of output: txt – ASCII (1 file will be returned), bin – binary (3 files will be returned: 2 *.bin and 1 *.txt).

Tab(s) or more than one space are allowed as delimiters in the input file.

We assume it is the user's responsibility to provide meaningful input. Neither aspect nor gcell check the input file for correctness, the only exception is to check if the given imolec is included. It is convenient to keep the input file(s) in the same folder with the aspect executable. Otherwise, the user is expected to provide a full path to the input file. If the input file is missing at the specified location, aspect will notify the user and stop execution. If the input file is not specified at all, aspect will run a default scenario for the oxygen A-band, O_2A, defined as follows:

```
7  6  -1.0  13050.0  13160.0  0.01  3  0.0 2.5 5.0 O2 txt
```

This default option is good for a quick check. As explained above, this input is for oxygen O_2 (molec_id = 7), standard US 1976 MODTRAN profile (iatm = 6, see Sec.6.1) and the total amount of gas from the same (column_amount = -1.0, see **Table 6** below), for the wavenumber grid ranging from 13050 (cm^{-1}) to 13160 (cm^{-1}) with step 0.01 (cm^{-1}), and for nzkm = 3 heights located at BOA, 0.0 (*km*), 2.5 (*km*), and 5.0 (*km*). The last parameter, txt, tells aspect to save output as an ASCII file. Note, again, that aspect returns partial column optical thicknesses (from TOA to the given altitudes), not the layer one calculated as difference between partial column optical thicknesses.

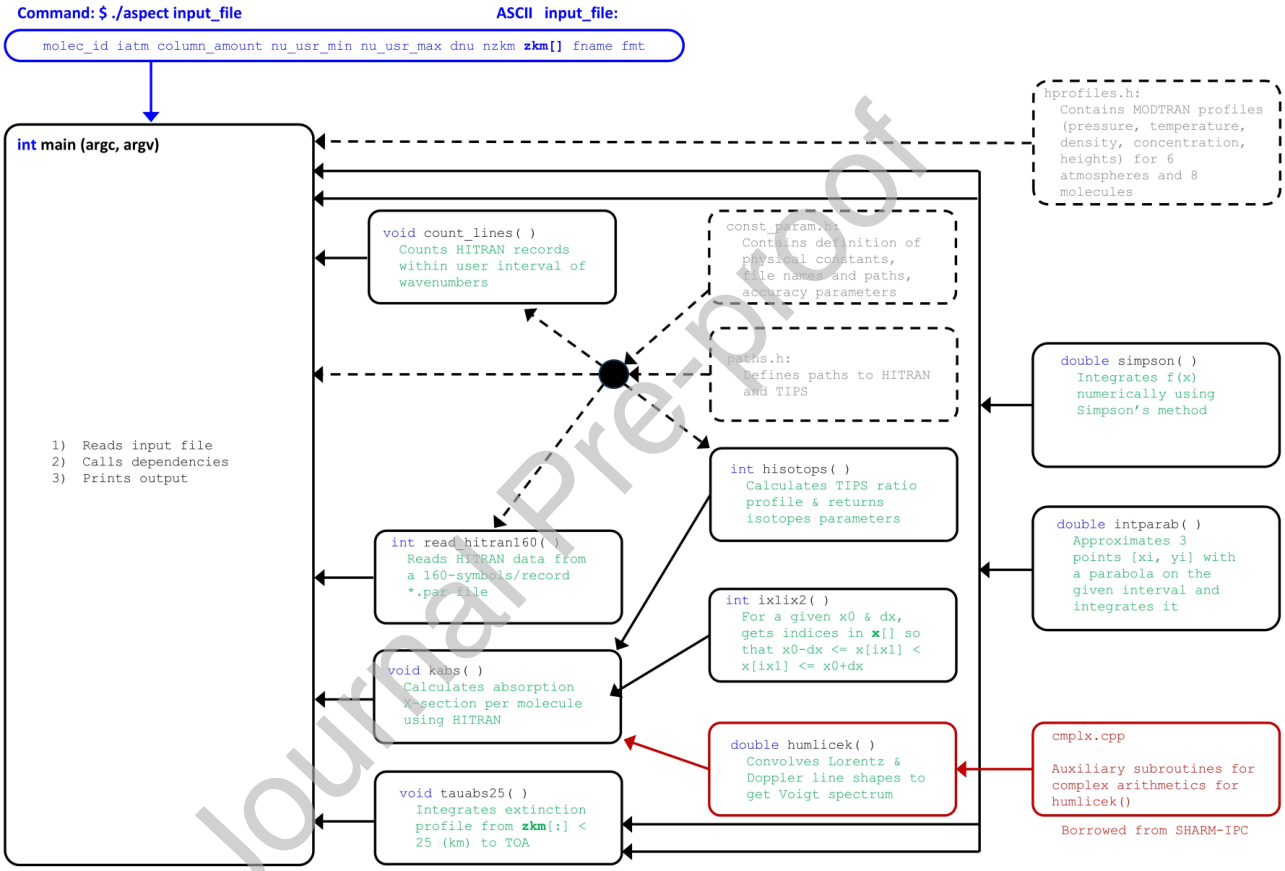

Fig.1(b): Structure of `aspect`. Dashed lines – headers, red – unaltered part from SHARM-IPC. Each block corresponds to a separate file. Except for cmplx.cpp, one file contains one function.

The output file `O2.txt` for the default case looks as follows (the first 4 and last 3 lines are shown; the result may look slightly different if the HITRAN database has changed, these correspond to HITRAN 2020 O_2 data as downloaded in October 2024)

```
# columns: [1] index inu, [2] nu (cm-1), [3:] tau from TOA to zkm =
0.000   2.500   5.000
0  13050.0000    2.725424e-01    1.365520e-01    6.542805e-02
1  13050.0100    2.838314e-01    1.421957e-01    6.812620e-02
2  13050.0200    2.958670e-01    1.482122e-01    7.100233e-02
…
10998  13159.9800    4.738309e-01    2.376659e-01    1.140908e-01
10999  13159.9900    4.857890e-01    2.432799e-01    1.166022e-01
11000  13160.0000    4.994583e-01    2.497651e-01    1.195352e-01
```

Starting from the second line onwards, the left column indicates an integer wavenumber index, `inu`, and the corresponding wavenumber **`nu`**`[inu]`, calculated as follows

```
nu[inu] = nu_usr_min + inu*dnu;
```

Next comes τ as integrated from TOA to 0.0, 2.5, and rightmost column 5.0 (*km*). Excluding the header line (#), the file contains 11001 records:

```
nnu = (13160 – 13050)/0.01 + 1 = 11001.
```

The ASCII file is convenient for visual inspection, e.g. at debugging stage. For a smaller size of the output file and faster reading of the data into memory, the binary format is preferable: `fmt = bin`, see file `aspect-o2a.inp` as an example. In this case, `aspect` generates three files on output. The first one, `O2_dat.txt`, contains information necessary to read in the binary files: the number of the spectral and height grid points. It also tells that floating-point numbers are stored in the single precision 32-bit format. The other two, `O2_inu.bin`, and `O2.bin`, contain 32-bit integer indices `inu` for the corresponding wavenumbers. In `O2.bin`, the height grid is the lead dimension; for each given wavenumber index, optical thicknesses at different heights are stored consecutively.

The following Python script reads τ from the binary file and converts the 1D array into a 2D array with heights changing column wise and wavenumbers – row wise:

```
import numpy as np
data = np.fromfile('O2.bin', dtype=np.float32)
```

```
tau[0:nnu, 0:nzkm] = np.reshape(data, (nnu, nzkm))
# O2_dat.txt contains nnu & nzkm
```

For the default O_2A case, `O2.bin` is about 5.5 times smaller than `O2.txt`: 709Kb/129Kb. Also, when saving and reading binary files on different machines, the user must care for endianness[35].

Based on the user-defined threshold for τ at the lowest height (usually, at BOA), `aspect` may skip insignificant values to reduce the size of the output `*.bin` file. In this case, the number of records will not match the number of grid points. The threshold τ is defined in `const_param.h`; the current setting is `tau_min = 1.0e-4`, which corresponds to a one-way vertical transmittance in atmosphere $T(\nu, \mu = 1) = 0.9999$ (see Eq.(24) below).

At this point, the reader is familiar with two modes of the code, and input and output format. This is the basic user level. An extension to the user level is understanding of the code structure: C-functions and their purpose, as charted in **Fig.1** (***a, b***). Now we proceed to the level of development. The first step is calculation of the absorption coefficient k ($cm^2/molec$) by a single line as parameterized by a corresponding HITRAN record. Since `gcell` does not consider height profiles, we recommend following our discussion with that code.

4. Calculation of absorption by a single HITRAN line

This section shows how to calculate the absorption cross-section k ($cm^2/molec$) for a single line using HITRAN parameters. As the units of k indicate, the cross-section is defined per one molecule of gas present. This standard practice will be assumed hereafter and the words "per molecule" will be dropped. As a prerequisite, we assume the user has downloaded the HITRAN database for molecules 1 through 7 and 10. The HITRAN ASCII `*.par` files with the line shape parameters come in the current 160-symbols-long format. The user should get acquainted with the HITRAN theoretical background using, e.g., online HITRAN manuals[36, 37] or papers (*Rothman*, 1998: p.708; *Pliutau & Roslyakov*, 2017 – note, the latter describes an educational software). Since typos are always possible, we recommend checking references from different

[35] https://en.wikipedia.org/wiki/Endianness
[36] https://hitran.org/docs/definitions-and-units/
[37] http://www.bytran.org/howtolbl.htm

authors, or different years from the same authors. All numerical results that we show in this paper correspond to HITRAN 2020 downloaded from the HITRANonline website[38].

4.1 Reading one record form the HITRAN `*.par` file

It is instructive to create and read a HITRAN file with only one record. As an example, we pick one O_2 line at ν = 13000.816219 (cm^{-1}) and read it using the `read_hitran160(…)` function. For reproducibility and simplicity of debugging, our `./hitran/` folder contains a file in the HITRAN 160-symbols-long format with only the named line `07_hitdb_one_line.par`. The main command executed in `read_hitran160(…)` is

```
fscanf(fin, "%2c%1c%12c%10c%10c%5c%5c%10c%4c%8c%93c%c",
str_molec_id, // molecule ID
str_isotop_id, // isotope ID
str_nuij, // transition wavenumber in vacuum
str_Sij, // line intensity at T=296K scaled by isotope abundance
str_Aij, // Einstein coefficient (not used in this paper)
str_gamma_air, // air-broadened Lorentzian HWHM
str_gamma_self, // self-broaden HWHM at T = 296 (K) and P = 1 (atm)
str_Elower, // Lower state energy, E''
str_n_air, // temperature exponent for the air-broadened HWHM
str_delta_air // air induced pressure shift referred to P = 1 (atm)
str_tail, // the rest of the line is not used
chr_end_of_line);
```

It explicitly shows the structure of the HITRAN `*.par` file. Note that the total number of characters being read is 160 as the function name says. However, it is easy to adapt this command for reading an old 100-characters long `*.par` file used until HITRAN 2004 edition (*Rothman*, 2005: Table 1). All these parameters, except for `str_molec_id` (known at input) and the Einstein coefficient (not used in our calculations), are converted from the character data type either to integer (using `atoi`) or the floating point number (`atof`), as appropriate.

Table 3: Output of the `read_hitran160(…)` function; the function `count_lines(…)` from **Table 1** defines the number of lines `nlines` to be read and the first line `iline0` to start reading. The reference temperature and pressure are $T_{ref} = 296^{o}(K)$ and

[38] https://hitran.org/lbl/

$p_{ref} = 1.0\ (atm) = 1013.25(Pa) = 760(torr)$, respectively. For list of all HITRAN parameters with units see (*Rothman*, 1986: p.4060) and (*Gordon*, 2017: p.5).

Name	type[size]	Notation	Units	Explanation
isotop_id	int[nlines]	-	none	Isotope ID, as in HITRAN, to get proper isotope properties (e.g., molar mass): 1 = most abundant, 2 = second, etc.
nuij	double[nlines]	ν_{ij}	cm^{-1}	Transition wavenumber between levels *i* and *j* (also called frequency)
Sij	double[nlines]	S_{ij}	$\frac{cm^{-1}}{molec \cdot cm^{-2}}$	Line intensity weighted with isotope abundance, I_a, at T_{ref}.
gamma_air	double[nlines]	γ_{air}	$\frac{1}{atm \cdot cm}$	Air-broadened Lorentzian HWHM at p = 1 (*atm*) and T = 296 (*K*) for Voight line shape.
gamma_self	double[nlines]	γ_{air}	$\frac{1}{atm \cdot cm}$	Self-broadened Lorentzian HWHM at p = 1 (*atm*) and T = 296 (*K*) for Voight line shape
Elower, Epp	double[nlines]	E''	cm^{-1}	Lower state energy
n_air	double[nlines]	n_{air}	none	Temperature-dependence exponent for the air-broadened HWHM, γ_{air}
delta_air	double[nlines]	δ_{air}	$\frac{1}{atm \cdot cm}$	Pressure shift induced by air, referred to p = 1 (*atm*)

Historically, the HITRAN database convention used one symbol for the isotope number thus assuming up to 9 isotopes (1 = most abundant, 2 = second…) per molecule at most. However, for some molecules more isotopes have been introduced over time. E.g., for CO_2 (`molec_id = 2`), HITRAN defines 12 isotopes using ID-s 0, A, and B for isotopes 10, 11, and 12, respectively, which must be checked before converting the isotope ID from character to integer. Note also that the line intensity, `Sij`, is already scaled by the isotope abundance (*De Biévre* et al., 1984; *Böhlke* et al., 2005) as found in the terrestrial atmosphere, so for such applications no further scaling is necessary.

Other than these two peculiarities, reading the standard HITRAN database in ASCII format is not a problem. For our example of the single O_2 line, we have `nline = 1` (total number of

lines), `iline0 = 0` (zero-offset index of the first line in the HITRAN file) and the line parameters are

```
isotop_id = 1
nuij = 13000.816219 (cm-1)
Sij = 2.708e-27 (cm-1/(molec cm-2))
gamma_air = 0.04580 (cm-1 atm-1)
gamma_self = 0.047 (cm-1 atm-1)
Epp = 1814.01040 (cm-1)
n_air = 0.67 (unitless)
delta_air = -0.007400 (cm-1 atm-1)
```

Negative `delta_air` means the center of the line is shifted towards the lower wavenumber ν ("left") in air w.r.t. its position in vacuum. Despite the simplicity, it is recommended to plot, e.g., line intensity and check the plots vs. HITRAN online tool (*Hill*, 2016) or figures reported in literature (*Rothman*, 2003: Fig.2; 2013: Fig.5; *Gordon*, 2017: Figs. 5, 6, 8; 2022: Fig. 5). The latter references also compare molecules from different HITRAN versions.

4.2 `Molparam.txt` and TIPS q-files.

The other two HITRAN files are `molparams.txt` and `TIPS.txt`. For all HITRAN molecules, `molparam.txt` contains a global ID molecule code (not used in this papers), the isotope abundance for the Earth environment (note again, `Sij` is already scaled by this), the total internal partition sum (TIPS) Q(296) (explained later) at the reference temperature $T = 296^o$ (K), the statistical weight g_j (not used in this paper), and the molar mass (in grams). In our codes, we moved all necessary information from `molparam.txt` file to the header `const_param.h`. Considering O_2 as an example, the content of the `molparam.txt` file[39]

```
Molecule # Iso Abundance     Q(296K)       gj    Molar Mass(g)
    O2 (7)
          66  9.95262E-01    2.1573E+02     1      31.989830
          68  3.99141E-03    4.5523E+02     1      33.994076
          67  7.42235E-04    2.6581E+03     6      32.994045
```

corresponds to the following in `const_param.h`:

```
// (7) O2:
int const niso_o2 = 3;
```

[39] To be exact, we used information from this page https://hitran.org/docs/iso-meta/, instead of the `txt` file.

```
char const fname_iso_o2[niso_o2][fname_len_max] =
   {"q36.txt", "q37.txt", "q38.txt"};
double const
   Qref_o2[niso_o2] = {215.73450400, 455.22995200, 2658.12071500},
   molar_mass_o2[niso_o2] = {31.989830, 33.994076, 32.994045},
   Ia_iso_o2[niso_o2] = {9.95262e-1, 3.99141e-3, 7.42235e-4};
```

Here `niso_o2` is the number of isotopes, ***Qref_o2*** are the TIPS at the reference temperature $T_{ref} = 296^o$ (*K*), ***molar_mass_o2*** are the isotope molar masses, and the isotope abundances are ***Ia_iso_o2***. Note that the isotope ID number, `isotope_id`, which one reads from the HITRAN `*.par` file, is used in our codes as an index to get the appropriate isotope parameters from the mentioned arrays. It is therefore easy to add a new isotope by adjusting the total number of isotopes and updating the arrays with new parameters. One must keep in mind that the HITRAN isotope number is a unit offset integer, contrary to the C-array zero offset indexing.

The array ***fname_iso_o2***, contains the file names with TIPS precomputed in a wide range of temperatures *T* from a few degrees to a few thousand (*Laraia*, 2011; *Gamache* 2017, 2021). The TIPS describes statistical properties of gas in thermodynamic equilibrium. In particular, the number of molecules (population) at different energy states E_i which in its turn determines the transition intensity of a line, S_{ij}. Since the dependence of the line intensity on TIPS is linear, the TIPS ratio is used to scale the intensity from the value at the reference temperature, $T_{ref} = 296^o$ (*K*) to an arbitrary one.

Each *q*-file contains only two columns: left is temperature *T* (*K*) in increasing order with equal step $\Delta T = 1^o$ (*K*), right is the TIPS value *Q*(*T*). This is convenient for reading and interpolation. Each *q*-file name is based on the global isotope ID. For example, for the oxygen, `isotope_id = 1`, the corresponding TIPS file `q36.txt` in line 296 reads 215.73450400, which is the TIPS value at the reference temperature Q(296^o*K*).

`Aspect` and `gcell`, use special functions for the isotope data. In `gcell` it is

```
niso = isotops(molec_id, T_kelvin, Qratio, mmass_iso, Ia_iso);
```

Using `molec_id`, and a given temperature `T_kelvin`, the function returns the total number of isotopes `niso` for the given molecule, ratio of TIPS $Q(T_{ref})/Q(T)$, the molar mass and abundances for all `niso` isotopes (hence all these output parameters are arrays). In `aspect`,

this function is slightly different because of the variation of temperature with height – `hisotops(…)`.

Specifically, based on `molec_id`, the `isotops(…)` function decides what isotopes to read from `const_param.h`

```
switch (molec_id)
{
      …
      case 7: // O2
            niso = niso_o2;
            for (iso = 0; iso < niso; iso++)
            {
                  Qref[iso] = Qref_o2[iso];
                  mmass_iso[iso] = molar_mass_o2[iso];
                  Ia_iso[iso] = Ia_iso_o2[iso];
                  strcpy(fname_iso[iso], fname_iso_o2[iso]);
            } // for iso
            break;
      …
}  // switch (molec_id)
```

Then, for each isotope, the function opens an appropriate `qXY.txt` TIPS file, reads it consecutively until the range of temperatures for `T_kelvin` is found, interpolates TIPS linearly and calculates the TIPS ratio

```
for (iso = 0; iso < niso; iso++)
{
      strcpy(fpath, path_TIPS);
      strcat(fpath, fname_iso[iso]);
      fin = fopen(fpath, "r");
      fscanf(fin, "%lf %lf", &T2, &Q2);
      while (T2 < T_kelvin)
      {
            T1 = T2;
            Q1 = Q2;
            fscanf(fin, "%lf %lf", &T2, &Q2);
      } // while T2 < T_kelvin
      Q = Q1 + (T_kelvin - T1)*(Q2 - Q1)/(T2 - T1);
      Qratio[iso] = Qref[iso]/Q;
      fclose(fin);
```

```
} // for iso
```

This straightforward, but not the most efficient way, could be improved by: (*a*) reducing the range of *T* (*K*) in the `qXY.txt` files to that typically found in the Earth atmosphere; (*b*) converting the `qXY.txt` files from ASCII to an array in header (e.g., in `const_param.h`) – this will allow to immediately find indices of the interval containing `T_kelvin`; (*c*) avoid files by coding an explicit expression for *Q*(*T*) (*Rothman*, 1998: p.695), or by using these Fortran or Python programs[40]. As we will see later, the performance of this subroutine is not a bottleneck. Because of that, and to avoid unnecessary alteration of the default HITRAN `qXY.txt` file, we use this simple LUT-based solution with consecutive search for the gas cell calculations.

4.3 Basic code for a single line

Now we are ready for calculation of the absorption cross section, *k* ($cm^2/molec$), in a gas cell. So far, we keep the abovementioned `*.par` file with one oxygen record. All commands in this section are operators of the `main(…)` function located in the `main_gcell.cpp` file.

For numerical calculations the user defines the following parameters:

`nu` – wavenumber to compute the absorption coefficient (cm^{-1});

`T_kelvin` – gas temperature (*K*);

`p_atm` – gas pressure (*atm*).

The first step is to compute the center of the spectra line ν_{ij}^{pshift} as it shifts w.r.t. its position in vacuum ν_{ij} due to user specified pressure *P* (*atm*) assumed constant – like in a gas cell or at a given level in the atmosphere (same for temperature and gas concentrations)

$$\nu_{ij}^{pshift} = \nu_{ij}(P) = \nu_{ij} + \delta_{air} P \qquad (1)$$

```
nuij_pshift = nuij + delta_air*p_atm;
13000.808819 = 13000.816219 + (-0.007400)*1
```

$cm^{-1} = cm^{-1} + cm^{-1}/atm \cdot atm$. Next, the intensity of the spectral line is scaled from the reference temperature $T_{ref} = 296^o$ (*K*) to the user-defined one. This step requires calculation of several exponential functions which can be combined to reduce the number of calls to the

[40] https://hitran.org/suppl/TIPS/TIPS2021/

computationally expensive `exp()` function. However, it would make the code less readable and does not provide much gain in performance.

$$e_{11} = \exp\left(-c_2 E''/T\right) \tag{2}$$

```
e11 = exp(-c2_rad*Epp/T_kelvin);
0.00016661 ≈ exp(-1.438777*1814.01040/300.0);
```

$$e_{21} = \exp\left(-c_2 E''/T_{ref}\right) \tag{3}$$

```
e21 = exp(-c2_rad*Epp/T_ref);
0.00014813 ≈ exp(-1.438777*1814.01040/296.0);
```

$$e_{12} = 1 - \exp\left(-c_2 \nu_{ij}^{pshift}/T\right) \tag{4}$$

```
e12 = 1.0 - exp(-c2_rad*nuij_pshift/T_kelvin);
1.0 ≈ 1.0 - exp(-1.438777*13000.808819/300.0);
```

$$e_{22} = 1 - \exp\left(-c_2 \nu_{ij}^{pshift}/T_{ref}\right) \tag{5}$$

```
e22 = 1.0 - exp(-c2_rad*nuij_pshift/T_ref);
1.0 ≈ 1.0 - exp(-1.438777*13000.808819/296.0).
```

In Eqs.(2)-(5), $c_2 = hc/k \approx 1.44$ ($cm \cdot K$) is the second black body radiation constant. Given its value, the spectral boundary for atmospheric remote sensing in the solar region, $\lambda_{max} \sim 2.5$ (μm) or $\nu_{min} \sim 4000$ (cm^{-1}), and the highest value temperature within $z = 0 \ldots 120$ (km) $T_{max} \sim 350^o$ (K), both exponents in Eqs.(4) and (5) vanish. We preserve these terms for a tutorial, rather than numerical reason, but note that they can be safely dropped for the Earth atmosphere remote sensing leveraging scattered sunlight. Also we note, that the two equations rely on Eq.(1). Apparently, similar equations in the HITRAN and BYTRAN manuals contain a typo: unshifted ν is used in both.

With Eqs.(2) - (5), one calculates the temperature-affected intensity of the spectral line as

$$S_{ij}(T) = S_{ij} Q_{ratio}(T) \frac{e_{11}}{e_{21}} \frac{e_{12}}{e_{22}} \tag{6}$$

```
SijT = Sij*Qratio*e11*e12/e21/e22
3.005168e-27 ≈ 2.708e-27*0.98664770*0.00016661*1.0/0.00014813/1.0
[SijT] = [Sij]
```

In Eq.(6), $Q_{ratio}(T)$ is the ratio of total internal partition functions Q at the reference and user-defined temperatures $Q(T_{ref})/Q(T)$ (note T_{ref} is in the numerator). As stated previously, by default the HITRAN line intensity S_{ij} is already scaled by the isotope abundance typical for the Earth environment, so users need make no changes.

In addition to the intensity, the line width is also affected by temperature and pressure. It is common to account for two effects contributing to the line broadening: the Doppler component and the Lorentzian component. The Doppler thermal (Brownian) motion broadening is caused by the Doppler effect of change of frequency of wave when the source of light (an emitting molecule) moves w.r.t. the observer. Kirchhoff's law requires the same change to happen for an absorbing molecule. The Doppler line shape is modeled by the Gaussian distribution with the following HWHM parameter

$$\alpha_D = \frac{\nu_{ij}^{pshift}}{c}\sqrt{\frac{2N_A kT\ln(2)}{m_{iso}}} \tag{7}$$

```
alf_doppler = nuij_pshift*
      sqrt(2.0*n_avogadro*k_boltzman*T_kelvin*ln2/mmass_iso)/c_light;
0.014257689 ≈ 13000.808819*
      sqrt(2.0*6.02214129e+23*1.3806488e-16*300.0*ln(2)/
      31.98983)/29979245800.0
```

The Lorentzian-broadening accounts for the natural broadening (finite radiative lifetime makes an excited atom eventually emit radiation) and collision/pressure broadening (emission of radiation by an excited atom when colliding against another atom of the same – self component – or another – foreign component – type). Again, Kirchhoff's law requires the same energy transition to happen during absorption. The HWHM parameter for Lorentzian effects is

$$\gamma_L = \left(\frac{T_{296}}{T}\right)^{n_{air}} \left(\gamma_{air}(P_{total} - P_{self}) + \gamma_{self} P_{self}\right) \tag{8}$$

```
gam_lorentz = pow(T_ref/T_kelvin, n_air)*
      (gamma_air*(p_tot - p_atm) + gamma_self*p_atm);
```

```
0.046579204 ≈
(296.0/300.0)^0.670*( 0.04580*(1.0 - 1.0) + 0.047*1.0 )
```

In Eq.(8), P_{self} is the partial pressure of the gas. In the case of the gas cell, it coincides with the total pressure and only self-broadening takes place: $P_{total} = P_{self}$ and the parameter γ_{air} becomes irrelevant. However, if the user slightly modifies input to provide the total and the partial pressures, the `gcell` code can be used for simulation of absorption along horizontal path in atmosphere that contains mixture of gases or in gas cell containing the same.

The Doppler and Lorentzian broadenings take place together and their combined effect is expressed as a convolution of the respective line shapes, resulting in the Voigt line shape model. This is an important step for modeling of the physics of the absorption process. Also, calculation of the Voigt contour is the most time-consuming step in both our codes. For these reasons, we consider details of the Voigt spectrum in a separate section.

4.4 Convolution – Voigt spectrum

The Voigt spectrum model is a result of the Lorentzian or pressure-broadening, that dominates in the lower atmosphere, and speed-dependent Doppler-broadening that dominates at higher temperatures and lower pressure (*van de Hulst & Reesinck*, 1947). Both are simulated by the normalized (unit integral over the wavenumber, ν) line shape functions. Like in Eqs. (7) - (8), we use subscripts *L* and *D* for the Lorentz and Doppler functions, respectively:

$$f_L(\nu - \nu_{ij}^*) = \frac{1}{\pi}\frac{\gamma_L}{\gamma_L^2 - (\nu - \nu_{ij}^*)^2}, \tag{9}$$

$$f_D(\nu - \nu_{ij}^*) = \sqrt{\frac{\ln 2}{\pi\alpha_D^2}}\exp\left(-\frac{(\nu - \nu_{ij}^*)^2 \ln 2}{\alpha_D^2}\right). \tag{10}$$

For simplicity, Eqs. (9) - (10) do not show *T* and *p* as arguments and indicate that the line shapes depend on distance between a given wavenumber ν and the line center ν_{ij}^* pressure-shifted according to Eq. (1). **Figure 2** schematically shows mutual broadening of the lines when the two effects take place at the same time.

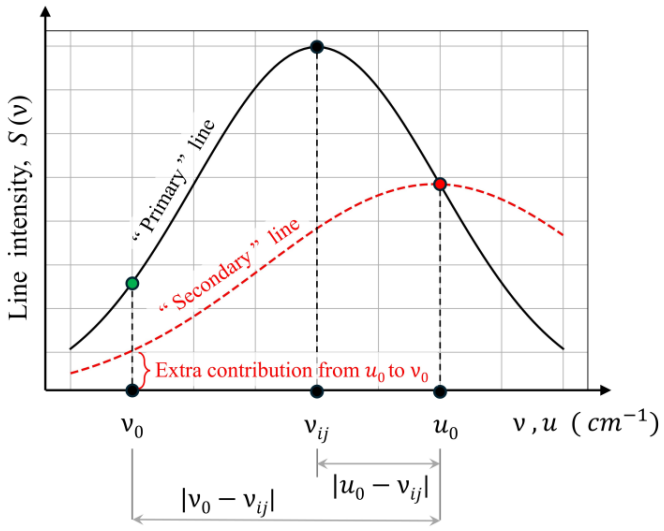

Fig.2: Schematic representation of "primary" line shape broadened by "secondary" one. Contribution at wavenumber ν_0 comes not only from the "primary" line, centered at ν_{ij}, but also from another wavenumber u_0 acting as a center of the secondary line. All points u_0 contribute to all points ν_0, hence both are in fact continuous variables u (for integration) and ν (wavenumber space):

$$f_V(\nu) = \int_{-\infty}^{+\infty} f_L(\nu - u)\, f_D(u)\, du\,.$$

See the main text for details.

Suppose we wish to calculate the line shape at a wavenumber ν considering the fact that wavenumbers u also contribute to ν due to broadening. Assuming the Doppler line as the primary one, we calculate the line intensity at u exactly as Eq.(10) shows

$$f_D(u) = \sqrt{\frac{\ln 2}{\pi \alpha_D^2}} \exp\left(-\frac{(u - \nu_{ij}^*)^2 \ln 2}{\alpha_D^2}\right). \qquad (11)$$

Eq.(11) is for the black solid line (**Fig.2**) centered at the HITRAN's pressure-shifted ν_{ij}^*. It is not indicated as the function argument because it is a constant parameter. Now, this line intensity $f_D(u)$ acts as a "secondary" line contributing to ν via Lorentzian broadening,

$$f_L(\nu - u) = \frac{1}{\pi} \frac{\gamma_L}{\gamma_L^2 - (\nu - u)^2}\,. \qquad (12)$$

In Eq.(12), we note a new line center, *u*. One accumulates the contribution from all points *u* to ν by integration:

$$f_V(\nu) = (f_L * f_D)(\nu) = \int_{-\infty}^{+\infty} f_L(\nu - u)\, f_D(u)\, du\,. \tag{13}$$

Eq.(13) is a convolution (*) of two functions, which commutativity tells that it is not important what line is called "primary". Also, negative wavenumbers are unphysical. However, we are far from wavenumbers close to zero and the line shapes attenuate quickly, within ~20-25 (cm^{-1}) in our band of interest. For mathematical reasons, which we consider shortly, it is beneficial to use the limits as in Eq.(13).

Eqs.(11) - (13) and an appropriate linear scaling of the integration variable *u* yields

$$f_V(\nu) = \sqrt{\frac{\ln 2}{\pi\alpha_D^2}}\,\frac{\gamma_L}{\pi}\int_{-\infty}^{+\infty}\frac{1}{\gamma_L^2 - (\nu - u)^2}\exp\left(-\frac{(u-\nu_{ij}^*)^2 \ln 2}{\alpha_D^2}\right)du = \sqrt{\frac{\ln 2}{\pi\alpha_D^2}}K(x,y)\,, \tag{14}$$

where

$$K(x,y) = \frac{y}{\pi}\int_{-\infty}^{+\infty}\frac{\exp(-t^2)}{y + (x-t)^2}dt,\quad x = \frac{\sqrt{\ln 2}}{\alpha_D}(\nu - \nu_{ij}^*),\quad y = \frac{\sqrt{\ln 2}}{\alpha_D}\gamma_L\,. \tag{15}$$

Code `gcell` implements calculation of the Voigt line shape, Eq.(15), in a straightforward manner, i.e. making commands look similar to what is published in literature. In the code snippet below we deliberately hide operators explained earlier and show only those corresponding to Eqs.(14)-(15).

```
nuij_pshift = …; // Eq.(1)
alf_doppler = …; // Eq.(7)
gam_lorentz = …; // Eq.(8)
y = sqrt_ln2*gam_lorentz/alf_doppler; // Eq.(15)
e11 = …; // Eq.(2)
e21 = …; // Eq.(3)
e12 = …; // Eq.(4)
e22 = …; // Eq.(5)
SijT = …; // Eq.(6)
for (inu = inu1; inu < inu2+1; inu++)
{
   x = sqrt_ln2*fabs(nu[inu] - nuij_pshift)/alf_doppler; // Eq.(15)
```

```
    k_abs[inu] = SijT*(sqrt_ln2/sqrt_pi)*
                        humlicek(x, y)/alf_doppler; //Eqs.(14)-(16)
} // inu = inu1 : inu2
```

We use the loop over `inu` to calculate absorption cross-section on the user's grid of the wavenumbers **`nu`**`[inu]`

$$k_{ij}(\nu, T, p) = S_{ij}(T)\, f_V(\nu, \nu_{ij}, T, p)\,. \qquad (16)$$

Note that absolute value `fabs(`**`nu`**`[inu] - nuij_pshift)` enforces symmetry of the line shape. However, the symmetry may be violated (see Sec.4.5 below).

Humlíček (1982) developed an algorithm for calculation of $K(x, y)$, Eq.(15), with reported relative error not exceeding 10^{-4} and published a corresponding FORTRAN function. Despite using complex arithmetic, the function contains only 30 lines, including 7 comments and 7 non-executable lines: `FUNCTION`, 4 `RETURN`-s, `END` statements and one line with definition of 3 local variables and the function output. Another 7 lines are mostly filled with precomputed values for 3 different "regions" of input parameters, accurate numerical evaluation of which is the main topic of that paper. A vectorized version of this subroutine (*Schreier*, 1992: Appendix 2) was translated into C (*Lyapustin*, 2002: function `humlicek(…)`), which we borrow for use in `gcell` and `aspect`.

Strictly speaking, calculation of $K(x, y)$ is of general mathematical nature, rather than spectroscopy (like calculation of weights for Gaussian quadrature or Legendre polynomials for use in multiple scattering of light). Therefore, for confident use of the `humlicek(…)` function it is sufficient to understand its input, x and y, Eq.(15). Here we only note that (*a*) *Humlíček* (1982: Eq.(1)) considered the entire complex probability function from which the Voigt line shape needs only the real part; and (*b*) calculation of the Voigt line shape is the slowest part of our code (takes ~ 90% of the runtime). *Schreier* (1992) compared accuracy and runtime for several techniques for computation of the Voigt function. It was found that depending on the method, the computational speed for the Voigt function varies by 2 orders of magnitude, even after code optimization. The *Humlíček* (1982) algorithm was found as overall best based on accuracy, speed, and flexibility (*Schreier*, 1992: p.760). We have used it for decades (*Lyapustin*, 2002) and stick to it in this paper.

However, "*accurate yet efficient computation of the Voigt … function is a challenge*" (*Schreier*, 2018(a): Abstract). *Kuntz* (1997), with corrections by *Ruyten* (2004), offered a new numerical implementation of the *Humlíček* algorithm. Depending on a computer architecture, a factor of 1.2 – 3.3 in acceleration was reported. Apart from computational efficiency, *Mohankumar & Sen* (2019) evaluated the Voight function with a 30-digit accuracy for reference purposes using trapezoidal integration, residue correction, and quadruple precision. Corresponding FORTRAN code and coefficients are reported in their paper.

Depending on application, it could be possible to use either Eq.(11) or Eq.(12) and avoid the time-consuming Voigt convolution, Eq.(13). Alternatively, the Voigt effect can be simulated approximately by a rectangular core (central) part and ν^{-2}- shaped wings (*Fels*, 1979), or using analytical, hence fast, approximations, e.g., as a sum of the Lorentzian profiles (*McLean et al.*, 1994: see Appendix for codes in C that approximately calculate the Voigt function and parameter derivatives). However, one must follow the analytical path with caution (*Schreier*, 2018b). *Wells* (1999) discuss an approximate algorithm tailored for atmospheric line-by-line calculations, which is efficient "*if the maximum relative error criteria can be relaxed* " (Abstract). It was suggested to express the algorithm in real arithmetic, use a simple analytical expression for a new "region" far from the line center, redefine boundaries of the regions (*Wells*, 1999: p.33). In the Appendix to *Wells* (1999), one finds codes in FORTRAN77 for calculation of the Voigt spectrum in `SUBROUTINE HUMLIK (…)`, and derivatives $\partial K(x,y)/\partial x$ and $\partial K(x,y)/\partial y$ in `SUBROUTINE HUMDEV(…)`. The Voigt code is longer than that of *Humlíček* (1982), also based on many precalculated numerical parameters, and yields a user-controlled accuracy. *Abrarov & Quine* (2015) approximate the Voigt function as an analytical – hence fast – series expansion (see their Eq.(17)). Their MATLAB code (in Appendix) also relies on a set of precomputed coefficients. For broadband atmospheric radiative transfer, *Nordebo* (2021) suggested replacing the Voigt with the Lorentzian calculation, but on the bounds altered as described in the paper, and based on the dominating role of the far wings of spectral lines in calculation of atmospheric transmittance.

This sparse literature review indicates that calculation of the Voigt function, despite decades of use, may be problematic. On top of that comes the fact that under some conditions the Voigt line

shape model may not be physically sufficient. Although our paper does not go "beyond Voigt", we feel obligated to say a few words supported by references.

4.5 Beyond Voigt: a few legacy and recent references

The Voigt line shape as convolution of the Doppler and Lorentzian contours, is only a model. Its limitations come, e.g., from the assumption of ideal gas to simulate elastic molecular collisions. In fact, the speed of molecules decreases at collision, so does the Doppler effect, causing "collision narrowing" of spectral lines and increasing absorption at the line centers – the *Dicke* (1953) effect[41]. Back in 1960's *Galatry* (1961) and *Rautian & Sobel'man* (1967) gave a non-Voigt expression for a spectral line accounting for the effect of change of speed on the line shape. This effect is most important for simulation of laser light absorption by narrow lines.

Likewise, the Lorentzian model works well near the center of spectral lines, where absorption is high, but less accurate at the line wings. Lower absorption in the wings is important for remote sensing in atmospheric windows. This effect is often accounted for as continuum (see references in the Introduction), based on measurements, and most important for broad lines in the microwave region. Like for the Doppler model, "generalized" Lorentzian contours exist. Two examples are the *van Vleck – Weisskopf* line shape and the *Benedict* scaling of the wings that reduces absorption (*Goody & Yung*, 1989: p.110, Eqs.(3.52) and (3.75), respectively).

HITRANonline[42] notes that "*the line shape function for many applications is much more complex*". The new line shape functions with better simulation of molecular collision are being applied, while the Voigt model for computation of radiative parameters pertains today to a "*not-so-distant past*". Indeed, literature has used the term "beyond Voigt" (*Ngo et al.*, 2013, 2014; *Wcisło et al.*, 2021) for cases where the Voight model is not satisfactory.

Spänkuch (1989) reviewed methods compensating deviations from the Lorentzian line shape. *Boone et al.* (2007) claims that "*the Voigt profile does not provide a sufficiently accurate representation of the line shape for air-broadened H_2O vapor over a significant range of conditions commonly encountered in atmospheric remote sensing*" – although "sufficiently accurate" depends on the end user's individual application. They offer a speed-dependent Voigt profile for analysis of infrared measurements collected by the Atmospheric Chemistry

[41] https://en.wikipedia.org/wiki/Dicke_effect
[42] https://hitran.org/docs/definitions-and-units/ (see between Eqs. (9) and (10))

Experiment (ACE) mission. A FORTRAN code for their line mixing approach, used in ACE, is publicly available from the journal website (*Boone et al.*, 2011).

The need for accurate modeling of the high-resolution spectral measurements spawned general terms like non-Voigt, beyond Voigt, speed-dependent Voigt, line-mixing, and Rautian profiles (*Ngo et al.*, 2013; *Schreier & Hochstaffl*, 2021; *Tran et al.*, 2013). Relevant, but more specific terms, found in literature are "partially-correlated quadratic-speed-dependent hard-collision profile (pCqSD-HCP)" and "quadratic speed dependent Voigt profile (qSDV)" (*Tran et al.*, 2013). An open-source FORTRAN code is available for *Tran et al.*, (2013) from the journal website. A typo in theoretical evaluations in *Ngo et al.*, (2013) and *Tran et al.*, (2013) was corrected in *Tran et al.*, (2014). In order to accurately capture the influence of pressure on line shape in high-resolution spectra (of water), the IUPAC Task Group recommends replacing the Voigt profile with use the pCqSD-HCP and call it the Hartmann-Tran profile for simplicity (*Tennyson et al.*, 2014). *Domysławska et al.* (2016) presented laboratory measurements of the oxygen B-band at low pressure (to make lines narrow). They used the qSDV-profile to simulate the speed-dependence of collisional broadening and shifting of the Voigt shape. *Schreier* (2017) analyzed different numerical approaches to calculation of the speed-dependent Voigt profile and suggested his own technique.

As a result of these studies, "beyond-Voigt" line shape parameters have been introduced into HITRAN (*Wcisło et al.*, 2021) for certain molecules and lines. However, for most molecules in atmospheric applications, the Voigt line model simulated is still the baseline[43]. Determining the need to go beyond-Voigt in remote sensing of the atmosphere is a separate problem. How important is it for the UV-Vis-NIR bands? What molecules are affected? For what temperature and pressure? We consider this beyond the scope of the present study but mention all that to prepare the reader for potential changes in standard practice soon. At present, we limited ourselves with a well-tested *Humlíček* algorithm explained in the relevant open source codes, and provided reference for further reading.

4.6 A few numbers for validation of code for an isolated line

In Sec.2 we noted that finding reliable (accurate and reproducible) numerical results to test the final output, not to mention unit testing, was not easy. It is, of course, possible to use tools like

[43] https://hitran.org/docs/definitions-and-units/

HAPI. But if results do not match, the developer is left with a question: "does my software have an error, or have I misunderstood the benchmark tool?". It is therefore desirable to tabulate some numbers, like we did in Sec.4 above and earlier in Sec.3.2.2, for a clearly defined input.

For checking purposes, here we plot the oxygen isotope #1 for 3 temperatures, T = 270, 300, 330 (^oK) at fixed pressure p = 1 (atm) and, vice versa, for 3 pressures p = 0.9, 1, 1.1 (atm) at a fixed T = 300^o (K).

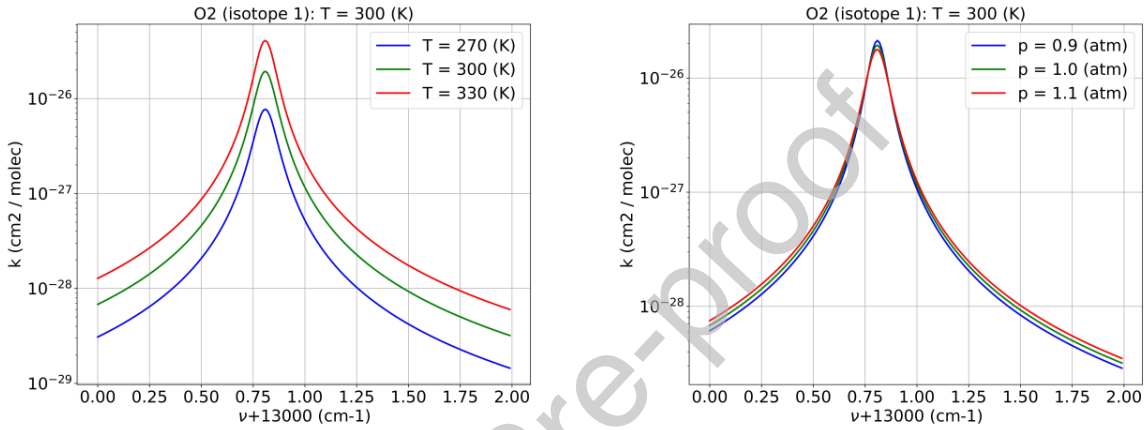

Fig.3: Dependence of the $k(\nu)$ shape on variation of T (left) and p (right) within 10% w.r.t. nominal values T = 300^o (K), p = 1 (atm). See **Table 4** for a few benchmark numbers at the peak.

Although the equations and the code described so far are simple this intermediate benchmark helps catch typos, e.g. the commonly encountered wrong order of magnitude caused by wrong units. It also leads to a better understanding of the physical background. For example, higher temperature causes higher absorption, and the dependence is strong. But for pressure, the dependence at the peak is the opposite and overall it is much weaker. **Table 4** shows some reference numbers for the absorption cross-section, k ($cm^2/molec$), and for input defined in Sec.4.1.

Table 4: The peak values for 6 curves shown in **Fig.3**. Because of the wavenumber grid step $\Delta\nu$ = 0.01 (cm^{-1}), the shown peak values are at ν = 13000.81 (cm^{-1}), which may not precisely coincide with the actual maximum value of the spectral line. Columns, left to right, indicate pressure p (atm), location of the maximum value of the line, Eq.(1), and three temperatures T (K).

p (atm)	$\nu(p)$ (cm^{-1})	T = 270 (K)	T = 300 (K)	T = 330 (K)

0.9	13000.80**9559**	-	2.125930E-26	-
1.0	13000.80**8819**	7.711446E-27	1.935411E-26	4.082727E-26
1.1	13000.80**8079**	-	1.774578E-26	-

Calculation of the optical thickness and transmittance requires scaling of the cross-section by number of particles in the gas cell. In the next chapter, we calculate absorption cross-section by multiple lines of the same gas, O_2 and separately CH_4 (all isotopes), compute spectral dependence of $\tau(\lambda)$, spectral transmittance $T(\lambda) = \exp(-\tau(\lambda))$, and compare our numerical results with a few published experiments.

5. Calculation of absorption in a gas cell

This section shows how to calculate the absorption cross-section k ($cm^2/molec$), optical thickness τ, and transmittance $T(\nu)$ for a group of spectral lines at a given temperature and pressure. Practically this scenario corresponds to simulation of absorption of light in a gas cell in laboratories and remote sensing systems. As a prerequisite, we assume the user has downloaded the HITRAN database files in the current 160-character ASCII format and compiled the package in the `gcell` mode (see Sec.3.2.1 and F**ig.1(a)**).

For the gas cell scenario, the user's input is

`molec_id` – molecule as numbered in HITRAN: 1-7 and 10 in the current version.

`T_kelvin` – gas temperature in Kelvins (*K*);

`p_atm` – gas pressure in atmospheres (*atm*);

`l_cm` – length of the gas cell in centimeters (*cm*);

`nu_usr_min` – lower boundary for the desired wavenumber spectral range (cm^{-1});

`nu_usr_max` – upper boundary for the same (cm^{-1});

`dnu` – wavenumber spectral resolution (cm^{-1}).

Using these parameters, in the next 3 parts, we begin by reading the HITRAN database, then we accumulate absorption from a group of spectral lines, and finally we test the result. Some steps

are the same for the atmospheric and the gas cell computations. We refer to these as `aspect/gcell`; otherwise, we use `gcell`. Sec.5.1 and 5.2 show commands from the `main(…)` functions located in the `main_gcell.cpp` and `main_aspect.cpp` respectively for the `gcell` and `aspect` modes.

5.1 Picking necessary lines from the HITRAN `*.par` files

After reading the input data with `read_hitran160(…)` in Sec. 4.1 above, `aspect/gcell` determines boundaries of the HITRAN spectral interval which lines contribute to the user defined interval either directly (the HITRAN line center belongs to the user interval) or via line wings – an "extended" spectral interval:

```
nu_hit_min = nu_usr_min - delta_nu;
nu_hit_max = nu_usr_max + delta_nu;
```

Following the common practice, we use $\Delta\nu = 25$ (cm^{-1}) for *`delta_nu`* (see Introduction).

Next, using these extended interval boundaries, `aspect/gcell` computes the number of the pertaining HITRAN records, `nlines`, and location of the first contributing line in the HITRAN `*.par` file `iline0` - both are output parameters of this function:

```
count_lines(molec_id, nu_hit_min, nu_hit_max, iline0, nlines);
```

Based on the value of `molec_id`, the function reads an appropriate `*.par` file sequentially from the beginning (lowest wavenumber). The number of the very first detected line that belongs to the extended spectral interval is saved in `iline0`; the total number of lines is counted and saved in `nlines`.

To comply with C's array indexing, we define `iline0` with zero offset: `iline0 = 0` corresponds to the first record in the HITRAN database that contributes to the user spectral interval (i.e., belongs to the extended interval). If `count_lines()` finds no lines contributing to the extended interval, it returns `iline0 = nlines = 0`. The `nlines` parameter yields memory allocation for parameters of all spectral lines. E.g., for H_2O in the interval $\lambda = [0.25, 2.5]$ (μm) or $\nu = [4000, 40000]$ (cm^{-1}), `nlines = 205134` (in HITRAN 2020). That many double precision floating point numbers occupy ~1.6Mb of memory. **Table 3** above shows that `aspect/gcell` store the HITRAN parameters in 7 arrays of the mentioned size and 1 integer

32-bits array. Thus, storing all necessary HITRAN parameters in memory for intermediate calculations is not a problem even for a wide band. It is the output that consumes memory most. Especially if one needs wide band, and high resolution over both wavenumber and height grids. We return to that problem later in Sec. 6.4 for `aspect` mode.

Allocation of 8 arrays to store parameters for each line and reading the HITRAN database has already been discussed in Sec.4.1 and 4.2. After that, `gcell` reads information about isotopes using the `isotops(…)` function, while `aspect` uses similar function `hisotops(…)` because of dependence of the TIPS ratio on height via temperature. Once completed, `aspect/gcell` proceed to the next step – simulation of a single line shape and accumulation of contribution from different lines.

5.2 The line-mixing effect, which we also neglect

Quoting from *Tonkov et al.* (1996: Abstract) "*It is well known that, due to line mixing effects, spectral regions with overlapping lines cannot be described by the sum of separate profiles*". Indeed, in general, the overlapping lines interfere with each other, changing the shape of the Lorentz contour (*Goody & Yung*, 1989; *Liou*, 2002). This effect is important in some lines of CO_2, CH_4, O_2 absorption in the microwave and in the A- bands, and O_3 in the IR, when the HWHM is comparable or exceeds distance between them.

Tran et al. (2006) considers the line mixing effect, combined with collision induced absorption (CIA), in the O_2A band at high pressure, 20-200 (*atm*), and temperature 200^o-300^o (*K*) for both pure O_2 and O_2-N_2 mixtures. They showed that neglecting the line mixing overestimates absorption in the wings and underestimates absorption at the peaks. Smooth spectral dependence of the effects allows treating them as "continuum" and model the difference between measurements and LBL simulation using some convenient fitting function.

Tran et al. (2006) used the resulting model and data to build a database and software suitable for the calculation of oxygen atmospheric (hence, "regular" pressure) absorption and for inclusion in RT codes. Then, they studied the influences of both line-mixing and collision-induced processes on atmospheric photon path escape factors and on cloud-top altitude retrievals such as this band is commonly used for such purposes (e.g. *Sayer et al.*, 2023). They concluded that the mentioned effects "*make significant contributions and explain a large part of the discrepancies between*

measured and calculated atmospheric absorption observed recently" (in particular, see their Fig.11 for numerical quantification of the effects). The model was later improved by *Tran & Harmtann* (2008: see Fig.1 for influence on transmission at oblique traces) and applied to O_2-CO_2 mixture by *Vangvichith* et al. (2009), also in the A-band.

Nevertheless, in this paper, we neglect the effect of line coupling for simplicity, and because HITRAN includes CIA as a separate dataset[44]. We simulate joint contribution of lines via simple summation of the absorption cross-sections.

5.3 Simulation of LBL absorption

Using a loop over `nlines` HITRAN records it is easy to account for their joint contribution to any user-defined wavenumber ν by simple accumulation, if the line-mixing effect is ignored

$$k(\nu) = \sum_{l}^{\text{nlines}} k_l(\nu, \nu_l)\, w(\nu - \nu_l)\ . \tag{17}$$

In Eq.(17), $k(\nu)$ is the total (accumulated) absorption cross-section at the user defined wavenumber ν, $k_l(\nu, \nu_l)$ is the cross-section at the user requested wavenumber ν by a line centered at ν_l, and the weight

$$w(\nu - \nu_l) = \begin{cases} 1, & \text{if } |\nu - \nu_l| \le 25\ (cm^{-1}) \\ 0, & \text{otherwise} \end{cases} \tag{18}$$

instructs to account for contribution only from those HITRAN records located no further then 25 (cm^{-1}) from the user's ν (*Schreier*, 1992: p.760; *Lyapustin*, 2003: p. p.870). This is standard practice when line parameters are derived and used to separate line and continuum absorption (*Clough* et al. 1981; *Burch*, 1982; *Mlawer* et al., 2023). The function `ix1ix2(…)` in `aspect/gcell` implements Eq.(18) with the following interface

```
code = ix1ix2(nuij, delta_nu, nu, nnu, inu1, inu2);
```

Namely, it returns indices `inu1` and `inu2` of elements of an array **`nu`**`[nnu]` falling within *`delta_nu`* from `nuij` and `code = 1` in case of success. If `code = -1` is returned, it means that all user-defined wavenumbers lie too far from the selected HITRAN record ν_l to receive any

[44] https://hitran.org/cia/

significant contribution. The corresponding pseudocode is (see also Sec. 4.4 between Eqs.(15) - (16))

```
for (inu = 0; inu < nnu; inu++)
     kabs[inu] = 0.0
for (iline = 0; iline < nlines; iline++) {
     if (ix1ix2(nuij, delta_nu, nu, nnu, inu1, inu2) > 0) {
          Calculate nuij_pshift
          Calculate Doppler and Lorentz HWHM
          Calculate e11, e12, e21, e22
          Calculate line intensity Sij
          for (inu = inu1; inu < inu2+1; inu++) {
               Calculate Voigt spectrum
               Accumulate absorption power:
               kabs[inu] += (line intensity) * (Voigt)
          } // for inu - all wavenumbers affected by iline
     } // if iline contributes to nu[]
} // for iline - all HITRAN lines within extended interval
```

This sequence of loops – over HITRAN lines first, over user's wavenumbers next – allows to calculate the HITRAN parameters only once and reuse these for all ν-s affected by the line wings. However, this option forces the user to keep the array **kabs**[nnu] in memory. This may cause memory issues if one needs a high spectral and altitude resolutions because the corresponding array has two dimension **kabs**[nnu*nkm] (recall, the codes unravel all arrays to 1D for efficient memory allocation). We briefly discuss this problem with regard to aspect further in Sec. 6.4.

The monochromatic cross-section, $k(\nu, T, p)$ ($cm^2/molec$), is defined per unit column number density of molecules of the absorbing gas, n ($molec/cm^2$), at a given temperature and pressure. The dimensionless absorption optical thickness is

$$\tau(\nu, T, p) = nk(\nu, T, p). \qquad (19)$$

Using the notation V, S, and l respectively for the volume, square and length of the column, N for the total number of molecules in it, k_B for the Boltzmann constant, and an assumption of an ideal gas, one writes

$$p = N k_B T/V = n k_B T/l. \qquad (20)$$

If the thermodynamic conditions do not change along the path, like in gas cell, the absorption optical thickness is

$$\tau(\nu, T, p) = \frac{p\,l}{k_B T} k(\nu, T, p) \tag{21}$$

```
// Note: a) n_column = l_cm * n_volume and b) units conversion
n_column = l_cm*atm_to_cm_g_s*p_atm/(k_boltzman*T_kelvin);
tau[inu] = k_abs[inu]*n_column;
```

The absorption coefficient a (cm^{-1}) is

$$a(\nu, T, p) = \tau(\nu, T, p) / l = \frac{p}{k_B T} k(\nu, T, p)\,. \tag{22}$$

If the thermodynamic conditions vary, e.g., with height h, the absorption optical thickness between two given heights would be (see Sec. 6.2 for relevant code)

$$\tau(\nu) = \int_{h_1}^{h_2} a(\nu, h)\,dh = \frac{1}{k_B} \int_{h_1}^{h_2} \frac{p(h)\,k(\nu, h)}{T(h)}\,dh\,. \tag{23}$$

In Eq.(23), the absorption cross-section depends on h via T and p. The monochromatic transmittance along the path, inclined at zenith angle $\theta = arccos(\mu)$ w.r.t normal, is

$$T(\nu, \mu) = \exp\left(-\tau(\nu)/\mu\right). \tag{24}$$

Finally, the spectrally integrated transmittance of the solar light $S(\nu)$ through a gas cell to a system with spectral response function (filter) $f(\nu)$ is

$$T(\mu) = \frac{\int_{\Delta\nu} T(\nu, \mu)\,S(\nu)\,f(\nu)\,d\nu}{\int_{\Delta\nu} S(\nu)\,f(\nu)\,d\nu}\,. \tag{25}$$

Using Eqs.(24) and (25), it is possible to derive a spectrally integrated (efficient) absorption optical thickness

$$\tau(\Delta\nu) = -\mu \log(T(\mu))\,. \tag{26}$$

Note that neither `gcell` nor `aspect` provide transmittance – the user is supposed to calculate it externally because Eq.(24) is trivial. Also integration in Eq.(25) often requires interpolation

from the HITRAN grid of wavenumbers to that of the Sun or spectral response functions, often defined as functions of wavelength. In the last part of this section, we report a few benchmark results for checking purpose.

5.4 Gas cell validation

Spectral calculations often involve hundreds and thousands of numbers which are rarely published making numerical comparisons difficult. In most cases, precise benchmark is possible if one uses software developed by others (proper understanding of that software – not only input - is therefore essential in this case) or ask the developer to generate numbers (which is not always convenient). Contrary to numerical results, graphical plots for absorption cross-section k (usually in $cm^2/molec$), absorption coefficient a (cm^{-1} or km^{-1}, depending on application), absorption optical thickness τ, or corresponding direct transmittance T (both dimensionless) have been published widely - see, e.g., *Hearn* (1961: Fig.1) for ozone. This simple visual test allows one to check magnitude (hence units conversion) and overall shape of the spectral dependence of transmittance, optical thickness, or cross-section. Thus, the key requirement for the published image is legibility.

Prischepa et al. (2023: Fig. 1) shows spectral dependences of absorption coefficients of pure N_2, O_2, H_2O within 500 - 12000 (cm^{-1}) at normal temperature and pressure. *Karlovets* et al. (2023: Fig.2) shows absorption coefficient for nitrous oxide, N_2O, measured at pressure 10 (*Torr*), or ~0.013 (*atm*), between 7250 and 7653 (cm^{-1}) and details showing separate lines near 7577 (cm^{-1}) at 2 different scales. Fig.3.21 in *Efremenko & Kokhanovsky* (2021) shows absorption cross-section of water vapor in a relatively wide 900-1000 (*nm*) and narrow 934-926 (*nm*) bands. Figs. 3.22 and 3.23 in the same show, respectively, absorption cross-section for oxygen A, B, and C-bands with 610-780 (*nm*), and O_2A band separately. *He* et al. (2019: Figs.1 & 6a) plot HITRAN-2016 line intensities for O_2 in 600-1300 (*nm*) – a simple but useful intermediate result for visual unit testing of, e.g., a HITRAN database reader. *Stamnes* et al. (2017: Fig.4.13) shows absorption coefficient spectrum for the 1510 – 1520 (cm^{-1}) part of the 6.3 (μm) water vapor band at 10 (*mbar*) and 240 (*K*), and at 1 (*bar*) and 296 (*K*) using HITRAN 1982 (!). Transmittance through 1 (*m*) of air at a pressure 150 (*hPa*) and a temperature of 215^o (*K*) near 15 ($m\mu$), where CO_2 is the dominant absorber, is shown in *Coakley & Yang* (2014: Fig. 5.4). *Rothman* (2013: Fig.7) plots absorption cross-section for CH_4 at T = 296^o (*K*) with 0.05 (cm^{-1}) resolution. *Bohren & Clothiaux*

(2006) show absorption cross-section of a water molecule for a temperature of 20^o (*C*) and a total pressure of 1 (*atm*) within 12-16 (μm) or 625 - 825 (cm^{-1}) (Fig.2.9); absorption cross-section for most strongly absorbing atmospheric gases in a wide range 0.1 (μm) - 0.1 (*m*) at 1013 (*mb*) and 294^o (*K*) (Fig.2.13); water vapor absorption at 1013 (*mbar*) and 10 (*mbar*) within 1084.7 - 1085.7 (cm^{-1}) with and without continuum absorption (Fig.2.19) and combination of the two (Fig.2.20). *Rothman* (2005: Fig.2) simulates CO_2 laboratory spectra in the 2-μm region at p = 30 (*torr*) and 25 (*m*) path. *Liou* (2002: Fig.4.5) shows absorption coefficient k $(atm \cdot cm)^{-1}$ within 600 : 0.01 : 700 (cm^{-1}) at p = 600 (*mbar*) and $T = 260^o$ (*K*). *Greenblatt* et al. (1990) plot results of measurement of O_2 absorption for 330-1140 (*nm*) (Fig.1) and 675-800 (*nm*) (Fig.2) at a high pressure of 55 (*atm*), 196^o (*K*), and a path length of 89.5 (*cm*). This list, by no means exhaustive, is intended to show that a wide range of reproducible "visual" tests have been published in the literature.

In this paper, we test `gcell` in two scenarios, one for the oxygen A-band and another one for methane, described in separate sections below. We use two strategies to test our code. For the A-band we reproduce published images and test `gcell` "visually". For methane, we numerically compare our result vs. independently calculated ones. Unlike broadly published pictures of spectra and contrary to numerical benchmarks for multiple scattering of radiation, numerical benchmarks for spectroscopy are rarely available from literature. A code developer has to either set up and run another code, like HAPI, or extract data from a huge database. Neither is convenient for quick testing. To help overcome this issue, we provide our numerical results for both tests in ASCII files together with our source code and report a few more numbers in the subsequent sections.

5.4.1 Oxygen A-band at 0.764 (μm)

The oxygen A-band, commonly shortened as O_2A, is located around $\lambda \approx 0.764$ (μm): $\Delta\lambda \approx 0.760 \ldots 0.768$ (μm), $\Delta\nu \approx 13000 \ldots 13160$ (cm^{-1}). We use an O_2A scenario described in *Predoi-Cross* et al., (2008); we will refer to their paper as *P-C* within this section. The spectral transmittance, Eq.(24), was recorded in a multiple path cell of the total pathlength l = 1633.6 (*cm*), at pressure of 0.724 (*bar*) ≈ 0.7145 (*atm*), at the room temperature, with spectral resolution 0.0222 (cm^{-1}) (*P-C: Sec.2*). The measurement error of the line intensity is claimed not to exceed ~1% (*P-C: Abstratct*). The room temperature varied from $\approx 294^o$ (*K*) to $\approx 298^o$ (*K*) (*P-C: Table 1*).

In our test, we do not intend to simulate the experiment with high precision. So, we use $T = 296^{o}$ (K) for calculation. For the given temperature, pressure and path length, Eq.(20) gives $n \approx 2.8921135 \cdot 10^{22}$ ($molec/cm^2$).

Fig.4 (*a*) shows the simulated transmittance vs. wavenumber $\nu = [13006, 13166]$ (cm^{-1}) and the optical thickness vs. corresponding wavelength. **Fig.4 (*b*)** reproduces the same but within a sub-band, $\nu = [13159.6, 13165.6]$ (cm^{-1}). These spectral intervals are borrowed from Fig.1 in (*P-C*). Images like that published in (*P-C*) and here help debug the program qualitatively by visually inspecting the picture for presence of lines and quantitatively by checking their order of magnitude.

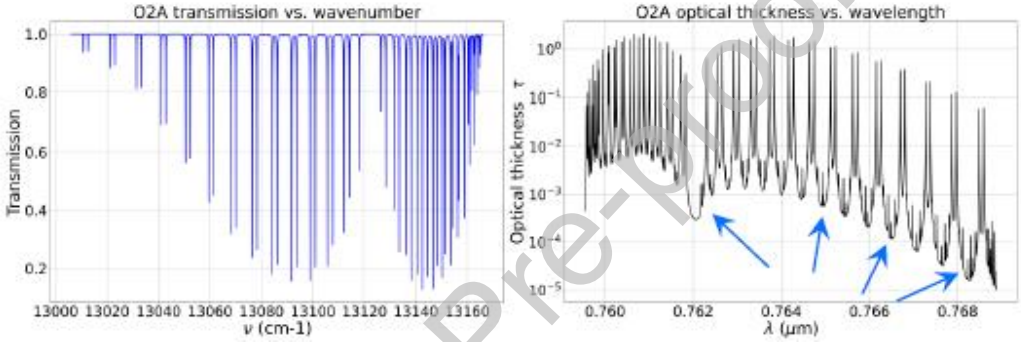

Fig.4 (*a*): Direct one way transmission (left) and corresponding optical thickness (right, log scale for *y*-axis) for the O_2A band. The left image reproduces Fig.1(A) from *Predoi-Cross et al.*, (2008: p. 91). Visual comparison of the two serves as qualitative validation of code `gcell`. The arrows in the right image indicate some weak absorption lines caused by isotopes with low abundance.

Our experience shows that once possible problems at these two steps are resolved, the code should work without major problems.

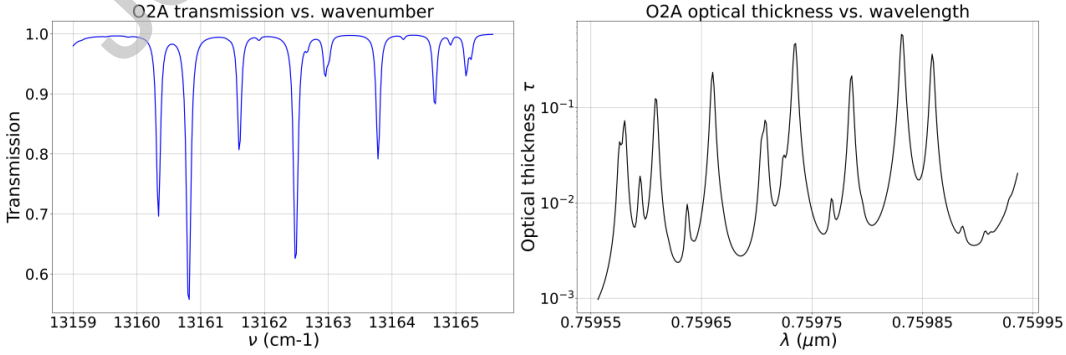

Fig.4 (*b*): Same as **Fig.4(*a*)**, except for narrow band. The left image reproduces Fig.1(B) from *Predoi-Cross et al.*, (2008).

An ASCII file `./benchmarks/Sec5p4p1___test_gcell_o2a.txt` contains results of our numerical simulation. The file contains 8000 rows, excluding three header ones, and two columns. The left column is the wavenumber ν (cm^{-1}) from 13006.00 to 13165.98 step 0.02. The right one contains τ (right images in **Fig.4 (*a*-*b*)**). Plotting $\exp(-\tau)$, Eq.(24), shows left images. .

5.4.2 Methane band at 2.3 (μm)

Our second benchmark scenario is for `imolec = 6`: methane, CH_4, which is a greenhouse gas. The gas is at the same room temperature, $T = 296^o$ (K), and slightly different pressure $p = 1000.0$ ($mbar$) ≈ 0.986923 (atm) compared to the previous scenario. Unlike for the published oxygen scenario, we compare our numerical simulation vs. the one kindly provided by the GATS[45] Inc. team. The GATS data contains the CH_4 spectral transmittance of an $l = 8$ (cm) gas cell, computed using the SpectralCalc[46] tool (*Gordley* et al., 1994), convolved with a spectral filter for their Digital-Array Gas-correlation Radiometer - DAGR[47]. The particles columnar number density, Eq.(20), for this case is $n \approx 1.9575594 \cdot 10^{20}$ ($molec/cm^2$).

The GATS data is based on HITRAN 2016 and defined within the inclusive interval ν = 4081.901…4505.699 (cm^{-1}), step $d\nu = 0.002$ (cm^{-1}). Considering their data as a benchmark, we calculated spectra of optical thickness (**Fig.5 (*a*)**), and corresponding direct one way transmittance (**Fig.5 (*b*)**), Eq.(24) with $\mu = 1$, and convolved the two. **Fig.5 (*c*)** shows the instrument filter (dash line), benchmark convolution (black curve), and absolute difference between our and the benchmark data (red line – almost at 0). The absolute difference, which is ~1000 times smaller compared to the convolution, is pictured separately in **Fig.5 (*d*)**.

[45] https://www.gats-inc.com/
[46] https://www.spectralcalc.com/ (note recent updates: "What's New at SpectralCalc!")
[47] https://www.gats-inc.com/future_missions.html#DAGR

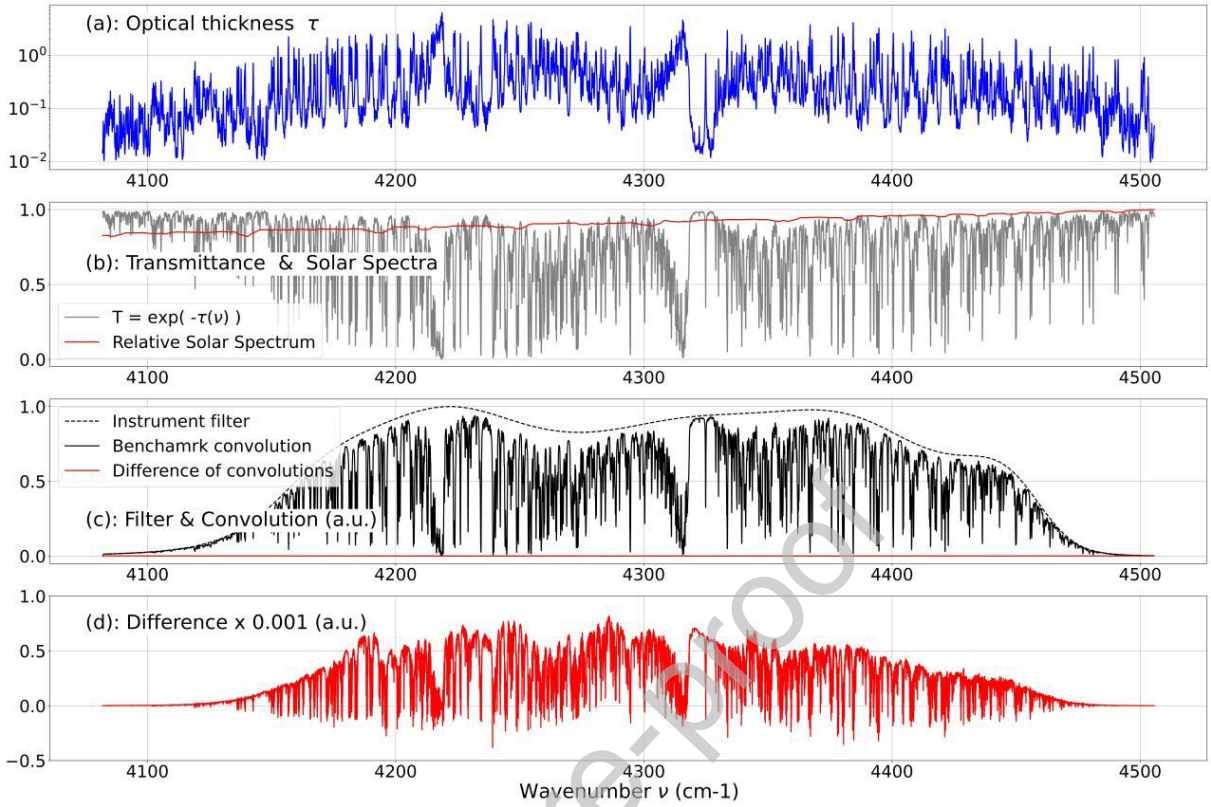

Fig.5: Graphical results for a methane gas cell test (see *y*-axis caption for letters (a-d)). (a) Optical thickness τ calculated using `gcell`; (b) Direct one-way transmittance, exp(-τ), and solar irradiance relative to maximum within the band; (c) Instrument filter function (dash line), convolved with transmittance (solid line – benchmark result), and absolute difference between the benchmark result and that computed with `gcell` (red line – almost at 0). (d) The same difference pictured separately – note the scaling factor 0.001 on *y*-axis, i.e. the difference does not exceed 0.0008 (*a.u.*)

Next, we calculated an absolute signal transmitted through the methane gas cell. For that, we used the *Chance-Kurucz* extraterrestrial solar irradiance spectrum defined from 50 (cm^{-1}) to 50000 (cm^{-1}) with 1 (cm^{-1}) resolution (*Kurucz*, 1992 & 1997; *Chance & Kurucz*, 2010). **Fig.5(*b*)** (second from top - red line) shows part of the solar spectrum relative to maximum value within the band and interpolated from 1 (cm^{-1}) grid to 0.002 (cm^{-1}) using Python's cubic spline. We then calculated the transmitted signal

$$u = \int_{\Delta\nu} S_0(\nu)\,\exp(-\tau(\nu))\; f(\nu)d\nu \qquad (27)$$

to obtain 187.03 (W/m^2) using benchmark convolution and 187.14 (W/m^2) using `gcell`. Switching between trapezoidal and Simpson integration in Eq.(27) did not change the numbers. For the spectrally integrated transmittances, Eq.(25), the values are 0.7007 (benchmark) and

0.7011 (`gcell`) or +0.0004 vs. the benchmark in absolute units (*a. u.*) of transmittance. Corresponding effective (spectrally integrated) absorption optical thicknesses, Eq.(26), are 0.3557 and 0.3552 (or –0.2% vs. the benchmark), respectively.

We compiled an ASCII file, `./benchmarks/Sec5p4p2___test_gcell_ch4.txt`, for accurate reproducibility of this numerical exercise. The file contains 211900 rows, excluding header. Columns, left to right, contain wavenumber (floating point format with 3 digits after decimal point), optical thickness calculated using our code `gcell` (scientific format, 7 digits total), direct transmittance for the same (floating point format, 6 digits), filter function, convolution of the `gcell` transmittance with the filter, benchmark convolution (all the three are in scientific format with 6 digits total and provided by the GATS team), and difference of the last two (scientific format, 2 digits). The header shows the total number of points and names of the columns.

6. Absorption in Earth's atmosphere

In the previous section we explained in detail how to calculate absorption by gas in a cell, where temperature, pressure, and the gas concentration are constant. In atmospheres, however, all these parameters vary with height. Their profiles come from another established package, MODTRAN, the elements of which we consider in the next section. After that, we integrate the MODTRAN profiles over height to get column amount of each considered molecule in atmosphere, discuss units expressing that amount, and calculate τ profile – one topic per section.

6.1 Elements of MODTRAN

MODTRAN is a comprehensive RT code, in Fortran, for calculation of atmospheric radiances and transmittance across the solar and thermal spectral region: from 100 to 50,000 (cm^{-1}) or 0.2 to 100 (μm). Multiple scattering is simulated using scalar RT code DISORT (*Stamnes* et al., 1988; *Laszlo* et al., 2016). MODTRAN v.6.0 (*Berk* et al., 2014, 2017, 2019) is the current release. It is not publicly available except for the online tool MODTRAN Demo[48]. However, the atmospheric profiles for `aspect` are published in a manual for MODTRAN v.2 / LOWTRAN v.7 (*Kneizys* et al., 1996), the latter being a precursor for MODTRAN.

[48] http://modtran.spectral.com/modtran_home

The MODTRAN/LOWTRAN package defines 6 atmospheres. They are “Tropical (15N Annual Average)”, “Mid-Latitude Summer (45N July)”, “Mid-Latitude Winter (45N Jan)”, “Sub-Arctic Summer (60N July)”, “Sub-Arctic Winter (60N Jan)”, and “U. S. Standard (1976)”. `Aspect` calls them by an index `iatm = 1 … 6`. The grid of heights, same for all profiles, consists of three parts (see **Fig.6 (*a*)**): lower - below 25 (*km*), middle – between 25 and 50 (*km*), and upper 50-120 (*km*). The corresponding steps are 1, 2.5, and 5 (*km*). For reference, about 50%, 70% and 95% of Rayleigh atmosphere are located below 5, 10, and 25 (*km*), respectively.

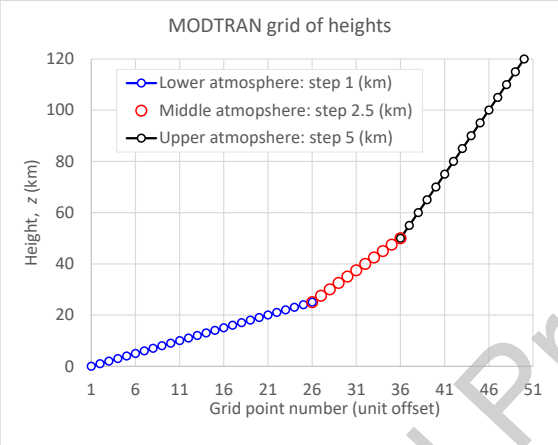

Fig.6(*a*): MODTRAN defines 3 intervals in the grid of heights: 1) lower atmosphere, 0-25 (*km*), step 1 (*km*) - 26 points; 2) middle atmosphere, 25-50 (*km*), 2.5 (*km*) step – 11 points; 3) upper atmosphere, 50-120 (*km*), step 5 (*km*) – 15 points. Boundary points #26 and #36 belong to both adjacent intervals.

For each of 6 atmospheres, MODTRAN/LOWTRAN provides LUTs with pressure *p* (*mbar*), temperature *T* (*K*), and molecular number density per unit volume (air density) *D* (cm^{-3}) – **Fig.6(*b*)**. The temperature profile shows the stronger variations, while the other two change little between 6 atmospheres. Lastly, for each of the 8 main atmospheric gases, the mixing ratio in parts-per-million in a volume (*ppmv*) is defined. **Fig.6(*c-f*)** illustrates the absolute number concentration in cm^{-3} for each molecule calculated as the product of the atmospheric air density and the volume mixing ratio (scaled by 10^{-6} to account for “per million”). In each figure, left charts show the full range of the MODTRAN heights, 0-120 (*km*); right columns show lower atmosphere 0-25 (*km*) with 1 (*km*) step. For another reference, we note that NASA’s ER-2 airplane carry airborne prototypes of satellite instruments at ~20 (*km*) altitude (*Diner* et al., 2013: Sec.2.6; *Puthukkudy* et al., 2020: Sec.3.1).

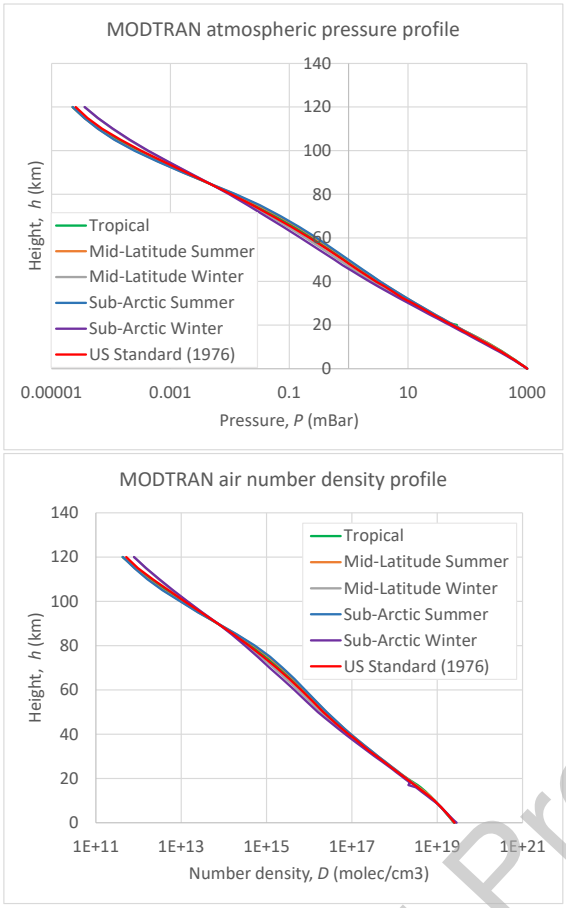

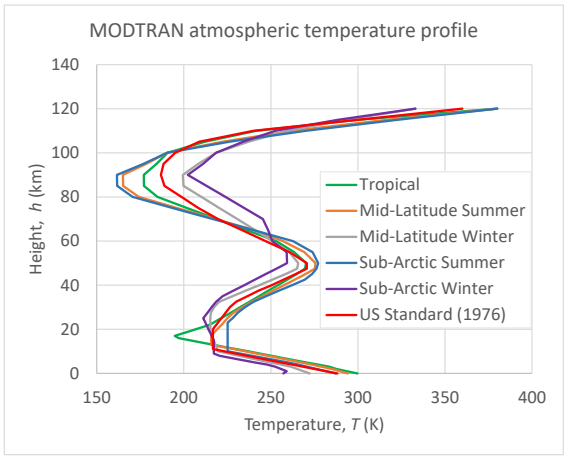

Fig.6(*b*): MODTRAN pressure *p* (top-left: log-scale on *x*-axis), temperature *T* (top-right: linear scale on *x* -axis) and number density *D* (bottom left: log scale on *x*-axis) profiles for 6 atmospheres. Note minor peculiarity in the Subarctic Winter *D*-profile (bottom-left, slightly below 20 (*km*)).

`Aspect` defines all the mentioned parameters in `hprofiles.h`. This simplifies updating the existing parameters or adding a new one, if needed.

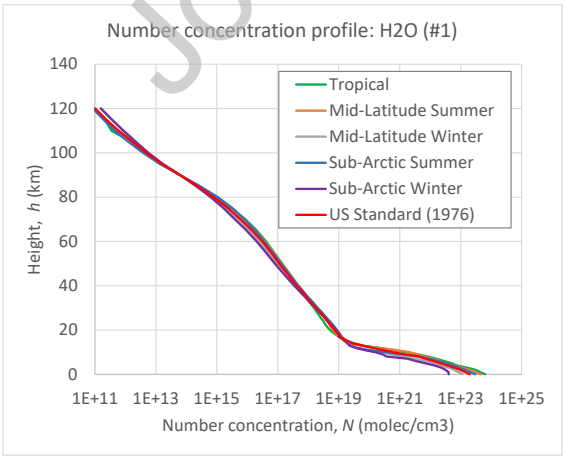

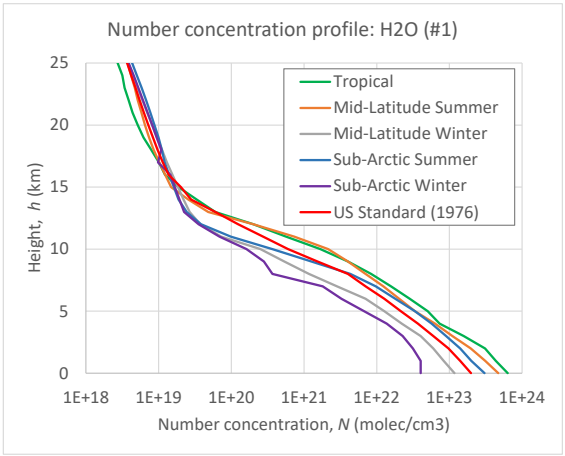

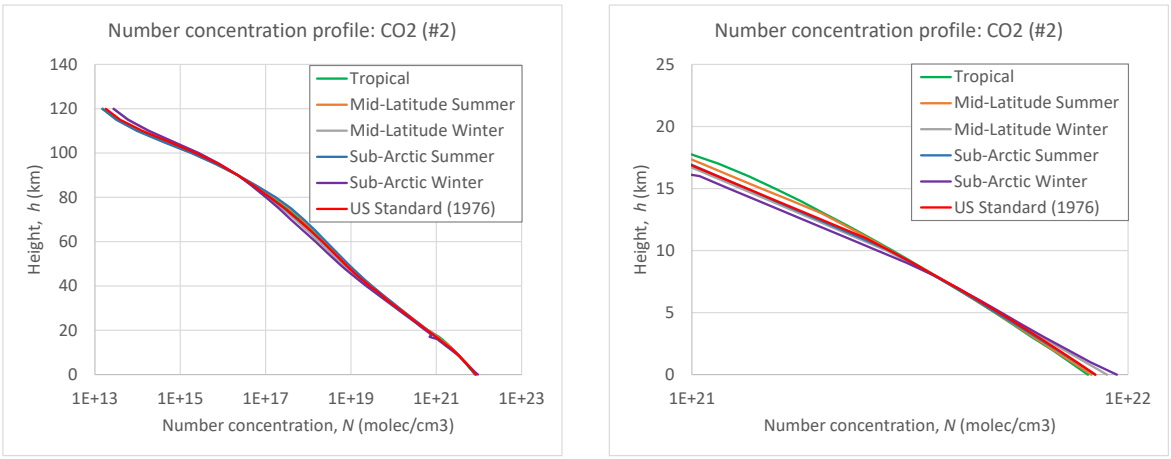

Fig.6(*c*): Number concentration profiles for H_2O (#1) and CO_2 (#2). The profiles are calculated based on the MODTRAN models for 6 atmospheric profiles. Left column: full range of the MODTRAN heights. Right column: lower atmosphere 0-25 (*km*) with 1 (*km*) step.

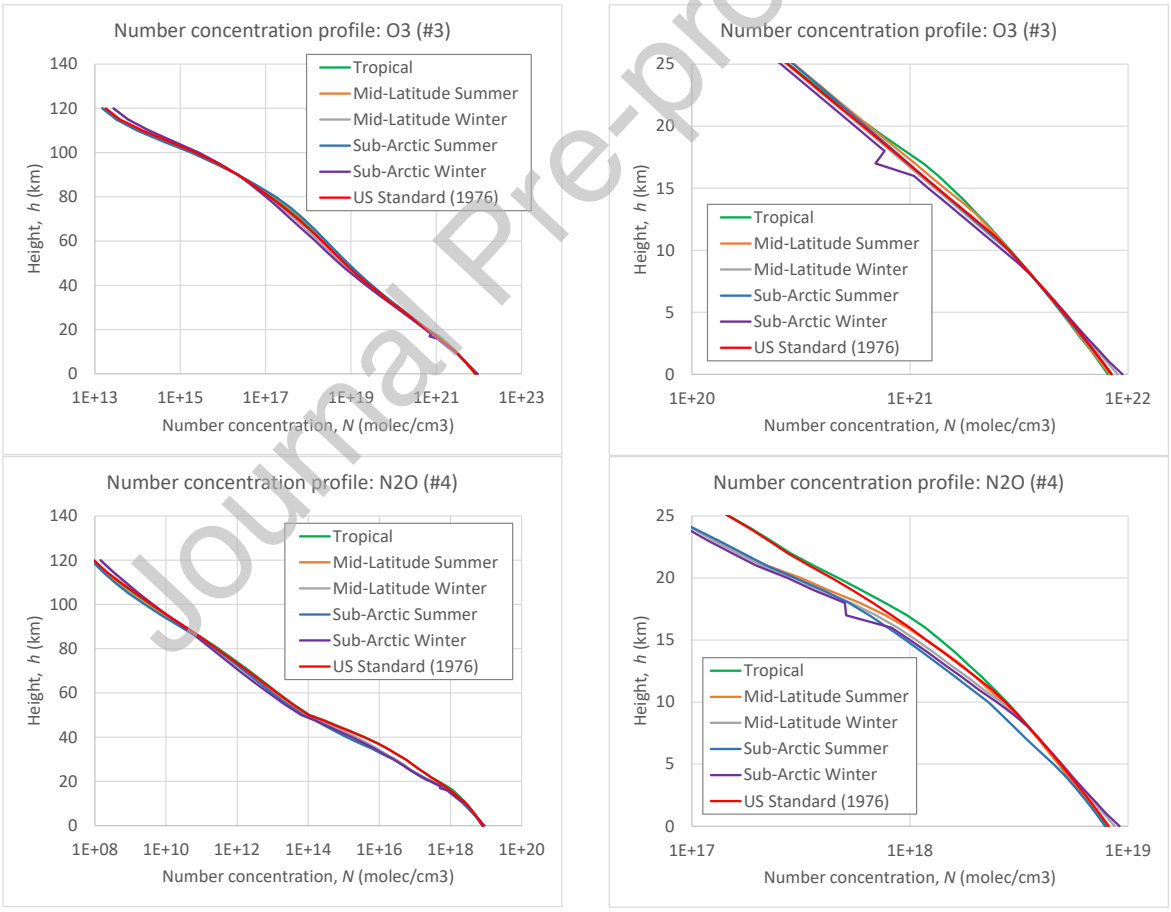

Fig.6(*d*): Same as **Fig.6(*c*)**, except for O_3 (#3) and N_2O (#4).

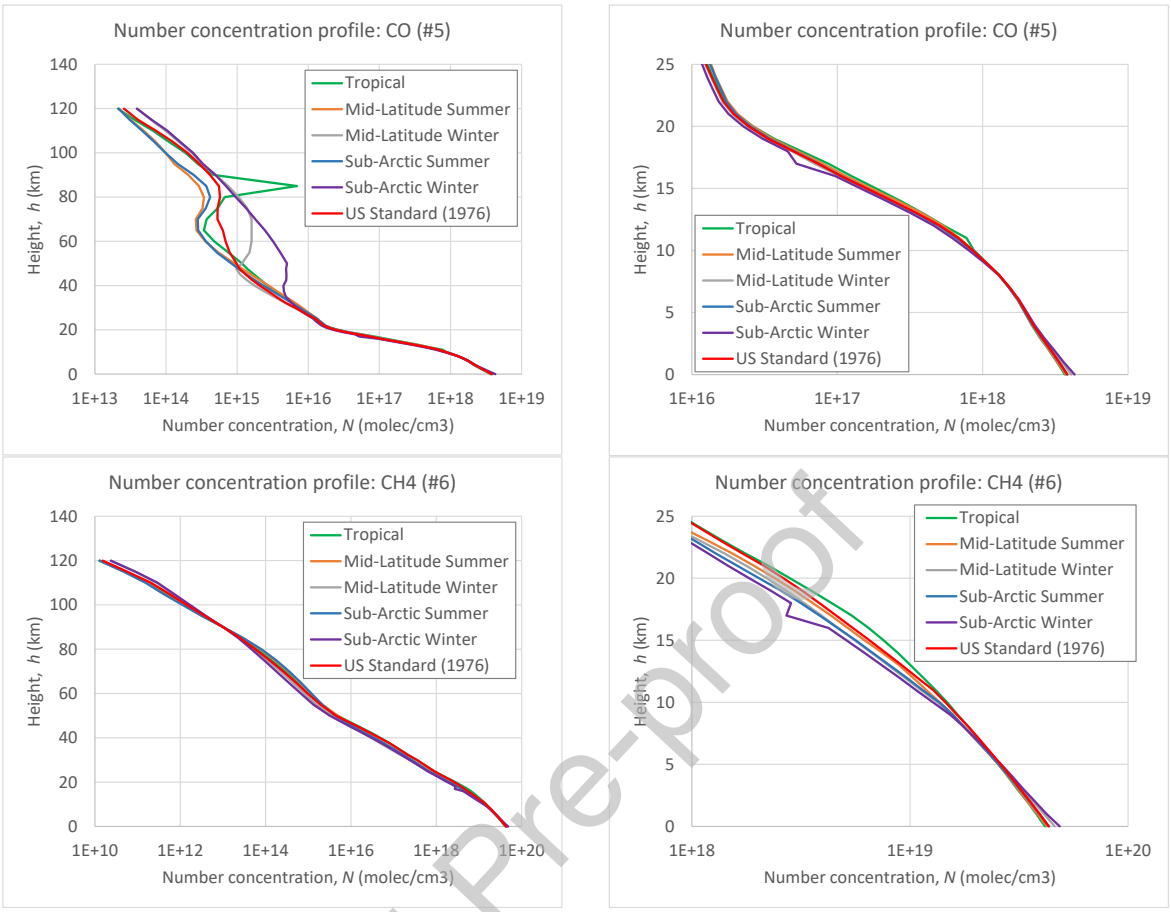

Fig.6(*e*): Same as **Fig.6(*c*)**, except for CO (#5) and CH_4 (#6).

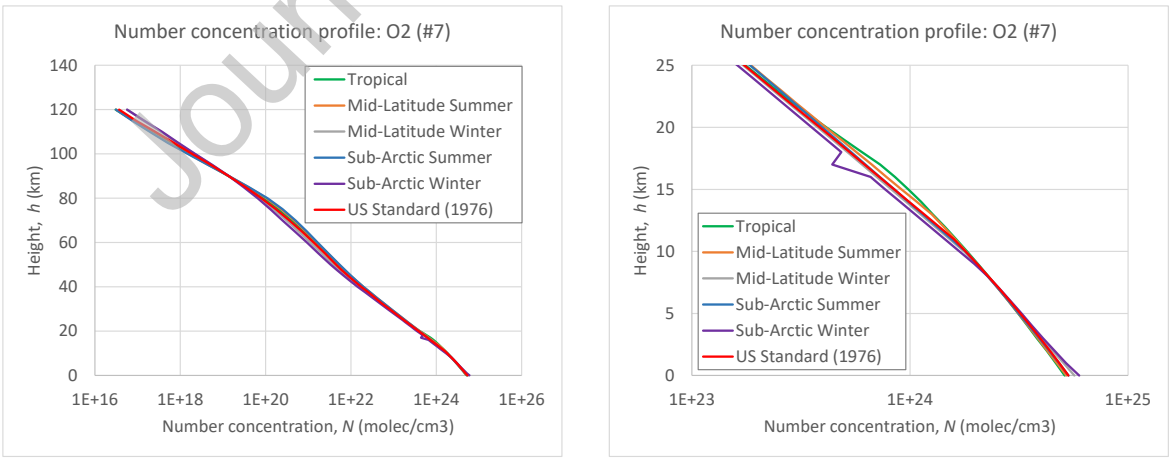

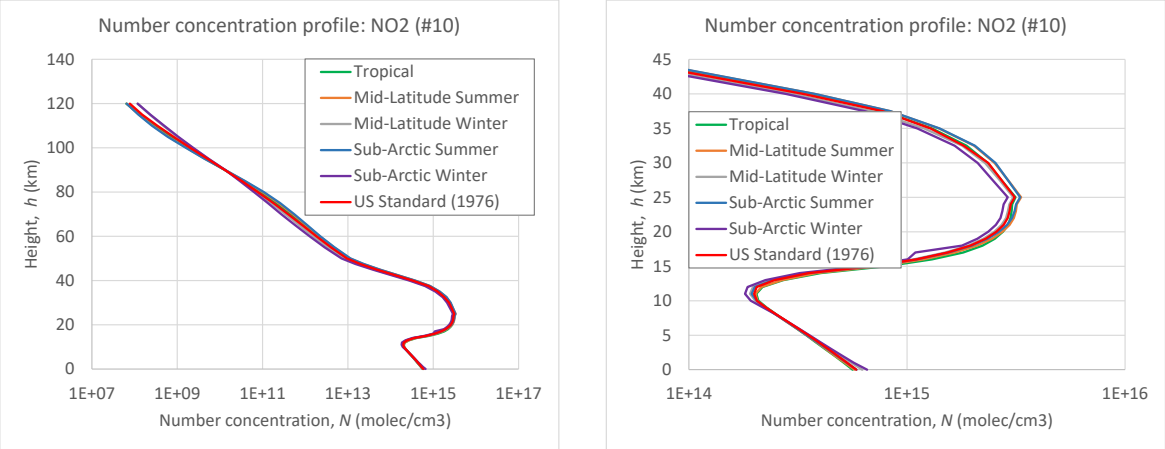

Fig.6(*f*): Same as **Fig.6(*c*)**, except for O_2 (#7) and NO_2 (#10). Note 0 – 45 (*km*) in the right chart.

6.2 Column amount of gas in atmosphere

Integration of the number concentration from BOA, $z = 0$ (*km*), to TOA, $z = 120$ (*km*), gives the columnar number density N_C (*molec*/*cm*^{2})

$$N_C = \int_{0km}^{120km} D(z)dz\,. \qquad (28)$$

Eq.(28) uses, as an example, the MODTRANS's density of air $D(z)$ (*molec*/*cm*^{3}) and integrates over z (*km*) . To account for different units of length, a conversion scaling factor 10^5 (*cm*/*km*) pops up in subsequent calculations. Numerical integration as in Eq.(28) involves a certain error, which we quantify below.

Absolute value of the optical thickness is directly proportional to the result of the integration. Hence, relative error of the numerical integration is transported to the value of τ as 1:1. We quantify the error by comparing 3 methods of numerical integration: trapezoidal, Simpson, on the native MODTRAN grid of heights, and Simpson on a fine grid using cubic spline interpolation from the native grid to a finer one. We did the test in Python, hence it is not part of our C-package, and picked one method to be coded in C-language.

Table 5 shows the result of the integration for all 6 atmospheric profiles and different methods of integration. In each number, one space separates digits that are not in agreement with others in the column. For the trapezoidal and Simpson integration we use Python's `numpy.trapz` and `scipy.integrate.simpson`, respectively. To get the numbers in the "spline" row, we first

interpolated the MODTRAN profiles from the default grid (**Fig.6(*a*)**) to an equidistant fine grid with step *dz* = 0.5 (*km*) using Pythons's cubic spline. Then we integrated the interpolated profiles on the fine grid using Simpson's technique. The last line, `aspect`, shows respective results of our implementation of the Simpson quadrature in C, which we picked based on the accuracy (better than trapezoidal) vs. coding burden (no dependence on splines). Numerical results from **Table 5** are suitable for intermediate validation of one's code (unit testing).

Table 5: Total atmosphere columnar number density $N_C \cdot 10^{25}$ (*molec*/*cm*^{2}), Eq.(28), for 6 model atmospheres, and different techniques of integration. ML and SA correspond to Midlatitude and Subarctic, respectively. The common scaling factor 10^{25} is dropped. Space separates digits that are not in agreement with others for the same atmosphere (same column).

Technique	Tropical	ML Summer	ML Winter	SA Summer	SA Winter	US 1976
Trapezoid	2.16 71	2.1 620	2.1 685	2.1 503	2.1 503	2.15 71
Simpson	2.164 6	2.159 3	2.165 5	2.147 7	2.146 6	2.154 5
Spline	2.164 5	2.159 3	2.165 3	2.147 6	2.146 1	2.154 4
`aspect`	2.164 2	2.159 5	2.165 1	2.147 4	**2.14 40**	2.154 6

Except for the Subarctic Winter model (see bold number in **Table 5**), `aspect` agrees with Python's spline and Simpson methods within 4 digits. In `aspect`, we use our self-coded Simpson's rule for the numerical integration over height. Simpson's rule approximates the function with a second-degree polynomial; hence the number of points must be odd. MODTRAN uses 26 points in the lower atmosphere (**Fig.6(*a*)**). So, we use Simpson's rule for the first 25 points - up to 24 (*km*)

```
hint0_24km = simpson(conc_all, 25, 1.0);
```

Then we draw and integrate a separate parabola for the 24-25 (*km*) region using 23 (*km*) as a third point (could be replaced just by trapezoidal integration)

```
hint24_25km = intparab(24.0, 25.0, zkm_mod[23], zkm_mod[24],
zkm_mod[25], conc_all[23], conc_all[24], conc_all[25]);
```

Afterwards, we use Simpson's rule again for the middle (11 points, 2.5 km step)

```
hint25_50km = simpson(&conc_all[25], 11, 2.5)
```

and upper (15 points, 5.0 km step)

```
hint50_120km = simpson(&conc_all[35], 15, 5.0)
```

parts of the atmosphere (note odd number of points for both). Adding all these gives one the column number concentration `nmolec_all` (*molec*/*cm*^{2}) in the whole atmosphere

```
nmolec_all = (hint0_24km + hint24_25km + hint25_50km +
hint50_120km)*km_to_cm;
```

where the scaling factor *`km_to_cm = 1.0e5`* relates kilometers in the grid of height and centimeters in the volume number density, and `_all` refers to all molecules in the air mixture.

Identically, by integrating a particular gas number concentration over height from BOA to TOA, one gets the total columnar number concentration for that gas only. E.g., for methane (#6: CH_4) we first calculate the gas mixing ratio from the *ppmv*-value

```
case 6:
    for (iz = 0; iz < nz_mod; iz++)
        gas_ratio[iz] = CH4_ppmv[iatm-1][iz]/1.0e6;
    break
```

and the height distribution of the volume number concentration **`conc_cm3[]`**

```
for (iz = 0; iz < nz_mod; iz++)
    …
    conc_cm3[iz] = Dcm3_mod[iatm-1][iz]*gas_ratio[iz];
    …
```

The abovementioned numerical integration of the methane number concentration over height gives `nmolec = 3.5523e+19` (*molec*/*cm*^{2}) or `ppm_ch4 = 1.6487`, in terms of *ppmv*

$$ppmv_{molec} = 10^6 \, n_{molec} / n_{all} \qquad (29)$$

```
column_amount_mod = nmolec*1.0e6/nmolec_all;
```

for the US 1976 standard atmosphere. This is the "standard" MODTRAN value, which is used in calculations by default if the user provides negative gas concentration as input parameter (see Sec.3.2.2). For validation purposes, **Table 6** indicates the "standard" columnar amount of the considered gases, for all atmospheres, in absolute units and in *ppmv* – i.e., relative to the values from the bottom row `aspect` in **Table 5**.

Table 6: Absolute (top: in number of molecules) and relative (bottom: in *ppmv* w.r.t. **Table 5**: row = `apsect`) columnar amount of atmospheric gases, calculated by `aspect`.

#	Molec	Tropical	Mid Lat Sum	Mid Lat Win	Sub Arc Sum	Sub Arc Win	US 1976
1	H_2O	1.3769E+23	9.8002E+22	2.8614E+22	6.9511E+22	1.4215E+22	4.7460E+22
		6362.24	4538.21	1321.60	3237.07	663.00	2202.72
2	CO_2	7.1420E+21	7.1263E+21	7.1449E+21	7.0863E+21	7.0752E+21	7.1102E+21
		330.00	330.00	330.00	330.00	330.00	330.00
3	O_3	7.6343E+18	8.9471E+18	1.0191E+19	9.3798E+18	9.9720E+18	9.2607E+18
		0.352747	0.414317	0.470691	0.436808	0.465114	0.429811
4	N_2O	6.6300E+18	6.3862E+18	6.4632E+18	5.8955E+18	6.4306E+18	6.6159E+18
		0.306346	0.295727	0.298517	0.274547	0.299937	0.307058
5	CO	2.3730E+18	2.3608E+18	2.4218E+18	2.3688E+18	2.4433E+18	2.3879E+18
		0.109647	0.109322	0.111855	0.110314	0.113961	0.110828
6	CH_4	3.5626E+19	3.4132E+19	3.4454E+19	3.3785E+19	3.4109E+19	3.5523E+19
		1.646144	1.580553	1.591323	1.573330	1.590893	1.648702
7	O_2	4.5232E+24	4.5133E+24	4.5251E+24	4.4880E+24	4.4810E+24	4.5031E+24
		209000	209000	209000	209000	209000	209000
10	NO_2	5.7520E+15	5.9628E+15	5.4231E+15	5.8875E+15	5.0470E+15	5.5625E+15
		0.000266	0.000276	0.000250	0.000274	0.000235	0.000258

To account for a different column amount of the gas, `column_amount_usr` (Sec.3.2.2) the user scales the vertical distribution of the number concentration and partial pressure, while the total pressure is not altered

```
scalef = column_amount_usr/column_amount_mod;
for (iz = 0; iz < nz_mod; iz++){
   conc_cm3[iz] *= scalef;
   Pgas[iz] *= scalef;
}
```

After rescaling, we recommend integration over the column again, with the user-defined gas concentration, and checking the new `ppmv` value. It must match the input. `Aspect` does it by default and prints the user input on the screen.

We note that the default MODTRAN values may be significantly outdated. For example, in recent years the average amount of CH_4 in the atmosphere has grown from the MODTRAN's ~1.6 (*ppmv*) to approximately 1.75 (*ppmv*) in 2020 (*Bernath* et al., 2020: Fig.21) and 1.92 (*ppmv*) in 2024 as indicated on the NOAA's Global Monitoring Laboratory website[49]. For CO_2 and N_2O these numbers have also grown, respectively, from 330 and 0.297 (*ppmv*) in MODTRAN to 422 and 0.337 (*ppmv*) at the present time, according to the NOAA website.

The physically correct scaling of the partial pressure has non-linear effect on the resulting optical thickness. However, **Fig.3** (right) shows that this effect may be overall insignificant. In this case, the resulting optical thickness would depend on the concentration linearly, which simplifies retrieval. For instance, one creates an optical thickness LUT for a unit amount of gas and scales it according to the change of concentration.

6.3 The mysterious *atm-cm/km*

In addition to *ppmv*, the atmosphere-centimeter per kilometer, *atm-cm/km*, is another way to define the relative (unitless) amount of gas in the atmosphere. It is widely used in practice by some atmospheric scientists but looks confusing to others. Finding the relation between the two units in literature is possible (see e.g., *Berk et al.*, 1999: Sec. 3.4.1) but not always easy, which induced us to compile this section.

The *atm-cm* in the numerator indicates height of the gas layer, in *cm*, if one would bring all molecules of the gas from the whole atmospheric column (which is measured in *km* - denominator) to standard conditions, $T_0 = 273.15^o$ (*K*), $p_0 = 1$ (*atm*), known as "standard (atmospheric) temperature and pressure" – SATP or STP, **Fig.7(*a*)**.

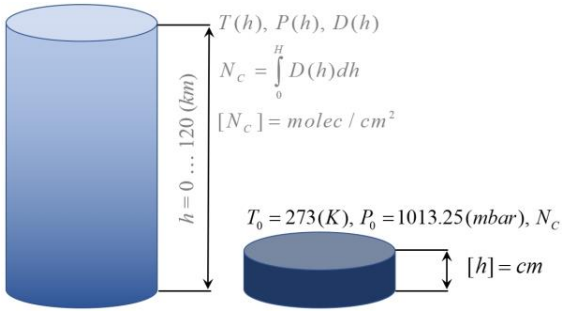

Fig.7(*a*): Definition of the units of *atm-cm/km*. The tall column on the left represents a realistic atmosphere with some temperature, pressure, and density profiles. The right column is at normal condition but holds the same number of the gas molecules *N* as the right one. Both columns stand on the unit area surface element *S*.

[49] https://gml.noaa.gov/ccgg/trends/gl_data.html

In order to convert the MODTRAN density profile in *molec*/*cm*^{3} into *atm-cm*/*km*, one uses

$$p = nk_B T = \frac{N}{Sh} k_B T \,, \tag{30}$$

where n (*molec*/*cm*^{3}) is the volume number concentration. From this equation one gets the ratio of two heights of gas in different thermodynamic conditions over the same (unit) area S of the atmospheric column (**Fig.7(*b*)**)

$$\frac{h(z_0)}{h(z)} = \frac{T_0}{p_0}\frac{p(z)}{T(z)} = \frac{T_0}{p_0} nk_B \left(\frac{atm\text{-}cm}{cm}\right) = \frac{T_0}{p_0} nk_B 10^5 \left(\frac{atm\text{-}cm}{km}\right). \tag{31}$$

In Eq.(31), the scaling factor 10^5 converts *km* to *cm*, and k_B and n are in SI units.

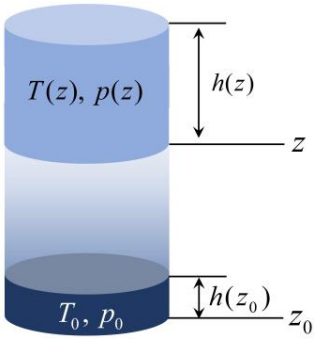

Fig.7(*b*): Graphical explanation for Eq.(31). Both heights h, measured at levels z and z_0, are small so that temperature and pressure are constant with the shown volumes; the number of molecules in both volumes is the same.

Any volume element $h(z)$, floating at level z in the atmosphere, can be reduced to the one at normal conditions, $h(z_0)$.

In terms of code, `aspect` converts MODTRAN's number density profiles into *atm-cm*/*km* as follows

```
c_stp = 1.0e5 * (k_boltzman * 1.0e-7) * To_stp / Po_stp * 1.0e6;
atmcm_km = new double [nz_mod];
for (iz = 0; iz < nz_mod; iz++) atmcm_km[iz] = c_stp*conc_cm3[iz];
```

Note, the factors `1.0e-7` and `1.0e6` bring the Boltzmann constant and the number density, respectively, to SI units; `_stp` stands for "standard temperature and pressure".

In fact, `aspect` does not use the `atmcm_km` array in calculations. However, it can be used to test numerical integration over height and to convert units from/to other data sources. For example, the MODTRAN website[50] reports numerical results (5 significant digits) for the total amount of species in *atm-cm* (integrated over height, hence no "per kilometer"). **Table 7** replicates their results in our paper for convenience (only molecules #1-7 and #10), while **Table 8** compares numbers from **Table 7**, assumed baseline, vs. those for `aspect` and SHARM-IPC. Negative sign in **Table 8** means our numerical result exceeds the one from **Table 7** .

Table 7: MODTRAN's total vertical column amounts (*atm·cm*) listed in HITRAN order. CO_2 is indicated for 380 (*ppmv*) as opposed to the default MODTRAN value of 330 (*ppmv*) – see **Table 6** and 2* below.

#	Molec	Tropical	Mid Lat Sum	Mid Lat Win	Sub Arc Sum	Sub Arc Win	US 1976
1	H_2O	5.1194E+03	3.6359E+03	1.0597E+03	2.5894E+03	5.1773E+02	1.7623E+03
2*	CO_2	3.0587E+02	3.0513E+02	3.0599E+02	3.0347E+02	3.0421E+02	3.0448E+02
3	O_3	2.7727E-01	3.3176E-01	3.7681E-01	3.4492E-01	3.7550E-01	3.4356E-01
4	N_2O	2.4649E-01	2.3743E-01	2.4037E-01	2.1920E-01	2.3993E-01	2.4593E-01
5	CO	3.0587E+02	3.0513E+02	3.0599E+02	3.0347E+02	3.0421E+02	3.0448E+02
6	CH_4	1.3243E+00	1.2684E+00	1.2806E+00	1.2556E+00	1.2719E+00	1.3203E+00
7	O_2	1.6823E+05	1.6782E+05	1.6829E+05	1.6691E+05	1.6732E+05	1.6746E+05
10	NO_2	2.1091E-04	2.1814E-04	1.9842E-04	2.1543E-04	1.8654E-04	2.0418E-04

Regarding **Table 8**, we note that profiles and numerical integration technique used in SHARM-IPC-LBL and `aspect` are not the same. First, in SHARM-IPC-LBL, the vertical distribution of molecules is defined in (*atm-cm/km*), instead of the number density concentration (*molec/cm*^{3}). Next, the number of points over height is different. The middle atmospheres 25-50 (*km*) uses 5 (*km*) step (6 points), and the upper atmosphere uses 25 (*km*) step. The TOA is assumed at 100

[50] http://modtran.spectral.com/modtran_faq, Table 1: Total vertical column amounts (atm·cm) for the 12 ambient band model species

(*km*), thus the upper part of atmosphere contains only 3 points. The total number of points in the height grid is 33 (compare with **Fig.6(*a*)**).

SHARM-IPC-LBL uses the following algorithm for integration of its profiles. For the lower, 0: 1:25 (*km*) the trapezoidal quadrature is used. For the middle atmosphere, 25:5:45 (*km*) atmosphere, the profile is first interpolated from 5 equidistant points, 5 (*km*) step, to 11 equidistant points, 2 (*km*) step, using the quadratic spline interpolation. Then, Simpson's rule is used on these 11 interpolated points. The last four points, 45, 50, 75, and TOA at 100 (*km*), are interpolated with an exp-function

$$f(z) = f(45)\exp(-\alpha(z-45)). \qquad (32)$$

In Eq.(32), the decay factor α (km^{-1}) is derived from the log-linear least squares fit at the last three points. We refer our reader back to Sec.6.2 for the vertical integration we use in `aspect`.

Table 8: Relative difference, in %, for MODTRAN (assumed as baseline, in **Table 7**) vs. `aspect` (left) and SHARM-IPC (right: gray). Negative values mean our result exceeds the one for MODTRAN.

#	Molec	Tropical		Mid Lat Sum		Mid Lat Win		Sub Arc Sum		Sub Arc Win		US 1976	
1	H_2O	0.1	2.0	0.3	2.0	0.5	1.5	-0.1	1.5	2.2	1.2	0.2	1.4
2	CO_2	0.1	0.0	0.1	0.0	0.1	0.1	0.1	0.0	-0.3	0.1	0.1	0.0
3	O_3	2.5	2.6	0.4	1.6	0.7	0.5	1.2	0.4	-1.2	0.2	0.3	0.7
4	N_2O	0.1	0.0	0.1	0.0	0.1	0.1	0.1	0.1	-0.2	0.1	0.1	0.0
5	CO	0.8	0.1	0.1	0.2	0.1	0.3	0.1	0.1	0.0	0.3	0.2	0.2
6	CH_4	0.1	0.0	0.2	0.0	0.1	0.0	0.1	0.0	-0.2	0.0	0.1	0.1
7	O_2	0.1	0.0	0.1	0.0	0.1	0.1	0.1	0.0	-0.3	0.1	0.1	0.1
10	NO_2	1.5	2.5	1.7	2.6	1.7	2.6	1.7	2.8	0.7	2.8	1.4	2.7

Because of the difference in profiles and numerical integration technique, the overall maximum (and average) relative deviation of `aspect` and SHARM-IPC-LBL w.r.t. the MODTRAN values are 2.5% (0.5%) and 2.8% (0.8%), respectively. **Table 8** shows that the Sharm-IPC deviation is always higher, while that for `aspect` changes sign w.r.t to the MODTRAN values.

We ignored the change of sign in the overall errors mentioned. Also, based on our literature search, we were unable to clarify MODTRAN's technique for vertical integration.

6.4 Profile of optical thickness

`Aspect` uses three steps to calculate the absorption optical thickness profile. For one, profile of the molecular absorption cross-section, k ($cm^2/molec$), is calculated in `kabs(…)` for each wavenumber ν from the user's grid [ν_{min}, ν_{max}] with step Δν. This is like the one for the gas cell (Sec.5): one picks all HITRAN line contributions to the user-defined band and accumulates them. The only two differences from simulation of the gas cell are: (1) one deals with a mixture of gases – hence Eq.(8) for the Lorentzian HWHM parameter uses both the total atmospheric and partial gas pressures, and two HITRAN parameters: γ_{self} and γ_{air}; and (2): the atmosphere is a stack of "gas cells", one on top of the other. Therefore, `kabs(…)` accepts as input the user's range of wavenumbers, parameters of the HITRAN lines (limited to those contributing to the user interval – see Sec.5.1), and profiles of temperature and pressure. The output of `kabs(…)` is the spectral and height dependence of the absorption cross-section, $k(\nu, z)$ ($cm^2/molec$), on the user grids of ν (cm^{-1}) and heights, z (km) – an array **`knu`**`[nz*nnu]`.

A few comments must be made here regarding the array **`knu`**`[]`. First, in order to allocate the elements of an array in memory consecutively, we prefer a 1D array over the 2D one (*Oliveira & Stewart*, 2006: Sec.8.3). Second, the grid of heights *z* is the lead dimension of the array for efficiency of the vertical integration performed independently for each ν. Third, the MODTRAN profiles are used. Before calling `kabs(…)`, the array **`knu`**`[nz_mod*nnu]` must be allocated for the number of the MODRAN points over height `nz_mod`. Fourth and the last one, at present `nz_mod = 53` and the user must be careful with the number of the spectral nodes, `nnu`. A wide spectral range combined with a very fine spectral resolution may lead to insufficient available memory. `Aspect` checks that and, if it happens, stops, and notifies the user. The easiest way to deal with the problem is to split the wide band into a few smaller ones, generate corresponding LUTs and, if needed, stitch them together into a single big file. Also, using single precision instead of double saves memory.

The next steps are trivial: for a given ν, `aspect` calculates the extinction profile by multiplying the cross-section and the number concentration profiles (the height grids must match); then it

integrates the extinction over height from TOA to a user-defined level to get the optical thickness between TOA and the given level (i.e., optical depth). The corresponding element of code in `aspect` is

```
for (inu = 0; inu < nnu; inu++) {
    for (iz = 0; iz < nz_mod; iz++)
          ext_km[iz] = knu[inu*nz_mod+iz]*conc_cm3[iz]*1.0e5;
    tauabs25(ext_km, zkm_mod, ztau, nzkm, tau_abs);
}
```

The scaling factor `km_to_cm = 1.0e5` relates cm^{-1} (in *k*) and km^{-1} (in the grid of heights).

The subroutine `tauabs25(…)` integrates the extinction profile, **`ext_km`**`[nzkm_mod]`, defined on the MODTRAN grid of heights, **`zkm_mod`**`[nzkm_mod]`, using the two functions already explained in Sec.6.2: `simpson(…)` and `intparab(…)`. On output, this subroutine gives an array, **`tau_abs`**`[nzkm]`, of optical depths at every user requested height **`ztau`**`[nzkm]`. For the code simplicity, we assume the user requests optical depths at levels not exceeding 25 (*km*). As Sec.6.1 shows, MODTRAN uses equidistant grid of heights with 1(*km*) step below the 25 (*km*) threshold. Therefore, it is easy to quickly get the left and right indices of the interval of heights containing the user requested altitude. Using these indices, one integrates from *z* = 25 (*km*) to the user level by accumulating Simpson integral and, optionally, trapezoidal integral to include the part not covered by Simpson's rule due to the odd vs. even number of points.

At and above *z* = 25 (*km*), `tauabs25(…)` provides the vertical integral from 25 to 120 (*km*) – regardless the user requested level. The 25-120 (*km*) value is calculated using only Simpson's rule for the middle (11 points, 2.5 km step) and top (15 points, 5 km step) atmosphere which are added to the final result.

Also, for code simplicity, `tauabs25(…)` loops through the user's heights independently. If the user requests many levels, `nzkm >> 1`, this is inefficient: a lower level includes integral from TOA to the level above it. However, our option *a*) helps keep the code simple; *b*) yields flexibility: the order of the user's levels is not important; and *c*) is not a bottleneck for the runtime – calculation of the Voigt line shape is.

The output result, **tau_abs**[nzkm], is saved either to ASCII or to a binary file as explained in Sec.3.3.2. In the former case, aspect prints out all values including 0.0. This is convenient for visual inspection, debugging, and smaller LUTs. Consider as an example only one HITRAN-2020 record for O_2 from Sec.4.2-4.3, default MODTRAN's amount of the gas in atmosphere, US 1976 profile, 4 user defined levels z = 0, 2, 4, 8 (*km*), and 6 user's ν = 13000 + [0.80 : 0.01 : 0.85] (cm^{-1}). The output file with optical thickness in ASCII format is

```
# nu, zkm =    0.000   2.000   4.000   8.000
0  13000.8000  3.077005e-02  1.877401e-02  1.106013e-02  3.841381e-03
1  13000.8100  3.533850e-02  2.287806e-02  1.461589e-02  6.374547e-03
2  13000.8200  3.425169e-02  2.232654e-02  1.442593e-02  6.519878e-03
3  13000.8300  2.782967e-02  1.723955e-02  1.043387e-02  3.993817e-03
4  13000.8400  2.084901e-02  1.196508e-02  6.532608e-03  1.837301e-03
5  13000.8500  1.554367e-02  8.344352e-03  4.179478e-03  9.014089e-04
```

These numbers are convenient for validation of integration over height because they correspond to a single HITRAN record.

In the case of binary output file, aspect checks the highest value (lowest level) against a threshold, tau_min, defined in const_param.h (at present, tau_min = 1.0e-4 which corresponds to the vertical one-way monochromatic transmittance of ~0.9999). If the highest thickness does not exceed the threshold, the whole wavenumber is not saved to the binary file. The check weather to save or skip **tau_abs**[nzkm] is made for each user's ν. For that reason, **tau_abs**[nzkm], does not depend on inu and is small even for a dense user's grid of heights **zkm**[nzkm].

6.5 Practical units for water vapor

MODTRAN defines profiles for the particles number concentration in *ppmv*. In practice, however, different units are commonly used for some molecules: *cm* (or sometimes *mm*) of precipitable liquid water for water vapor (WV), and Dobson units (DU) for O_3. In this part we convert the atmospheric columnar amounts of WV from *ppmv* to *cm* of precipitated (liquid) water.

The atmosphere-centimeters shown in **Table 7** for MODTRAN's US 1976 atmosphere corresponds to apsect's h = 1766.42 (*cm*). It is the heigh of a column of the water vapor (ideal

gas) at the normal conditions. When the vapor is condensed into the liquid water, the number of molecules does not change, but the mass density does. Ratios of the mass densities and columns of water in two physical states are the same:

$$h_{LW} = h_{WV} \frac{\rho_{LW}}{\rho_{WV}} \tag{33}$$

In Eq.(33), the subscript LW means "Liquid Water" and $\rho_{LW} = 1.0$ (g/cm^3) is the liquid water mass density. The water vapor mass density is calculated via scaling the molar mass of the H_2O molecule $\mu_{H_2O} = 18.01528$ (*g/mole*) by the number of moles. The latter is computed as the ratio of the Loschmidt number[51] $N_L = 2.6867811 \cdot 10^{19}$ ($molec/cm^3$) and the Avogadro number $N_A = 6.02214129 \cdot 10^{23}$ (*molec/mole*)

$$\rho_{WV} = \mu_{H_2O} \frac{N_L}{N_A}. \tag{34}$$

Eqs.(33) and (34) result in ≈1.42 (*cm*) of liquid water for the MODTRAN's Standard US1976 atmosphere. Recall, `aspect` expects the LW amount as input for H_2O.

6.6 `Aspect` validation

6.6.1 Literature references

As for the gas cell, we recommend starting with a visual comparison of the spectral dependencies calculated using `aspect` vs. figures published in literature. This helps catch misunderstandings of units, which manifest as wrong order of magnitude. The existence and location of the spectral line peaks (or drops in atmospheric transmittance, also called transmission, or transmissivity – in the right-most column "Brief description" we borrow the term from the respective source) help verify the proper reading and understanding of the HITRAN database. In **Table 9**, we combine some references to published images that can be used for validation of separate molecules and the whole atmosphere. The list is sporadic, non-exhaustive, and contains references to papers and books that we found while working on this paper.

[51] In 2018, the temperature at which the Loschmidt constant is defined, has changed from 296° to 273.15° (*K*). Thus its numerical value in legacy and modern codes may differ. If not compensated via ratio of the temperatures, this difference noticeably impacts output (https://en.wikipedia.org/wiki/Loschmidt_constant)

Table 9: References to published benchmark images that can be used to test codes like `aspect`. The bottom row "total" refers to results for all gases mixed in atmosphere.

#	Mol.	Ref.	≈ Δν (cm^{-1})	≈ Δλ (μm)	Brief description
1	H_2O	*Gao* et al., 1993: Fig.2		0.4 - 2.5	Atmospheric water vapor transmittance spectrum, at 10 (*nm*) resolution, using LOWTRAN7 (*Kneizys* et al., 1988)
		Goody & Yung, 1995: p.68, p.71	630 – 710 (p.71)	1 - 13 (p.68)	Low-resolution atmospheric absorption spectrum; high-resolution transmission near 14.9 (μm) at 0 (*km*) and SZA = 30^o and terrestrial concentration x 0.03
		Petty, 2006: p.179		0.3 - 50	Zenith transmittance of a midlatitude summertime atmosphere.
		Thorpe et al., 2013: Fig.1		0.5 - 2.5 2.0 - 2.5	Transmittance spectra generated using MODTRAN v.5.3 for a sensor located at 8.9 (*km*) altitude.
		Yang et al., 2013: Fig.1		0.6 – 0.8	Atmospheric columnar water vapor absorption transmittance calculated using LBLRTM.
		Ibrahim et al., 2018: Fig.1		0.3 – 1.1	Columnar atmospheric transmittance for 3.3 (*cm*) of water vapor
		Coakley & Yang, 2014: p.157	800 - 900		Total atmospheric water vapor transmission for the 1976 US Standard Atmosphere. The water vapor continuum was not included "*in order to better show the line structure*".
		Gordon, 2019: p.328		0.4 – 1.0 0.4 – 2.5	Water vapor transmittance in the US Standard Atmosphere at 20 (cm^{-1}) resolution (p.327)
		Mobley, 2022: Fig. 15.15	300 - 1000		Transmittance by a moist tropical atmosphere at 1 (*nm*) resolution.
		Docter et al., 2023: Fig. 2		0.6 – 2.35	Atmospheric transmittance.
		Gordon et al., 2022: Fig.3	9000 - 19000		Terrestrial atmospheric transmittance for HITRAN 2020 and 2016.

2	CO_2	*Gao* et al., 1993: Fig.2		0.4 – 2.5	Atmospheric carbone dioxide transmittance spectrum, at 10 (*nm*) resolution, using LOWTRAN7 (*Kneizys* et al., 1988)
		Goody & Yung, 1995: p.68, p.71	786 – 796 (p.71)	1.5 – 13 (p.68)	Low-resolution atmospheric absorption spectrum; high-resolution transmission near 12.64 (*μm*) at 15 (*km*) and SZA = 30^o and terrestrial concentration × 10.
		Bohren & Clothiaux, 2006: Fig.2.22	746 - 758 756.5 - 758.0 1074 - 1086 1082.0-1082.75		Absorptivity along a vertical path for a Mid-latitude Summer atmosphere and 4 different concentrations of carbon dioxide; note non-zero values for 0 (*ppm*) of CO_2.
		Petty, 2006: p.179		0.3 - 50	Zenith transmittance of a midlatitude summertime atmosphere.
		Docter et al., 2023: Fig. 2		0.6 – 2.35	Atmospheric transmittance.
3	O_3	*Gao* et al., 1993: Fig.3		0.4 – 2.5	Atmospheric ozone transmittance spectrum, at 10 (*nm*) resolution, using LOWTRAN7 (*Kneizys* et al., 1988)
		Goody & Yung, 1995: pp. 68 & 72	1039 – 1041 (p.72)	3.5 – 15.5 (p.68)	Low-resolution atmospheric absorption spectrum; high-resolution transmission near 9.61 (*μm*) at 30 (*km*) and SZA = 30^o.
		Petty, 2006: p.179		0.3 - 50	Zenith transmittance of a midlatitude summertime atmosphere.
		Ibrahim et al., 2018: Fig.1		0.3 – 1.1	Columnar atmospheric transmittance for 277 DU of ozone
		Gordon, 2019: p.329		0.4 – 0.8	Ozone transmittance in the US Standard Atmosphere.
		Mobley, 2022: Fig. 15.16	300 - 1000		Vertical atmospheric transmittance for 200, 350, and 500 DU. Strong absorption in the Blue-UV band, not available from HITRAN's LBL database, is visible.
4	N_2O	*Gao* et al., 1993:		0.4 – 2.5	Atmospheric nitrous oxide transmittance spectrum, at 10 (*nm*)

		Fig.3			resolution, using LOWTRAN7 (*Kneizys* et al., 1988)
		Goody & Yung, 1995: p.68, p.70, p.96	1245 - 1325 (p.70) 1160.0 – 1160.6 (p.96)	2 – 9.5 (p.68)	Low-resolution atmospheric absorption spectrum (p.68); high-resolution transmission near 7.78 (μm) at 15 (*km*) and SZA = 30^o (p.70); ultra-high resolution transmission for "*physical conditions very different from those occurring in Earth's atmosphere*" (also useful for gas cell validation).
		Petty, 2006: p.179		0.3 - 50	Zenith transmittance of a midlatitude summertime atmosphere.
		Coakley & Yang, 2014: p.153	1120 - 1220		N_2O transmissivity near 8.6 (μm) for 1976 US Standard Atmosphere, HITRAN 2008, at ground level for SZA = 0^o.
5	CO	*Gao* et al., 1993: Fig.3		0.4 – 2.5	Atmospheric carbon monoxide transmittance spectrum, at 10 (*nm*) resolution, using LOWTRAN7 (*Kneizys* et al., 1988)
		Goody & Yung, 1995: p.68, p.70	2102 - 2182 (p.70)	2 – 6 (p.68)	Low-resolution atmospheric absorption spectrum; high-resolution transmission near 4.67 (μm) at 10 (*km*) and SZA = 30^o.
		Petty, 2006: p.179		0.3 - 50	Zenith transmittance of a midlatitude summertime atmosphere.
6	CH_4	*Gao* et al., 1993: Fig.3		0.4 – 2.5	Atmospheric methane transmittance spectrum, at 10 (*nm*) resolution, using LOWTRAN7 (*Kneizys* et al., 1988)
		Goody & Yung, 1995: p.68, p.69	2874 – 2946 2904 - 2908	1.5 – 8.5 (p.68)	Low-resolution atmospheric absorption spectrum (p.68); and medium and high-resolution transmission spectra near 3.44 (μm) at 10 (*km*) above the ground for SZA = 30^o (p.69)
		Petty, 2006: p.179		0.3 - 50	Zenith transmittance of a midlatitude summertime atmosphere.
		Thorpe et al., 2013: Fig.1		0.5 - 2.5 2.0 - 2.5	Transmittance spectra generated using MODTRAN v.5.3 for a sensor located at 8.9 (*km*) altitude.

		Docter et al., 2023: Fig. 2		0.6 – 2.35	Atmospheric transmittance.
7	O_2	*Gao* et al., 1993: Fig.3		0.4 – 2.5	Atmospheric oxygen transmittance spectrum, at 10 (*nm*) resolution, using LOWTRAN7 (*Kneizys* et al., 1988)
		Goody & Yung, 1995: p.196	842 - 7922		IR atmospheric band of molecular oxygen near 1.27 (μm) based on AFGL data at 0 (*km*) and SZA = 30^o.
		Pfeilsticker et al., 1998: Fig. 2		0.768 – 0.772 (A-band)	Direct Sun observations of the atmospheric O_2 A-band at different solar zenith angles.
		Stam et al., 2000: Figs.1, 2(a), & 3		0.755 - 0.775 0.765 - 0.766	Fig.1: Molecular scattering and absorption columnar optical thickness based on HITRAN-92 for the A-band. Fig.2(a): Like Fig.1 but for a narrow band $\Delta\lambda = 1$ (*nm*) resolves peaks from the isotope minorities. Fig.3: Like Fig.2(a) but for absorption cross-section as a function for 0 (*km*) and 30 (*km*) with specified temperature and pressure (also useful for gas cell validation).
		Petty, 2006: p.179		0.3 - 50	Zenith transmittance of a midlatitude summertime atmosphere.
		Nowlan et al., 2007: Figs.1, 3		0.690 – 0.692 0.680 – 0.700 0.755 – 0.780	A- and B-bands cross-sections (Figs. 1 & 3) and transmittances (Fig.1 only) in atmosphere at 0, 30 (A-band only), and 50 (*km*); temperature and pressure are specified (also useful for gas cell validation).
		Natraj et al., 2007: Fig.1	12,995 - 13,020		Atmospheric columnar optical depth calculated using HITRAN 2000; corresponding Rayleigh optical depth is also shown.
		Gordon et al., 2011: Figs. 2 & 4	15,050 - 15,930 14,496 - 14,504		Oxygen B- and γ-bands: atmospheric transmittance.

		Yang et al., 2013: Figs.1 & 2(ab)		0.6 - 0.8	Oxygen transmittance in the A- and B -bands (Fig.1). Figs. 2(a) and 2(b) show details for the A- and B-bands, respectively.
		Ibrahim et al., 2018: Fig.1		0.3 – 1.1	Columnar transmittance for tropical atmosphere.
		Mobley, 2022: Fig. 15.15	300 - 1000		Atmospheric columnar transmittance at 1 (*nm*) resolution.
10	NO_2	*Ibrahim* et al., 2018: Fig.1		0.3 – 1.1	Columnar transmittance for tropical atmosphere
		Gordon, 2019: p.328		0.35 – 0.90	Columnar transmittance for the US 1976 Standard Atmosphere.
		Mobley, 2022: Fig. 15.17	300 - 1000		Vertical atmospheric for low, typical, and high concentrations of NO_2.
-	Total	*Goody & Yung*, 1995: p.4		0.1 - 100	Atmospheric absorption at ground level and at 11 (*km*)
		Petty, 2006: p.179		0.3 - 50	Zenith transmittance of a midlatitude summertime atmosphere.
		Bohren & Clothiaux, 2006: Fig.2.13		0.1 (μm) – 10 (***cm***)	Atmospheric transmissivity along a vertical path in a very broad band. There are 6 panels, each panel is one wavelength decade - hence the top covered limit: 10 ***centimeters***. Ozone absorption, not included in our HITRAN-based LBL calculations, is visible in the 0.1 (μm) – 1 (μm) panel.
		Thompson et al.,2015: Fig.1		0.4 – 2.4	Atmospheric transmittance due to atmospheric gases.
		Ibrahim et al., 2018: Fig.1		0.3 – 1.1	Tropical atmosphere transmittance for 3.3 (*cm*) of H_2O, 277 DU of O_3, O_2, and NO_2 combined.
		Gordon, 2019: p.329		0.4 – 1.0 0.4 – 2.5	Columnar transmittance for the US Standard Atmosphere.

		Chen et al., 2021: Fig.2(a)		0.25 - 2.50	Atmospheric transmittance in the Solar reflectance band. Note, the ozone absorption at wavelength shorter than 700 (*nm*) is not included in HITRAN, hence, in our paper as well.

Once the user has verified the order of magnitude, it is time for accurate numerical comparison vs. tools mentioned in the Introduction. With this paper, we distribute our numbers for the oxygen A-band and methane optical thickness integrated from TOA to several levels in the atmosphere (see Sec. 3.2.2).

6.6.2 Numerical validation of atmospheric absorption

This section presents examples of numerical validation of `aspect` against another code (*Ibrahim et al.*, 2018) simulating LBL atmospheric absorption spectroscopy for the PACE-OCI instrument. That code, assumed benchmark, was developed independently of `aspect`. It is a completely refactored and updated version of the ATREM code (*Gao et al.*, 1993; *Thompson et al.*, 2015). Two key modifications in the benchmark code include the translation from Fortran into Python and the use of the HAPI tool (*Kochanov* et al., 2016) for simulating the absorption cross-section k ($cm^2/molec$) at a given temperature, pressure (i.e., in a layer at a specific altitude) and for the Voigt line shape via the `absorptionCoefficient_Voigt(…)` function. The wing cut-off was set to 25 (cm^{-1}).

Like `aspect`, the benchmark code uses prescribed MODTRAN atmospheric profiles with 50 boundaries; however, the calculation of optical thickness τ differs. The benchmark code models the atmosphere as consisting of 49 layers, where pressure, temperature, and particles number concentrations are assumed constant in each layer and calculated as the average of those at the layer boundaries. Thus, the atmosphere is treated as a vertical stack of gas cells, whose absorption properties can be tested using `gcell`. The atmospheric optical thickness is then accumulated from TOA to BOA or to any desired altitude in the atmosphere. For tests presented in this section, both codes calculated $\tau(\nu)$ in LBL mode with a spectral resolution $\Delta\nu = 0.01$ (cm^{-1}), using MODTRAN US 1976 atmospheric profile (Sec.6.1) and HITRAN-2020 edition. We

considered absorption by two molecules: H_2O within 550-900 (*nm*) and O_2 in the B- and A-bands: 680-700 and 750-780 (*nm*), respectively. We ignored continuum for both.

To provide a practical perspective for our comparison and to enhance visual clarity, we compare the total atmosphere one-way vertical transmittance within the PACE-OCI instrument bands as defined by Eq.(25). The OCI relative spectral response functions (RSRs) are available from the NASA GSFC Ocean Color website[52] in a netCDF file. All RSRs are defined on the same grid of 20926 equidistant wavelength points beginning at 306 (*nm*) with 0.1 (*nm*) step. **Fig.8** shows the RSRs for all OCI bands, however, we are interested only in "hyperspectral" mode which extends up to ~894(*nm*), with 5 (*nm*) resolution bandwidth (full width at half maximum), and spectral steps 2.5 (*nm*) (between band centers) for most bands and 1.25 (*nm*) for a few.

In addition to the RSRs, **Fig.8** also shows the solar spectral irradiance normalized to its maximum value, ≈2.4 ($W\,m^{-2}\,nm^{-1}$). For this, we use a new solar irradiance reference spectrum recently published by *Coddington* et al. (2023). The solar spectrum is available online[53] for the wavelength range from 202 (*nm*) to 2730 (*nm*), with native (unconvolved) spectral resolution 0.001 (*nm*), as reported in `hybrid_reference_spectrum_c2022-11-30_with_unc.nc` file, which we use in our calculations.

Since both the solar irradiance spectrum and RSRs are defined in the wavelength domain, we integrate Eq. (25) over λ. This requires converting the HITRAN-LBL absorption optical thickness from wavenumbers to wavelengths, and then interpolating between different wavelength grids. The constant step $\Delta\nu = 0.01$ (cm^{-1}) for the HITRAN-LBL calculations corresponds to a step $\Delta\lambda$ not exceeding 0.001 (*nm*) for $\lambda < 1000$ (*nm*). Therefore, we interpolate the solar spectrum and hyperspectral RSRs from their wavelength grid to match that of LBL τ. We developed a Python script for cubic interpolation and Simpson integration, and used it for both `aspect` and benchmark LBL data. This ensures that no discrepancies arise from interpolation and integration in Eq. (25).

[52] https://oceancolor.gsfc.nasa.gov/images/data/PACE_OCI_L1B_LUT_RSR_baseline_1.1.1.nc
[53] https://lasp.colorado.edu/lisird/data/tsis1_hsrs_p1nm

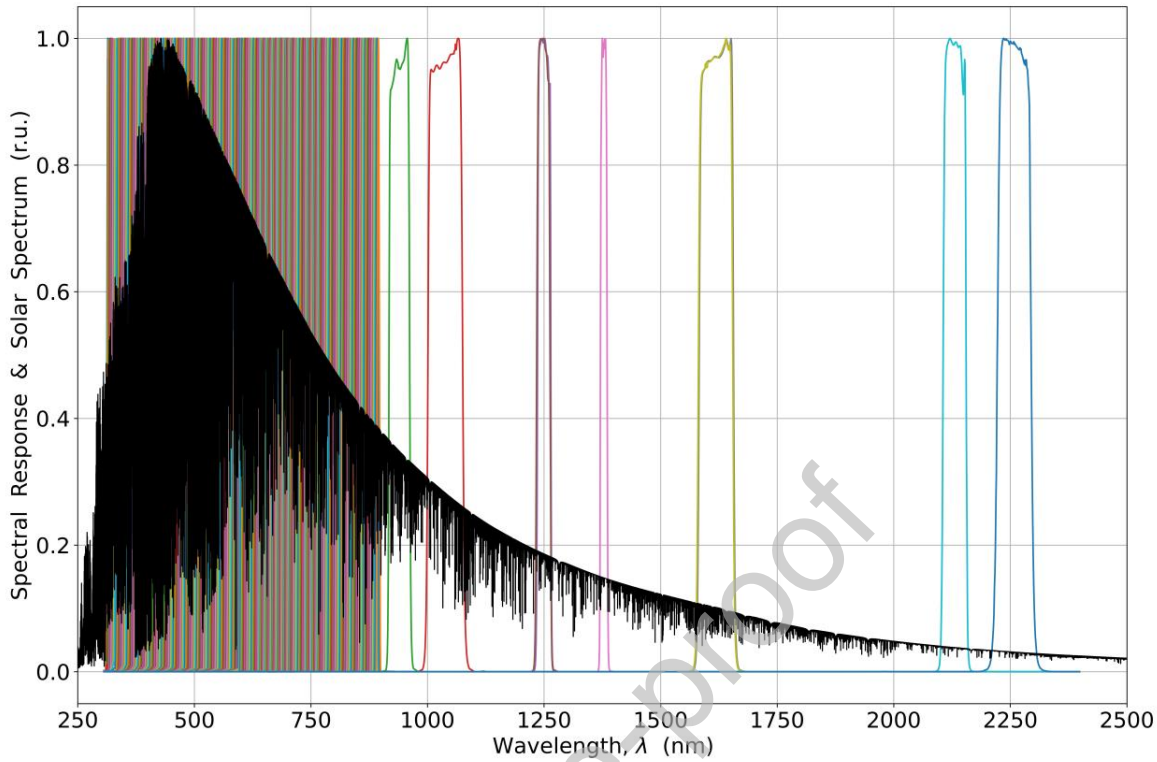

Fig.8: PACE-OCI RSRs (colored lines) and solar spectrum (black) normalized to its maximum value ≈ 2.4 ($W\,m^{-2}\,nm^{-1}$). The multiple colored bands below 900 (*nm*) correspond to the hyperspectral mode.

Fig.9(*a*) compares one-way vertical transmittances, expressed as percentages (%), where 100% corresponds to total transparency (T = 1), within OCI bands for 0.5 and 5 (*cm*) of liquid water. **Fig.9(*b*)** shows the absolute difference between `aspect` and the benchmark code in the same percentage units. Given the different approaches to simulating absorption cross-sections (self-coded vs. HAPI) and to vertical integration (Simpson rule vs. layer-averaged) in `aspect` and the benchmark code, we are satisfied with the result.

Fig.9(*c*) compares true `aspect` calculations with those obtained through linear scaling of absorption optical thickness in the same code:

$$\tau_{WV}(\nu) = \frac{LW}{LW_{Std}}\tau_{Std}(\nu)\,, \tag{35}$$

where $LW_{Std} \approx 1.4197655$ (*cm*) is the amount of water vapor condensed into a liquid for the standard MODTRAN US 1976 atmosphere, $\tau_{Std}(\nu)$ is the LBL optical thickness calculated for the same, and LW is the user-defined amount (e.g., 0.5 or 5 (*cm*) in our examples, as shown in

Fig.9). This simple scaling is convenient for retrievals; however, it must be treated with caution depending on the absorption characteristics of the media (strong absorption lines and/or large amount of absorbent). We refer the reader to Eq.(12) in *Gueymard* (2001) for one modification of the scaling rule, Eq. (35).

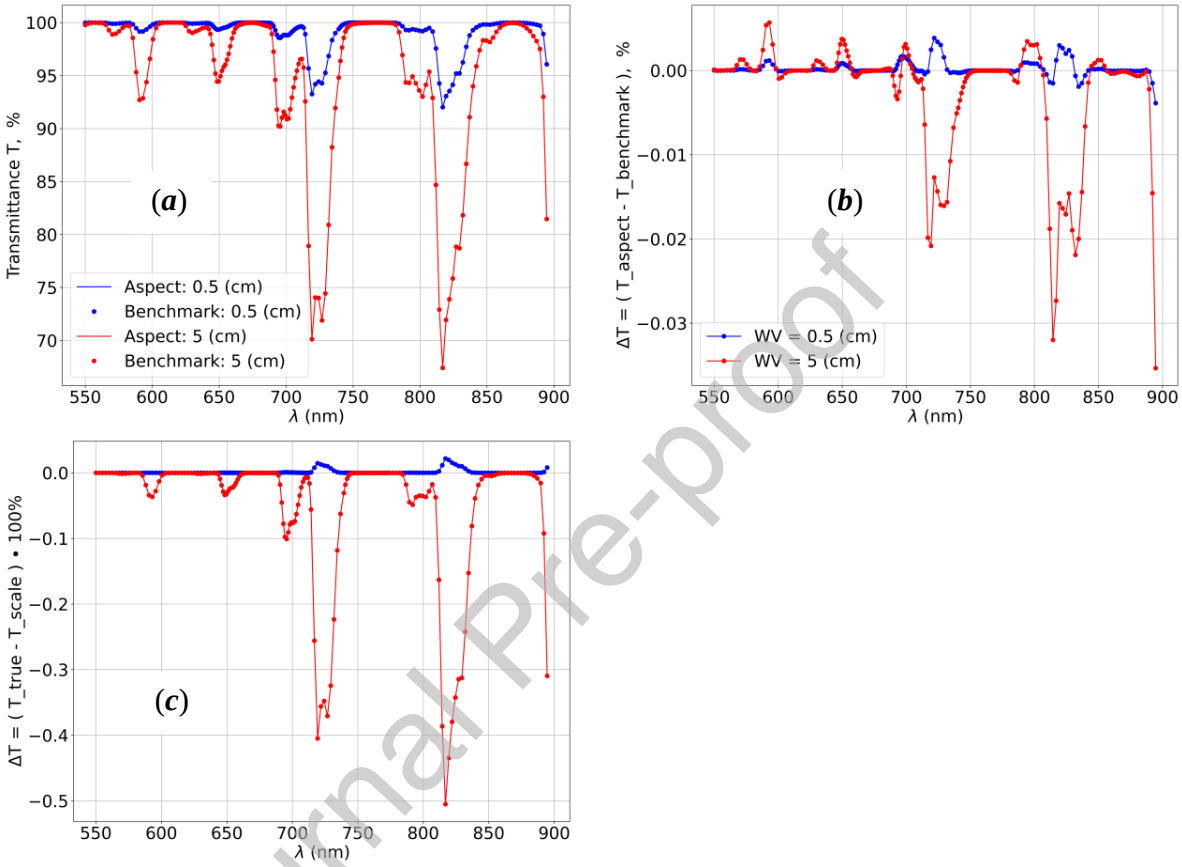

Fig.9: (***a***) Vertical one-way transmittances (top-left) within PACE-OCI bands (dots indicate band centers) for the condensed water vapor (WV) amount of 0.5 (blue lines) and 5 (red lines) (*cm*) as percentages (%), where 100% corresponds to $T = 1$ (no absorption). (***b***) Absolute difference between `aspect` and the benchmark code in the same units. (***c***) Absolute difference between true `aspect` calculations and those obtained from linear scaling of optical thickness, as given in Eq.(35), for the same amounts of WV.

Fig.10 shows another comparison of `aspect` versus the benchmark code for O_2 B- and A-bands, shown in the left and right charts, respectively. As in **Fig.9**, we plot one-way vertical transmittance as percentages (%; left y-axes) and the absolute difference in the simulated

transmittances between the two codes (right y-axes), also expressed as percentages (%). Like in Fig.9 (***b***), we attribute the difference to different approaches to simulating absorption cross-sections and to its vertical integration. To confirm this, we applied the Simpson integration from Python's `scipy.integrate` package (hence independently developed by experts) in the benchmark HAPI-based code. The pattern of the deviation remained the same; however, the maximum deviation decreased by factors of 5 and 3 in the B- and A-bands, respectively.

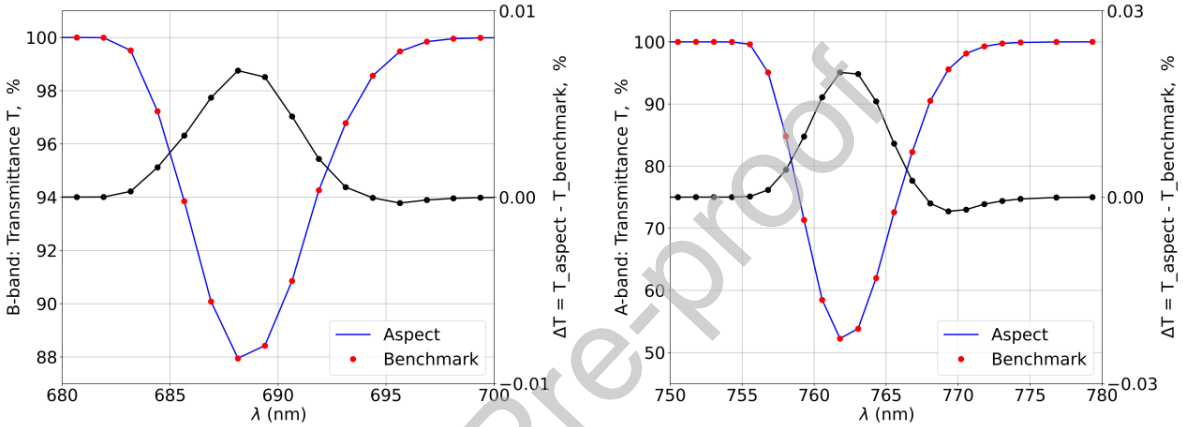

Fig.10: Comparison of one-way vertical transmittance in O_2 B (left image) and A (right image) bands. Red dots in the benchmark results correspond to PACE-OCI RSR band centers, while `aspect` results are shown with continuous blue lines for better visual perception. In each of the two charts, left y-axes show the absolute values of the transmittances, while the right y-axes show the absolute difference between `aspect` and benchmark codes.

For the cases considered in **Figs. 9** and **10**, we have prepared five `txt` files with LBL values of absorption optical thickness, which are distributed with our code in the `./benchmarks/` folder. Three of the files correspond to H_2O at 0.5, ≈1.42 (standard atmosphere), and 5 (*cm*) of liquid; the other two correspond to the oxygen A- and B-bands, as indicated in their respective file names. The optical thickness is calculated at 0, 1, 2.5, and 8 (*km*) altitudes; figures in this section show results for BOA, 0 (*km*). Structure of each file is explained in Sec.3.2.2 above. We used `aspect` to prepare the `txt` files.

7. Conclusion

Following our published "A practical guide to writing a radiative transfer code", this paper explains the development of a code for line-by-line trace gas absorption in Earth atmosphere within the solar reflectance band, 250-2500 (*nm*). We focus on the code, as opposed to theoretical background or practical applications, thoroughly discussed elsewhere. We start by reading the HITRAN database and simulate absorption by a single spectral line. Then we consider absorption by many lines in a gas cell at a given temperature and pressure. Finally, using the MODTRAN profiles, we simulate atmospheric absorption at user-defined altitudes. This sequence deals with one problem at a time: reading and understanding HITRAN, calculation of absorption for fixed thermodynamic conditions in a gas cell (code `gcell`), and lastly dealing with atmospheric profiles in the code `aspect`. In terms of the code text, `gcell` and `aspect` largely overlap.

Unlike the mentioned "guide to writing a radiative transfer code", which shows an entire scalar plane-parallel RT code, the current paper explains only key parts of each program. All the source codes and test data are available from the journal website and from our GitHub repository[54]. The sources are carefully commented. In this paper, we pay particular attention to unit testing and provide numerical and graphical material for debugging. We believe this detailed explanation leads to a thorough understanding of our software. This, in its turn, should simplify the completion of the basic tasks (e.g., the replacement for the current HITRAN database with a newer version, or vice versa, reproducing results with an older version), moderate modification of the code (acceleration of the *Humlíček* convolution algorithm; updating TIPS; adding a new molecule or profile; account for the wavenumber shift due to refractive index of air, which changes with height, as opposed to the HITRAN's line positions in vacuum), and fundamental changes (eventual replacement of the Voigt line shape with the speed-dependent Voigt, or other "beyond Voigt" models of line shape). The mentioned changes become necessary when one faces the everlasting question: "is this effect important in my case?". And even if numerical simulation proves that no changes are required so far, our approach assures confident exploitation of the code over time and smooth transition of knowledge between generations of atmospheric scientists.

[54] https://github.com/korkins/aspect_gcell

Both our “practical guide”-papers differ from most scientific papers because they do not present new information but rather act as an instructive resource to present necessary but disparate materials that are not often discussed together in a practically convenient form of “get to coding quickly”. Repeating our “RT guide”, we say here that a real understanding of how software applications of a general type of work is, in most cases, truly only attainable by developing your own. We encourage the reader to use our presented open-source scripts as an example to aid their understanding and a basis to develop tools for their own needs, and not merely as a shortcut.

Naturally, this paper and code have many limitations. We have restricted ourselves to absorption in spectral lines under conditions typical for the Earth environment – the area of our expertise. We take the line parameters from only one database – HITRAN. The main part of the HITRAN database simulates the line shape using convolution of the Doppler and Lorentzian contours – the Voigt profile. We mentioned above that we didn’t go “beyond Voigt”: e.g., the speed dependence (affecting the Doppler contour) and line mixing effects (affecting the Lorentzian contour) are not considered. We have hard-coded atmospheric profiles from MODTRAN. Therefore, our program is not ready for profile retrieval. Most importantly, we do not consider spectrally smooth absorption, like water vapor or ozone continuum. Hence, our tools cannot be used for ozone correction or in the microwave. We skip collision induced absorption (CIA), which seems important for cloud top height retrieval in the oxygen A-band. The number of gas species is limited to only the first few from a long HITRAN list.

Each limitation comes for a reason. Due to different theoretical backgrounds and scaling of the LBL and continuum-type absorption, e.g., for variations of temperature and pressure, it makes little sense to combine LBL and continuum in one program. Parameters for CIA are still not included in the “main” HITRAN database but come as separate ones. Same for non-Voigt line shapes. In order to partially close the gap in capabilities, we provide a broad list of literature references, 186 items, including some from the XIX-th century to give a historical perspective. Separate sections of our papers are devoted to the effects that we have dropped and to multiple tools for atmospheric spectroscopy that have been developed – many as open source, some with tutorial goal in developers’ mind. We encourage the reader to study literature focusing on their spectral band, as well as the light source (e.g., Sun vs. laser) and figure out what effects are

important, and what are not so. One common reason for all the limitations was to balance the simplicity of our codes with their practical value.

As to the limitations on the list of molecules, we believe our explanation of the source code bundled with theoretical background will help potential users to build-in and test any molecule from the HITRAN list quickly yet confidently. Our belief is based on the feedback to our proposal "The paper-and-code bundle as a new paradigm supporting the TOPS initiative in Earth Science" (NASA ROSES-22 program element F.15 High Priority Open-Source Science: NNH22ZDA001N-HPOSS). Although we received no funding from the program, the "selectable" status and overall positive review encouraged us to find extra time and finish this work, as proposed, but largely on a volunteer basis.

Acknowledgements

The authors are grateful to Laurence Rothman, Iouli Gordon (Harvard, USA) and the broader HITRAN team for the years of work developing and maintaining the database and associated resources. Sergey Korkin and Alexei Lyapustin thank Larry Gordley, Tom Marshall, and the GATS Inc. team (USA) for sharing numerical results discussed in Sec.5.3.2 "Methane band at 2.3 (μm)". Andrew M. Sayer thanks Keith Shine and Jon Elsey (University of Reading, UK) for useful discussions which aided our understanding of the history and conventions of line shape models, and Luca Lelli (DLR, Germany) for independent verification of some numerical results from his implementation of absorption line code. Sergey Korkin, Andrew M. Sayer, and Amir Ibrahim are thankful to Bo-Cai Gao (Naval Research Laboratory, USA) for help with understanding of the nature of "minor" lines in the oxygen absorption (see arrows in **Fig.4(*a*)**; private communication, May 2020). OpenAI's ChatGPT helped us create Makefiles for our codes; it also helped the first author with the initial editing of the text, although submitted and revised texts have been independently and fully checked by the authors.

Sergey Korkin thanks the Richard M. Goody Award Selection Committee for their decision, anonymous colleagues for their nomination, and numerous fellow workers collaboration with whom resulted in the 2016 Award.

Authors contribution

SK: original draft and development of codes `gcell` and `aspect`; AMS: critical revision and editing of the original draft, numerical validation of intermediate results in `gcell`; AI: development of HAPI-based Python code for atmospheric absorption spectroscopy and validation of `aspect` results; AL: development of the original SHARM-IPC package, which LBL part we have refactored and updated in the current paper; funding acquisition for SK. All: review and editing of the manuscript.

Funding information

This work received no target funding (see Conclusion: last paragraph). However, the work of S. Korkin was partially supported by NASA Atmosphere Observing System (AOS) mission; the work of A. Lyapustin and S. Korkin was partially supported by NASA VIIRS, DSCOVR, and PACE programs via respective ROSES proposals (PI: A. Lyapustin); the work of A. M. Sayer and A. Ibrahim was partially supported by NASA PACE Project Science.

References

1. Abrarov S. M. and Quine B. M., “Sampling by incomplete cosine expansion of the sinc function: Application to the Voigt/complex error function”, *Applied Mathematics and Computation*, **258**, pp. 425-435, 2015. doi: https://doi.org/10.1016/j.amc.2015.01.072
2. Adorf C.S., Ramasubramani V., Anderson J. A., and Glotzer S.C., "How to Professionally Develop Reusable Scientific Software—And When Not To", *Computing in Science & Engineering*, **21** (2), pp. 66-79, 2019. doi: https://doi.org/10.1109/MCSE.2018.2882355
3. Amato U., Masiello G., Serio C., and Viggiano M., “The σ-IASI code for the calculation of infrared atmospheric radiance and its derivatives”, *Environmental Modelling & Software*, **17** (7), pp. 651–667, **2002**. doi: https://doi.org/10.1016/S1364-8152(02)00027-0
4. Armstrong B.H., “Spectrum line profiles: The Voigt function,” *Journal of Quantitative Spectroscopy and Radiative Transfer*, **7** (1), pp. 61-88, 1967. doi: https://doi.org/10.1016/0022-4073(67)90057-X
5. Arrhenius S., “On the influence of carbonic acid in the air upon the temperature of the ground”, *Philosophical Magazine and Journal of Science*, **41** (251), pp. 237-276, 1896. doi: https://doi.org/10.1080/14786449608620846
6. Arrhenius S., “On the influence of carbonic acid in the air upon the temperature of the Earth,” *Publications of the Astronomical Society of the Pacific*, **9** (54), pp. 14-24, 1897. https://www.jstor.org/stable/40670917

7. Bailey J. and Kedziora-Chudczer L., "Modelling the spectra of planets, brown dwarfs and stars using vstar", *Monthly Notices of the Royal Astronomical Society*, **419** (3), pp.1913-1929, 2012. doi: https://doi.org/10.1111/j.1365-2966.2011.19845.x

8. Baldridge A.M., Hook S.J., Grove C.I., and Rivera G., "The ASTER spectral library version 2.0", *Remote Sensing of Environment*, **113** (4), pp. 711-715, 2009. doi: https://doi.org/10.1016/j.rse.2008.11.007

9. Berk A., Conforti P., Kennett R., Perkins T., Hawes F., and van den Bosch J., "MODTRAN® 6: A major upgrade of the MODTRAN® radiative transfer code", *6th Workshop on Hyperspectral Image and Signal Processing: Evolution in Remote Sensing*, pp. 1-4, 2014. doi: https://doi.org/10.1109/WHISPERS.2014.8077573

10. Berk A. and Hawes F., "Validation of MODTRAN®6 and its line-by-line algorithm," *Journal of Quantitative Spectroscopy and Radiative Transfer*, **203**, pp. 542-556, 2017. doi: https://doi.org/10.1016/j.jqsrt.2017.03.004

11. Berk A., J. van den Bosch J., Hawes F., Perkins T., Conforti P. F., Acharya P.K., Anderson G.P., and Kennett R.G., *MODTRAN 6.0 User's Manual*. Kirtland AFB, NM: Air Force Research Laboratory, 2019. link: https://wiki.harvard.edu/confluence/download/attachments/301915384/MODTRAN 6 User's Manual.pdf

12. Bernath P. F., Steffen J., Crouse J., Boone C.D., Sixteen-year trends in atmospheric trace gases from orbit, *Journal of Quantitative Spectroscopy and Radiative Transfer*, 253, 107178, 2020. doi: https://doi.org/10.1016/j.jqsrt.2020.107178

13. Bertaux J.L., Lallement R., Ferron S., Boonne C., and Bodichon R., "TAPAS, a web-based service of atmospheric transmission computation for astronomy", *Astronomy & Astrophysics*, **564**, A46, 2014. doi: https://doi.org/10.1051/0004-6361/201322383

14. Binkley D., Davis M., Lawrie D., and Morrell C., "To camelcase or under_score", IEEE 17th International Conference on Program Comprehension, Vancouver, BC, Canada, pp. 158-167, 2009. doi: https://doi.org/10.1109/ICPC.2009.5090039

15. Bogumil K. and Coauthors, "Measurements of molecular absorption spectra with the SCIAMACHY pre-flight model: instrument characterization and reference data for atmospheric remote-sensing in the 230–2380 nm region", *Journal of Photochemistry and Photobiology A: Chemistry*, **157** (2–3), pp.167-184, 2003. doi: https://doi.org/10.1016/S1010-6030(03)00062-5

16. Bohren C. F., and Clothier E. E., *Fundamentals of Atmospheric Radiation: An Introduction with 400 Problems*, Wiley, 2006. doi: https://onlinelibrary.wiley.com/doi/book/10.1002/9783527618620

17. Boone C.D., Walker K.A., and Bernath P.F., "Speed-dependent Voigt profile for water vapor in infrared remote sensing applications", *Journal of Quantitative Spectroscopy and Radiative Transfer*, **105** (3), pp. 525–532, 2007. doi: https://doi.org/10.1016/j.jqsrt.2006.11.015

18. Boone C.D., Walker K.A., and Bernath P.F., "An efficient analytical approach for calculating line mixing in atmospheric remote sensing applications", *Journal of Quantitative Spectroscopy and Radiative Transfer*, **112** (6), pp. 980–989, 2011. doi: https://doi.org/10.1016/j.jqsrt.2010.11.013

19. Bourassa A.E., Degenstein D.A., and Llewellyn E.J., "SASKTRAN: A spherical geometry radiative transfer code for efficient estimation of limb scattered sunlight", *Journal of Quantitative Spectroscopy and Radiative Transfer*, **109** (1), pp. 52-73, 2008. doi: https://doi.org/10.1016/j.jqsrt.2007.07.007

20. Böhlke J. K., de Laeter J. R., De Bièvre P., Hidaka H., Peiser H. S., Rosman K. J. R., and Taylor P. D. P., "Isotopic Compositions of the Elements, 2001", *Journal of Physical and Chemical Reference Data*, **34** (1), pp. 57 - 67, 2005. doi: https://doi.org/10.1063/1.1836764

21. Buehler S.A., Mendrok J., Eriksson P., Perrin A., Larsson R., and Lemke O., "ARTS, the Atmospheric Radiative Transfer Simulator – version 2.2, the planetary toolbox edition", *Geoscientific Model Development*, **11** (4), pp. 1537-1556, 2018. doi: https://doi.org/10.5194/gmd-11-1537-2018

22. Burch D.E., "Continuum absorption by H_2O", AFGL Technical Report, 1982. link: https://apps.dtic.mil/sti/citations/ADA112264

23. Carissimo A., De Feis I., and Serio C., "The physical retrieval methodology for IASI: the δ-IASI code", *Environmental Modelling & Software*, **20** (9), pp. 1111-1126, 2005. doi: https://doi.org/10.1016/j.envsoft.2004.07.003

24. Chance K. and Kurucz R.L., "An improved high-resolution solar reference spectrum for earth's atmosphere measurements in the ultraviolet, visible, and near infrared", *Journal of Quantitative Spectroscopy and Radiative Transfer*, **111** (9), pp.1289-1295, 2010. doi: https://doi.org/10.1016/j.jqsrt.2010.01.036

25. Chapman I.M., Naylor D., Gom B.G., Querel R.R., and Davis-Imhof P., "BTRAM : An Interactive Atmospheric Radiative Transfer Model" in *The 30th Canadian Symposium on Remote Sensing*, pp. 22–25, 2010. link: https://blueskyspectroscopy.com/

26. Chen W., Ren T., and Zhao C., "A machine learning based model for gray gas emissivity and absorptivity of H2O-CO2-CO-N2 mixtures", *Journal of Quantitative Spectroscopy and Radiative Transfer*, **312**: 108798, 2024. doi: https://doi.org/10.1016/j.jqsrt.2023.108798

27. Chen X. and Coauthors, "First retrieval of absorbing aerosol height over dark target using TROPOMI oxygen B band: Algorithm development and application for surface particulate matter estimates", *Remote Sensing of Environment*, **265**, 112674, 2021. doi: https://doi.org/10.1016/j.rse.2021.112674

28. Clough S.A., Kneizys F.X., Rothman L.S., and Gallery W.O., "Atmospheric Spectral Transmittance And Radiance: FASCOD1B", *Proceedings of SPIE*, **277**, pp. 152–166, 1981. doi: https://doi.org/10.1117/12.931914

29. Clough S.A., Kneizys F.X., and Davies R.W., "Line shape and the water vapor continuum," *Atmospheric Research*, **23** (3-4), pp. 229–241, 1989. doi: https://doi.org/10.1016/0169-8095(89)90020-3

30. Clough S.A., Shephard M.W., Mlawer E.J., Delamere J.S., Iacono M.J., Cady-Pereira K., Boukabara S., and Brown P.D., "Atmospheric radiative transfer modeling: A summary of the AER codes", *Journal of Quantitative Spectroscopy and Radiative Transfer*, **91** (2), pp. 233–244, 2005. doi: https://doi.org/10.1016/j.jqsrt.2004.05.058

31. Coakley J., and Yang P., *Atmospheric Radiation: A Primer with Illustrative Solutions*, Willey Series in Atmospheric Radiation and Remote Sensing (Ed. A. Kokhanovsky), 2014. link: N/A.

32. Coddington O. M., Richard E. C., Harber D., Pilewskie P., Woods T. N., Chance K., Liu X., and Sun K., "The TSIS-1 Hybrid Solar Reference Spectrum", *Geophysical Research Letters*, **48**, e2020GL091709, 2023. doi: https://doi.org/10.1029/2020GL091709

33. Collange S., Daumas M., and Defour D., "Line-by-line spectroscopic simulations on graphics processing units", *Computer Physics Communications*, **178** (2), pp. 135–143, 2008. doi: https://doi.org/10.1016/j.cpc.2007.08.013

34. Cornette W.M., Acharya P.K., and Anderson G.P., "Using the MOSART code for atmospheric correction", *Proceedings of IGARSS '94 - 1994 IEEE International Geoscience and Remote Sensing Symposium*, pp. 215–219, 1994. doi: https://doi.org/10.1109/IGARSS.1994.399084

35. De Biévre P., Gallet M., Holden N. E., and Barnes I. L., "Isotopic abundances and atomic weights of the elements", *Journal of Physical and Chemical Reference Data*, **13**, pp. 809 - 891, 1984. doi: https://doi.org/10.1063/1.555720

36. Delahaye T. and Coauthors, "The 2020 edition of the GEISA spectroscopic database", *Journal of Molecular Spectroscopy*, **380**, 111510, 2021. doi: https://doi.org/10.1016/j.jms.2021.111510

37. Dicke R.H., "The effect of collisions upon the Doppler width of spectral lines", *Physical Review*, **89** (2), pp.472-473, 1953. doi: https://link.aps.org/doi/10.1103/PhysRev.89.472

38. Diner D. J. and Coauthors, "The Airborne Multiangle SpectroPolarimetric Imager (AirMSPI): a new tool for aerosol and cloud remote sensing", *Atmospheric Measurement Techniques*, **6**, pp. 2007–2025, 2013. doi: https://doi.org/10.5194/amt-6-2007-2013

39. Docter N., Preusker R., Filipitsch F., Kritten L., Schmidt F., and Fischer, J., "Aerosol optical depth retrieval from the EarthCARE Multi-Spectral Imager: the M-AOT product", Atmospheric Measurement Techniques, **16**, pp. 3437–3457, 2023. doi: https://doi.org/10.5194/amt-16-3437-2023

40. Domysławska J., Wójtewicz S., Masłowski P., Cygan A., Bielska K., Trawiński R.S., Ciuryło R., and Lisak D., "A new approach to spectral line shapes of the weak oxygen transitions for atmospheric applications", *Journal of Quantitative Spectroscopy and Radiative Transfer*, 169, pp.111-121, 2016. doi: https://doi.org/10.1016/j.jqsrt.2015.10.019

41. Dudhia A., "The Reference Forward Model (RFM)," *Journal of Quantitative Spectroscopy and Radiative Transfer*, **186**, pp. 243–253, 2017. doi: https://doi.org/10.1016/j.jqsrt.2016.06.018

42. Dubey A., "Good Practices for High-Quality Scientific Computing", *Computing in Science & Engineering*, 24 (6), pp. 72-76, 2022. doi: https://doi.ieeecomputersociety.org/10.1109/MCSE.2023.3259259

43. Easterbrook S.M. and Johns T.C., "Engineering the Software for Understanding Climate Change", *Computing in Science & Engineering*, **11** (6), pp. 65-74, 2009. doi: https://doi.org/10.1109/MCSE.2009.193

44. Edwards D.P., "GENLN2: A General Line-by-line Atmospheric Transmittance and Radiance Model. Version 3.0 Description and Users Guide", University Corporation for Atmospheric Research (UCAR) Technical Report, No. NCAR/TN-367+STR, 1992. doi: http://dx.doi.org/10.5065/D6W37T86

45. Efremenko D., and Kokhanovsky A., *Foundations of Atmospheric Remote Sensing*, Springer, 2021. doi: https://doi.org/10.1007/978-3-030-66745-0

46. Elsasser W.M., *Heat transfer by infrared radiation in the atmosphere*, Harvard University Press, Cambridge, 108 pp., 1942. link: https://archive.org/details/ElsasserFull1942

47. Emde C. and Coauthors, "The libRadtran software package for radiative transfer calculations (version 2.0.1)", *Geoscientific Model Development*, **9** (5), pp. 1647-1672, 2016. doi: https://doi.org/10.5194/gmd-9-1647-2016

48. Fels S.B., "Simple strategies for inclusion of Voigt effects in infrared cooling rate calculations", *Applied Optics*, **18** (15), pp. 2634 - 2637, 1979. doi: https://doi.org/10.1364/AO.18.002634

49. Foote E., "Circumstances Affecting the Heat of the Sun's Rays", *American Journal of Art and Science*, 22 (66), pp. 383–384, 1856. link: https://en.wikipedia.org/wiki/Eunice_Newton_Foote (see Section "Scientific Career")

50. Galatry L., "Simultaneous Effect of Doppler and Foreign Gas Broadening on Spectral Lines", *Physical Review*, **122** (4), pp. 1218–1223, 1961. doi: https://doi.org/10.1103/PhysRev.122.1218

51. Gamache R.R. and Coauthors, "Total internal partition sums for 166 isotopologues of 51 molecules important in planetary atmospheres: Application to HITRAN2016 and beyond," *Journal of Quantitative Spectroscopy and Radiative Transfer*, **203**, pp. 70–87, 2017. doi: https://doi.org/10.1016/j.jqsrt.2017.03.045

52. Gamache R.R., Vispoel B., Rey M., Nikitin A., Tyuterev V., Egorov O., Gordon I.E., and Boudon V., "Total internal partition sums for the HITRAN2020 database", *Journal of Quantitative Spectroscopy and Radiative Transfer*, **271**, 107713, 2021. doi: https://doi.org/10.1016/j.jqsrt.2021.107713

53. Gao B.-C., Heidebrecht K.B., and Goetz A.F.H., "Derivation of scaled surface reflectances from AVIRIS data", *Remote Sensing of Environment*, **44** (2-3), pp. 165–178, 1993. doi: https://doi.org/10.1016/0034-4257(93)90014-O

54. Goldenstein C.S., Miller V.A., Spearrin R.M., and Strand C.L., "SpectraPlot.com: Integrated spectroscopic modeling of atomic and molecular gases," *Journal of Quantitative Spectroscopy and Radiative Transfer*, **200**, pp. 249–257, 2017. doi: https://doi.org/10.1016/j.jqsrt.2017.06.007

55. Goody R.M., and Yung Y.L., *Atmospheric Radiation. Theoretical Basis*. Oxford University Press, 2nd Edition, 1989. link: N/A.

56. Gordley L.L., Marshall B.T., and Chu D.A., "Linepak: Algorithms for modeling spectral transmittance and radiance", *Journal of Quantitative Spectroscopy and Radiative Transfer*, **52** (5), pp. 563–580, 1994. doi: https://doi.org/10.1016/0022-4073(94)90025-6

57. Gordon H. R., *Physical Principles of Ocean Color Remote Sensing*, University of Miami, 2019. doi: https://doi.org/10.33596/ppocrs-19

58. Gordon I.E., Rothman L.S., and Toon G. C., "Revision of spectral parameters for the B- and γ-bands of oxygen and their validation against atmospheric spectra", *Journal of Quantitative Spectroscopy and Radiative Transfer*, **112** (14), pp. 2310–2322, 2011, doi: 10.1016/j.jqsrt.2011.05.007.

59. Gordon I.E., Potterbusch M.R., Bouquin D., Erdmann C.C., Wilzewski J.S., and Rothman L. S., "Are your spectroscopic data being used?", *Journal of Molecular Spectroscopy*, **327**, pp. 232–238, 2016. doi: https://doi.org/10.1016/j.jms.2016.03.011

60. Gordon I.E. and Coauthors, "The HITRAN2016 molecular spectroscopic database," *Journal of Quantitative Spectroscopy and Radiative Transfer*, **203**, pp. 3–69, 2017. doi: https://doi.org/10.1016/j.jqsrt.2017.06.038

61. Gottschling P., *Discovering Modern C++. An Intensive Course for Scientists, Engineers, and Programmers*, 2nd Edition, Addison-Wesley Professional, 576 pp. 2021. link: N/A.

62. Greenblatt G. D., Orlando J. J., Burkholder J. B., and Ravishankara A. R., "Absorption measurements of oxygen between 330 and 1140 nm", *Journal of Geophysical Research*, 95(D11), pp.18577 – 18582, 1990. doi: https://doi.org/10.1029/JD095iD11p18577

63. Gueymard C.A., "Parameterized transmittance model for direct beam and circumsolar spectral irradiance", *Solar Energy*, **71** (5), pp. 325 – 346, 2001. doi: https://doi.org/10.1016/S0038-092X(01)00054-8

64. Havemann S., Thelen J.C., Taylor J.P., and Harlow R.C., "The Havemann-Taylor Fast Radiative Transfer Code (HT-FRTC): A multipurpose code based on principal components", *Journal of Quantitative Spectroscopy and Radiative Transfer*, **220**, pp. 180–192, 2018. doi: https://doi.org/10.1016/j.jqsrt.2018.09.008

65. He W., Wu K., Feng Y., Fu D., Chen Z., and Li F., "The Radiative Transfer Characteristics of the O2 Infrared Atmospheric Band in Limb-Viewing Geometry", *Remote Sensing*, 11(22): 2702, 2019. doi: https://doi.org/10.3390/rs11222702

66. Hearn A.G., "The Absorption of Ozone in the Ultra-violet and Visible Regions of the Spectrum", *Proceedings of the Physical Society*, **78** (5), pp. 932-940, 1961. link: https://iopscience.iop.org/article/10.1088/0370-1328/78/5/340

67. Heaton D. and Carver J.C., "Claims about the use of software engineering practices in science: A systematic literature review", Information and Software Technology, 67, pp. 207-219, 2015. doi: https://doi.org/10.1016/j.infsof.2015.07.011

68. Hinsen K., "Dealing With Software Collapse", *Computing in Science & Engineering*, 21 (3), pp.104-108, 2019. doi: https://doi.org/10.1109/MCSE.2019.2900945

69. Hollis M.D.J., Tessenyi M., and Tinetti G., "Tau: A 1D radiative transfer code for transmission spectroscopy of extrasolar planet atmospheres", *Computer Physics Communications*, **184** (10), pp. 2351–2361, 2013. doi: https://doi.org/10.1016/j.cpc.2013.05.011

70. Hollis M.D.J., Tessenyi M., and Tinetti G., “TAU: A 1D radiative transfer code for transmission spectroscopy of extrasolar planet atmospheres”, *Computer Physics Communications*, 185 (2), p. 695, 2014. doi: https://doi.org/10.1016/j.cpc.2013.05.011

71. Hill C., Gordon I.E., Rothman L.S., and Tennyson J., “A new relational database structure and online interface for the HITRAN database”, *Journal of Quantitative Spectroscopy and Radiative Transfer*, **130**, pp. 51–61, 2013. doi: https://doi.org/10.1016/j.jqsrt.2013.04.027

72. Hill C., Gordon I.E., Kochanov R.V., Barrett L., Wilzewski J.S., and Rothman L.S., “HITRANonline: An online interface and the flexible representation of spectroscopic data in the HITRAN database,” *Journal of Quantitative Spectroscopy and Radiative Transfer*, **177**, pp. 4-14, 2016. doi: https://doi.org/10.1016/j.jqsrt.2015.12.012

73. Humlíček J., “Optimized computation of the Voigt and complex probability functions,” *Journal of Quantitative Spectroscopy and Radiative Transfer*, 27 (4), pp. 437-444, 1982. doi: https://doi.org/10.1016/0022-4073(82)90078-4

74. Ibrahim A., Franz B., Ahmad Z., Healy R., Knobelspiesse K., Gao B-C, Proctor C, and Zhai P.-W., “Atmospheric correction for hyperspectral ocean color retrieval with application to the Hyperspectral Imager for the Coastal Ocean (HICO)”, *Remote Sensing of Environment*, **204**, pp.60-75, 2018. doi: https://doi.org/10.1016/j.rse.2017.10.041

75. Iwabuchi H. and Okamura R., “Multispectral Monte Carlo radiative transfer simulation by the maximum cross-section method”, *Journal of Quantitative Spectroscopy and Radiative Transfer*, **193**, pp. 40-46, 2017. doi: https://doi.org/10.1016/j.jqsrt.2017.01.025

76. Kanewala U. and Bieman J.M., “Testing scientific software: A systematic literature review”, Information and Software Technology, **56** (10), pp. 1219-1232, 2014. doi: https://doi.org/10.1016/j.infsof.2014.05.006

77. Kendall R., Fisher D., Henderson D., Carver J., Mark A., Post D., Rhoades Jr. C.E., and Squires S., "Development of a Weather Forecasting Code: A Case Study", *IEEE Software*, **25** (4), pp. 59-65, 2008. doi: https://doi.org/10.1109/MS.2008.86

78. Karlovets E.V., Mondelain D., Tashkun S.A., and Campargue A., “The absorption spectrum of nitrous oxide between 7250 and 7653 cm-1”, *Journal of Quantitative Spectroscopy and Radiative Transfer*, **301**, 108511, 2023. doi: https://doi.org/10.1016/j.jqsrt.2023.108511

79. Karman T., Koenis M. A. J., Banerjee A., Parker D. H., Gordon I. E., van der Avoird A., van der Zande W. J., and Groenenboom G. C., “O2−O2 and O2−N2 collision-induced absorption mechanisms unravelled”, *Nature Chemistry*, **10** (5), pp. 549-554, 2018. doi: https://doi.org/10.1038/s41557-018-0015-x

80. Karman T., and Coauthors, “Update of the HITRAN collision-induced absorption section”, *Icarus*, **328**, pp.160-175, 2019. doi: https://doi.org/10.1016/j.icarus.2019.02.034

81. Key J.R. and Schweiger A.J., “Tools for atmospheric radiative transfer: STREAMER and FLUXNET”, *Computers & Geosciences*, **24** (5), pp. 443-451, 1998. doi: https://doi.org/10.1016/S0098-3004(97)00130-1

82. Kistenev Yu.V., Skiba V.E., Prischepa V.V., Vrazhnov D.A., and Borisov A.V., “Super-resolution reconstruction of noisy gas-mixture absorption spectra using deep learning”,

Journal of Quantitative Spectroscopy and Radiative Transfer, 289: 108278, 2022. doi: https://doi.org/10.1016/j.jqsrt.2022.108278

83. Kneizys F.X., Shettle E.P., Abreu L.W., Chetwynd J.H., Anderson G.P., Gallery W.O., Selby J.E.A., and Clough S.A., "Users Guide to LOWTRAN 7", Hanscom AFB, MA: Air Force Geophysics Laboratory, 1988. link: https://apps.dtic.mil/sti/citations/ADA206773
84. Kneizys F. X. and Coauthors, *The MODTRAN 2/3 Report and LOWTRAN 7 Model*, North Andover, MA, 1996. link: https://web.gps.caltech.edu/~vijay/pdf/modrept.pdf
85. Kochanov R.V., Gordon I.E., Rothman L.S., Wcisło P., Hill C., and Wilzewski J.S., "HITRAN Application Programming Interface (HAPI): A comprehensive approach to working with spectroscopic data", *Journal of Quantitative Spectroscopy and Radiative Transfer*, **177**, pp. 15-30, 2016. doi: https://doi.org/10.1016/j.jqsrt.2016.03.005
86. Kochanov R. V., and Coauthors, "Infrared absorption cross-sections in HITRAN2016 and beyond: Expansion for climate, environment, and atmospheric applications", *Journal of Quantitative Spectroscopy and Radiative Transfer*, **230**, pp. 172-221, 2019. doi: https://doi.org/10.1016/j.jqsrt.2019.04.001
87. Korkin S., Sayer A.M., Ibrahim A., and Lyapustin A., "A practical guide to writing a radiative transfer code", *Computer Physics Communications*, **271**, 108198, 2022. doi: https://doi.org/10.1016/j.cpc.2021.108198
88. Kuntz M., "A new implementation of the Humlíček algorithm for the calculation of the Voigt profile function", *Journal of Quantitative Spectroscopy and Radiative Transfer*, **57** (60), pp. 819-824, 1997. doi: https://doi.org/10.1016/S0022-4073(96)00162-8
89. Kurucz R.L., "Synthetic infrared spectra", *Infrared Solar Physics*, IAU Symp. **154**, edited by D.M. Rabin and J.T. Jefferies, Kluwer, Acad., Norwell Massachusetts, pp. 523-531, 1992. link: https://adsabs.harvard.edu/full/1994IAUS..154..523K
90. Kurucz R.L., "The solar irradiance by computation", (unpublished) 1997. link: http://kurucz.harvard.edu/sun/irradiance/solarirr.tab
91. Laraia A.L., Gamache R.R., Lamouroux J., Gordon I.E., and Rothman L.S., "Total internal partition sums to support planetary remote sensing", *Icarus*, **215** (1), pp. 391-400, 2011. doi: https://doi.org/10.1016/j.icarus.2011.06.004
92. Laszlo I., Stamnes K., Wiscombe W., and Tsay S.-C., "The Discrete Ordinate Algorithm, DISORT for Radiative Transfer," in *Light Scattering Reviews*, Springer., A. A. Kokhanovsky, Ed. Berlin, 2016, pp. 3–65. doi: https://doi.org/10.1007/978-3-662-49538-4_1
93. LeVeque R.J., Mitchell I.M., and Stodden V., "Reproducible research for scientific computing: Tools and strategies for changing the culture", *Computing in Science & Engineering*, **14** (4), pp. 13-17, 2012. doi: https://doi.org/10.1109/MCSE.2012.38
94. Liou K. N., *An Introduction to Atmospheric Radiation* (2nd Ed.), Academic Press, 2002. link: https://shop.elsevier.com/books/an-introduction-to-atmospheric-radiation/liou/978-0-12-451451-5
95. Liu X., Yang Q., Li H., Jin Z., Wu W., Kizer S., Zhou D.K., and Yang P., "Development of a fast and accurate PCRTM radiative transfer model in the solar spectral region", *Applied Optics*, **55** (29), pp. 8236-8247, 2016. doi: https://doi.org/10.1364/AO.55.008236

96. Lyapustin A.I., "Interpolation and Profile Correction (IPC) Method for Shortwave Radiative Transfer in Spectral Intervals of Gaseous Absorption," *Journal of the Atmospheric Sciences*, **60** (6), pp. 865–871, 2003. doi: https://doi.org/10.1175/1520-0469(2003)060%3C0865:IAPCIM%3E2.0.CO;2

97. Lyapustin A., Muldashev T., and Wang Y., "Code SHARM: fast and accurate radiative transfer over spatially variable anisotropic surfaces," in *Light Scattering Reviews 5. Single light scattering and radiative transfer* (A. Kokhanovsky, Ed.), Chichester, UK: Springer, 2010, pp. 205–247. doi: https://doi.org/10.1007/978-3-642-10336-0_6

98. Luther F. M., Ellingson R. G., Fouquart Y., Fels S., Scott N. A., and Wiscombe W. J., "Intercomparison of Radiation Codes in Climate Models (ICRCCM): Longwave Clear-Sky Results – A Workshop Summary", *Bulletin of the American Meteorological Society*, **69**, pp. 40 – 48, 1988. doi: https://doi.org/10.1175/1520-0477-69.1.40

99. McClatchey R.A., Benedict W.S., Clough S.A., Burch D.E., Calfee R.F., Fox K., Rothman L.S., and Garing J.S., "AFCRL Atmospheric Absorption Line Parameters Compilation", Air Force Cambridge Research Laboratories, Bedford MA, 1973. link: https://modis-images.gsfc.nasa.gov/JavaHAWKS/AFCRL_AALPC.pdf

100. McLean A. B., Mitchell C. E. J., and Swanston D. M., "Implementation of an efficient analytical approximation to the Voigt function for photoemission lineshape analysis", *Journal of Electron Spectroscopy and Related Phenomena*, **69** (2), pp. 125–132, 1994. doi: https://doi.org/10.1016/0368-2048(94)02189-7

101. Mlawer E.J., Taubman S.J., Brown P.D., Iacono M.J., and Clough S.A., "Radiative transfer for inhomogeneous atmospheres: RRTM, a validated correlated-*k* model for the longwave," *Journal of Geophysical Research: Atmospheres*, **102** (D14), pp. 16663–16682, 1997. doi: https://doi.org/10.1029/97JD00237

102. Mlawer E.J., Payne V.H., Moncet J.L., Delamere J.S., Alvarado M.J., and Tobin D.C., "Development and recent evaluation of the MT-CKD model of continuum absorption", *Philosophical Transactions of the Royal Society A*, **370**, pp. 2520–2556, 2012. doi: https://doi.org/10.1098/rsta.2011.0295

103. Mlawer E.J., Cady-Pereira K.E., Mascio J., and Gordon I.E., "The inclusion of the MT_CKD water vapor continuum model in the HITRAN molecular spectroscopic database", *Journal of Quantitative Spectroscopy and Radiative Transfer*, **306**, 108645, 2023. doi: https://doi.org/10.1029/97JD00237

104. Mobley C. D. (Editor), *The Oceanic Optics Book*, International Ocean Colour Coordinating Group (IOCCG), Dartmouth, NS, Canada, 924 pp., 2022. doi: http://dx.doi.org/10.25607/OBP-1710

105. Mohankumar N. and Sen S., "On the very accurate evaluation of the Voigt functions," *Journal of Quantitative Spectroscopy and Radiative Transfer*, **224**, pp. 192–196, 2019. doi: https://doi.org/10.1016/j.jqsrt.2018.11.022

106. Müller H.S.P., Schlöder F., Stutzki J., and Winnewisser G., "The Cologne Database for Molecular Spectroscopy, CDMS: a useful tool for astronomers and spectroscopists", *Journal*

of Molecular Structure, **742** (1-3), pp. 215–227, 2005. doi: https://doi.org/10.1016/j.molstruc.2005.01.027

107. Natraj V., Spurr R. J. D., Boesch H., Jiang Y., and Yung Y. L., "Evaluation of errors from neglecting polarization in the forward modeling of O2 A band measurements from space, with relevance to CO2 column retrieval from polarization-sensitive instruments", *Journal of Quantitative Spectroscopy and Radiative Transfer*, **103** (2), pp. 245–259, 2007, doi: 10.1016/j.jqsrt.2006.02.073.

108. Ngo N. H., Lisak D., Tran H., and Hartmann J. M., "An isolated line-shape model to go beyond the Voigt profile in spectroscopic databases and radiative transfer codes", *Journal of Journal of Quantitative Spectroscopy and Radiative Transfer*, **129**, pp. 89–100, 2013. doi: https://doi.org/10.1016/j.jqsrt.2013.05.034

109. Ngo N. H., Lisak D., Tran H., and Hartmann J. M., "Erratum to 'An isolated line-shape model to go beyond the Voigt profile in spectroscopic databases and radiative transfer codes' [J. Quant. Spectrosc. Radiat. Transf. 129 (2013) 89-100]", *Journal of Journal of Quantitative Spectroscopy and Radiative Transfer*, **134**, p. 105, 2014. doi: http://dx.doi.org/10.1016/j.jqsrt.2013.10.016

110. Nordebo S., "Uniform error bounds for fast calculation of approximate Voigt profiles" *Journal of Quantitative Spectroscopy and Radiative Transfer*, **270**, 107715, 2021. doi: https://doi.org/10.1016/j.jqsrt.2021.107715

111. Nowlan C. R., McElroy C. T., and Drummond J. R., "Measurements of the O2A - and B-bands for determining temperature and pressure profiles from ACE-MAESTRO: Forward model and retrieval algorithm", *Journal of Quantitative Spectroscopy and Radiative Transfer*, **108** (3), pp. 371–388, 2007. doi: https://doi.org/10.1016/j.jqsrt.2007.06.006

112. Oliveira S., and Stewart D., *Writing Scientific Software: A Guide to Good Style*, Cambridge University Press, New York, 303 pp., 2006.

113. Orphal J., and Coauthors, "Absorption cross-sections of ozone in the ultraviolet and visible spectral regions: Status report 2015", Journal of Molecular Spectroscopy, **327**, pp. 105-121, 2016. doi: http://dx.doi.org/10.1016/j.jms.2016.07.007

114. Pannier E. and Laux C.O., "RADIS: A nonequilibrium line-by-line radiative code for CO2 and HITRAN-like database species", *Journal of Quantitative Spectroscopy and Radiative Transfer*, **222–223**, pp. 12–25, 2019. doi: https://doi.org/10.1016/j.jqsrt.2018.09.027

115. Payne V.H. and Coauthors, "Absorption coefficient (ABSCO) tables for the Orbiting Carbon Observatories: Version 5.1", *Journal of Quantitative Spectroscopy and Radiative Transfer*, **255**, 2020. doi: https://doi.org/10.1016/j.jqsrt.2020.107217

116. Petty G. W., *A First Course in Atmospheric Radiation* (2nd ed.), Sundog Publishing, Madison, Wisconsin, 2006. Link: N/A.

117. Pfeilsticker K., Erle F., Funk O., Veitel H., and Platt U., "First geometrical pathlengths probability density function derivation of the skylight from spectroscopically highly resolving oxygen A-band observations: 1. Measurement technique, atmospheric observations and model calculations", *Journal of Geophysical Research: Atmospheres*, **103** (D10), pp. 11483–11504, 1998. doi: https://doi.org/10.1029/98JD00725

118. Pickett H.M., Poynter R.L., Cohen E.A., Delitsky M.L., Pearson J.C., and Muller H.S.P., "Submillimeter, millimeter, and microwave spectral line catalog", *Journal of Quantitative Spectroscopy and Radiative Transfer*, **60** (5), pp. 883–890, 1998. doi: https://doi.org/10.1016/S0022-4073(98)00091-0

119. Pincus R. and Coauthors, "Benchmark calculations of radiative forcing by greenhouse gases", *Journal of Geophysical Research*, **125**: e2020JD033483, 2020. doi: https://doi.org/10.1029/2020JD033483

120. Pipitone J. and Easterbrook S., "Assessing climate model software quality: a defect density analysis of three models", *Geoscientific Model Development*, **5**, 1009–1022, 2012. doi: https://doi.org/10.5194/gmd-5-1009-2012

121. Pliutau D. and Roslyakov K., "Bytran - |- spectral calculations for portable devices using the HITRAN database", *Earth Science Informatics*, **10**, pp. 395–404, 2017. doi: https://doi.org/10.1007/s12145-017-0288-4

122. Pouillet C., "Memoir on the solar heat, on the radiating and absorbing powers of atmospheric air, and on the temperature of space", in *Scientific Memoirs, Selected from the Transactions of Foreign Academies of Science and Learned Societies, and from Foreign Journals* (Taylor R., Editor), London, England: Richard and John E. Taylor, pp.44-90, 1846. link: https://en.wikipedia.org/wiki/Claude_Pouillet (see Ref. 6: English translation for pdf)

123. Predoi-Cross A., Hambrook K., Keller R., Povey C., Schofield I., HurtmansD., Over H., and Mellau G. Ch., "Spectroscopic lineshape study of the self-perturbed oxygen A-band", *Journal of Molecular Spectroscopy*, **248** (2), pp. 85–110, 2008. doi: https://doi.org/10.1016/j.jms.2007.11.007

124. Press W.H., Teukolsky S.A., Vettering W.T., and Flannery B.P , *Numerical Recipes in C: the Art of Scientific Computing*, Cambridge University Press, New York, 1992. link: link: https://numerical.recipes/

125. Press W.H., Teukolsky S.A., Vettering W.T., and Flannery B.P , *Numerical Recipes. The Art of Scientific Computing*, Cambridge University Press, New York, 2007. link: https://numerical.recipes/

126. Prischepa V.V., Skiba V.E., Vrazhnov D.A., Kistenev Yu. V., "Gas mixtures IR absorption spectra decomposition using a deep neural network", *Journal of Quantitative Spectroscopy and Radiative Transfer*, **301**: 108521, 2023. doi: https://doi.org/10.1016/j.jqsrt.2023.108521

127. Puthukkudy A., Martins J. V., Remer L. A., Xu X., Dubovik O., Litvinov P., McBride B., Burton S., and Barbosa H. M. J., "Retrieval of aerosol properties from Airborne Hyper-Angular Rainbow Polarimeter (AirHARP) observations during ACEPOL 2017", *Atmospheric Measurement Techniques*, **13**, 5207–5236, 2020. doi: https://doi.org/10.5194/amt-13-5207-2020

128. Rautian S. G., and Sobel'man I. I., "The effect of collisions on the Doppler broadening of spectral lines", *Soviet Physics Uspekhi*, **9** (5), pp.701-716, 1967. doi: https://dx.doi.org/10.1070/PU1967v009n05ABEH003212

129. Richard C., and Coauthors, "New section of the HITRAN database: Collision-induced absorption (CIA)", *Journal of Quantitative Spectroscopy and Radiative Transfer*, 113 (11), pp. 1276-1285, 2012. doi: https://doi.org/10.1016/j.jqsrt.2011.11.004

130. Rothman L.S., "Update of the AFGL atmospheric absorption line parameters compilation", *Applied Optics*, **17** (22), pp. 3517–3518, 1978. doi: https://doi.org/10.1364/AO.17.003517

131. Rothman L.S. and Coauthors, "The HITRAN database: 1986 edition", *Applied Optics*, **26** (19), pp. 4058–4097, 1987. doi: https://doi.org/10.1364/AO.26.004058

132. Rothman L.S. and Coauthors, "The HITRAN molecular spectroscopic database and HAWKS (HITRAN atmospheric workstation): 1996 edition", *Journal of Quantitative Spectroscopy and Radiative Transfer*, 60 (5), pp. 665-710, 1998. doi: https://doi.org/10.1016/S0022-4073(98)00078-8

133. Rothman L.S. and Coauthors, "The HITRAN molecular spectroscopic database: edition of 2000 including updates through 2001", *Journal of Quantitative Spectroscopy and Radiative Transfer*, **82** (1-4), pp. 5–44, 2003. doi: https://doi.org/10.1016/S0022-4073(03)00146-8

134. Rothman L.S. and Coauthors, "The HITRAN 2004 molecular spectroscopic database", *Journal of Quantitative Spectroscopy and Radiative Transfer*, **96** (2), pp. 139–204, 2005. doi: https://doi.org/10.1016/j.jqsrt.2004.10.008

135. Rothman L.S., Jacquinet-Husson N., Boulet C., and Perrin A. M., "History and future of the molecular spectroscopic databases", *Comptes Rendus Physique*, **6**(8), pp.897-907, 2005. doi: https://doi.org/10.1016/j.crhy.2005.09.001

136. Rothman L.S. and Coauthors, "The HITRAN 2008 molecular spectroscopic database," *Journal of Quantitative Spectroscopy and Radiative Transfer*, **110** (9–10), pp. 533–572, 2009. doi: https://doi.org/10.1016/j.jqsrt.2009.02.013

137. Rothman L.S., "The evolution and impact of the HITRAN molecular spectroscopic database", *Journal of Quantitative Spectroscopy and Radiative Transfer*, **111** (11), pp. 1565–1567, 2010. doi: https://doi.org/10.1016/j.jqsrt.2010.01.027

138. Rothman L.S., and Coauthors, "The HITRAN2012 molecular spectroscopic database", *Journal of Quantitative Spectroscopy and Radiative Transfer*, **130**, pp. 4-50. doi: http://dx.doi.org/10.1016/j.jqsrt.2013.07.002

139. Rothman L.S., "History of the HITRAN Database", *Nature Reviews Physics*, **3** (5), pp. 302–304, 2021. doi: https://doi.org/10.1038/s42254-021-00309-2

140. Rozanov V.V., Rozanov A.V., Kokhanovsky A.A., and Burrows J.P., "Radiative transfer through terrestrial atmosphere and ocean : Software package SCIATRAN," *Journal of Quantitative Spectroscopy and Radiative Transfer*, **133**, pp. 13–71, 2014 doi: https://doi.org/10.1016/j.jqsrt.2013.07.004

141. Ruyten W., "Comment on 'A new implementation of the Humlíček algorithm for the calculation of the Voigt profile function' by M. Kuntz [JQSRT 57(6) (1997) 819–824]", *Journal of Quantitative Spectroscopy and Radiative Transfer*, **86** (2), pp. 231-233, 2004. doi: https://doi.org/10.1016/j.jqsrt.2003.12.027

142. Sanders R. and Kelly D., "Dealing with Risk in Scientific Software Development", *IEEE Software*, **25** (4), pp. 21-28, 2008. doi: https://doi.org/10.1109/MS.2008.84

143. Sayer A.M., Lelli L., Cairns B., van Diedenhoven B., Ibrahim A., Knobelspiesse K.D., Korkin S., and Werdell P.J., "The CHROMA cloud-top pressure retrieval algorithm for the Plankton, Aerosol, Cloud, ocean Ecosystem (PACE) satellite mission", Atmospheric Measurement Techniques, 16 (4), pp.969-996, 2023. doi: https://doi.org/10.5194/amt-16-969-2023

144. Saunders R., Matricardi M., and Brunel P., "An improved fast radiative transfer model for assimilation of satellite radiance observations", *Quarterly Journal of Royal Meteorological Society*, **125** (556), pp. 1407-1425, 1999. doi: https://doi.org/10.1002/qj.1999.49712555615

145. Segal J. and Morris C., "Developing Scientific Software", *IEEE Software*, **25** (4), pp. 18-20, 2008. doi: https://doi.ieeecomputersociety.org/10.1109/MS.2008.85

146. Schreier F., "The Voigt and complex error function: A comparison of computational methods", *Journal of Quantitative Spectroscopy and Radiative Transfer*, **48** (5), pp. 743-762, 1992. doi: https://doi.org/10.1016/0022-4073(92)90139-U

147. Schreier F. and Schimpf B., "A New Efficient Line-By-Line Code for High Resolution Atmospheric Radiation Computations incl. Derivatives", IRS 2000: Current Problems in Atmospheric Radiation, A. Deepak Publishing, pp.381-385, 2001. link: https://www.gbv.de/dms/goettingen/333853989.pdf

148. Schreier F. and Böttger U., "MIRART, a line-by-line code for infrared atmospheric radiation computations incl. derivatives", *Atmospheric and Oceanic Optics*, **16** (3), pp. 262–268, 2003. link: https://ao.iao.ru/en/content/vol.16-2003/iss.03

149. Schreier F., Gimeno García S., Hedelt P., Hess M., Mendrok J., Vasquez M., and Xu J., "GARLIC - A general purpose atmospheric radiative transfer line-by-line infrared-microwave code: Implementation and evaluation", *Journal of Quantitative Spectroscopy and Radiative Transfer*, **137**, pp. 29–50, 2014. doi: https://doi.org/10.1016/j.jqsrt.2013.11.018

150. Schreier F., "Computational aspects of speed-dependent Voigt profiles", *Journal of Quantitative Spectroscopy and Radiative Transfer*, **187**, pp. 44–53, 2017. doi: https://doi.org/10.1016/j.jqsrt.2016.08.009

151. Schrier F., "The Voigt and complex error function: Humlíček's rational approximation generalized", *Monthly Notices of the Royal Astronomical Society*, **479** (3), pp. 3068–3075, 2018**(a)**. doi: https://doi.org/10.1093/mnras/sty1680

152. Schreier F., "Comments on the Voigt function implementation in the Astropy and SpectraPlot.com packages", *Journal of Quantitative Spectroscopy and Radiative Transfer*, **213**, pp. 13–16, 2018**(b)**. doi: https://doi.org/10.1016/j.jqsrt.2018.03.019

153. Schreier F., Gimeno García S., Hochstaffl P., and Städt S., "Py4CAtS—PYthon for Computational ATmospheric Spectroscopy", *Atmosphere*, **10** (5), 262, 2019. doi: https://doi.org/10.3390/atmos10050262

154. Schreier F. and Hochstaffl P., "Computational aspects of speed-dependent Voigt and Rautian profiles", *Journal of Quantitative Spectroscopy and Radiative Transfer*, **258**, 107385, 2021. doi: https://doi.org/10.1016/j.jqsrt.2020.107385

155. Scott N.A. and Chedin A., "A Fast Line-by-Line Method for Atmospheric Absorption Computations: The Automatized Atmospheric Absorption Atlas", *Journal of Applied Meteorology and Climatology*, 20 (7), pp. 802–812, 1981. doi: https://doi.org/10.1175/1520-0450(1981)020%3C0802:AFLBLM%3E2.0.CO;2

156. Shine K. P., Ptashnik I.V., and Rädel G., "The water vapour continuum: brief history and recent developments", *Surveys in Geophysics*, **33**, pp. 535 – 555, 2012. doi: https://doi.org/10.1007/s10712-011-9170-y

157. Smette A. and Coauthors, "Molecfit: A general tool for telluric absorption correction", *Astronomy & Astrophysics*, **576**, A77, 2015. doi: https://doi.org/10.1051/0004-6361/201423932

158. Spänkuch D., "Effects of line shapes and line coupling on the atmospheric transmittance," *Atmospheric Research*, **23**(3), pp. 323–344, 1989. doi: https://doi.org/10.1016/0169-8095(89)90024-0

159. Stam D. M., de Haan J. F., Hovenier J. W., and Stammes P., "A fast method for simulating observations of polarized light emerging from the atmosphere applied to the oxygen-A band", *Journal of Quantitative Spectroscopy and Radiative Transfer*, **64** (2), pp. 131–149, 2000. doi: https://doi.org/10.1016/S0022-4073(99)00009-6

160. Stamnes K., Tsay S.-C., Wiscombe W., and Jayaweera K., "Numerically stable algorithm for discrete-ordinate-method radiative transfer in multiple scattering and emitting layered media", *Applied Optics*, **27** (12), pp. 2502–2509, 1988. doi: https://doi.org/10.1364/AO.27.002502

161. Stamnes K., Thomas G. E., and Stamnes J. J., *Radiative Transfer in the Atmosphere and Ocean* (2nd Ed.), Cambridge University Press, 2017. doi: https://doi.org/10.1017/9781316148549

162. Stiller G.P., von Clarmann T., Funke B., Glatthor N., Hase F., Höpfner M., and Linden A., "Sensitivity of trace gas abundances retrievals from infrared limb emission spectra to simplifying approximations in radiative transfer modelling", *Journal of Quantitative Spectroscopy and Radiative Transfer*, **72** (3), pp. 249–280, 2001. doi: https://doi.org/10.1016/S0022-4073(01)00123-6

163. Storer T., "Bridging the Chasm: A Survey of Software Engineering Practice in Scientific Programming", *ACM Computing Surveys*, 50(4), 47, pp.1-32, 2017. doi: https://doi.org/10.1145/3084225

164. Tennyson J. and Coauthors, "Recommended isolated-line profile for representing high-resolution spectroscopic transitions (IUPAC technical report)", *Pure and Applied Chemistry*, **86** (12), pp. 1931–1943, 2014. doi: https://doi.org/10.1515/pac-2014-0208

165. Thompson D.R., Gao B.-C., Green R.O., Roberts D.A., Dennison P.E., and Lundeen S.R., "Atmospheric correction for global mapping spectroscopy: ATREM advances for the HyspIRI preparatory campaign", *Remote Sensing of Environment*, **167**, pp. 64–77, 2015. doi: https://doi.org/10.1016/j.rse.2015.02.010

166. Thorpe A. K., Roberts D.A., Bradley E.S., Funk C.C., Dennison P.E., and Leifer I., "High resolution mapping of methane emissions from marine and terrestrial sources using a Cluster-Tuned Matched Filter technique and imaging spectrometry", *Remote Sensing of Environment*, **134**, pp. 305-318, 2013. doi: https://doi.org/10.1016/j.rse.2013.03.018

167. Tonkov M. V., Filippov N. N., Timofeyev Yu. M., and Polyakov A.V., "A simple model of the line mixing effect for atmospheric applications: Theoretical background and comparison with experimental profiles", *Journal of Quantitative Spectroscopy and Radiative Transfer*, **56** (5), pp.783-795, 1996. doi: https://doi.org/10.1016/S0022-4073(96)00113-6

168. Tran H., Boulet C., and Hartmann J.-M., "Line mixing and collision-induced absorption by oxygen in the A band: Laboratory measurements, model, and tools for atmospheric spectra computations", *Journal of Geophysical Research*, **111**, D15210, 2006. doi: https://doi.org/10.1029/2005JD006869

169. Tran H. and Hartmann J.-M., "An improved O2 A band absorption model and its consequences for retrievals of photon paths and surface pressures", *Journal of Geophysical Research*, **113**, D18104, 2008. doi: https://doi.org/10.1029/2008JD010011

170. Tran H., Ngo N.H., and Hartmann J.-M., "Efficient computation of some speed-dependent isolated line profiles", *Journal of Quantitative Spectroscopy and Radiative Transfer*, **129**, pp. 199–203, 2013, doi: https://doi.org/10.1016/j.jqsrt.2013.06.015

171. Tran H., Ngo N.H., Hartmann J.-M., "Erratum to "Efficient computation of some speed-dependent isolated line profiles" [J. Quant. Spectrosc. Radiat. Transfer 129 (2013) 199–203]", *Journal of Quantitative Spectroscopy and Radiative Transfer*, **134**, p.104, 2014. doi: https://doi.org/10.1016/j.jqsrt.2013.10.015

172. Turner E., Rayer P., and Saunders R., "AMSUTRAN: A microwave transmittance code for satellite remote sensing", *Journal of Quantitative Spectroscopy and Radiative Transfer*, **227**, pp. 117–129, 2019. doi: https://doi.org/10.1016/j.jqsrt.2019.02.013

173. Tyndall J., "Note on the transmission of radiant heat through gaseous bodies", *Proceedings of the Royal Society of London*, **10**, pp. 37-39, 1860. doi: https://doi.org/10.1098/rspl.1859.0017

174. Urban J., Baron P., Lautié N., Schneider N., Dassas K., Ricaud P., and De La Noë J., "Moliere (v5): A versatile forward- and inversion model for the millimeter and sub-millimeter wavelength range," *Journal of Quantitative Spectroscopy and Radiative Transfer*, **83** (3–4), pp. 529–554, 2004. doi: https://doi.org/10.1016/S0022-4073(03)00104-3

175. van de Hulst H.C. and Reesinck J. J. M., "Line Breadths and Voigt Profiles", *The Astrophysical Journal*, **106**, pp. 121-127, 1947. link: https://adsabs.harvard.edu/pdf/1947ApJ...106..121V

176. Vangvichith M., Tran H., and Hartmann J.-M., "Line-mixing and collision induced absorption for O2–CO2 mixtures in the oxygen A-band region", *Journal of Quantitative Spectroscopy and Radiative Transfer*, **110** (18), pp.2212-2216, 2009. doi: https://doi.org/10.1016/j.jqsrt.2009.06.002

177. Villanueva G.L., Smith M.D., Protopapa S., Faggi S., and Mandell A.M., "Planetary Spectrum Generator: An accurate online radiative transfer suite for atmospheres, comets,

small bodies and exoplanets", *Journal of Quantitative Spectroscopy and Radiative Transfer*, **217**, pp. 86-104, 2018. doi: https://doi.org/10.1016/j.jqsrt.2018.05.023

178. Wcisło P. and Coauthors, "The first comprehensive dataset of beyond-Voigt line-shape parameters from ab initio quantum scattering calculations for the HITRAN database: He-perturbed H2 case study", *Journal of Quantitative Spectroscopy and Radiative Transfer*, **260**, 2021. doi: https://doi.org/10.1016/j.jqsrt.2020.107477

179. Wells R.J., "Rapid approximation to the Voigt/Faddeeva function and its derivatives", *Journal of Quantitative Spectroscopy and Radiative Transfer*, **62** (1), pp. 29–48, 1999. doi: https://doi.org/10.1016/S0022-4073(97)00231-8

180. Werdell P. J., and Coauthors, "The Plankton, Aerosol, Cloud, Ocean Ecosystem Mission: Status, Science, Advances", *Bulletin of the American Meteorological Society*, **100** (9), pp. 1775–1794, 2019. doi: https://doi.org/10.1175/BAMS-D-18-0056.1

181. Wilson G., and Coauthors, "Best practices for scientific computing", *PLOS Biology*, **12** (1), e1001745, 2014. doi: https://doi.org/10.1371/journal.pbio.1001745

182. Xie Y., Sengupta M., and Dudhia J., "A Fast All-sky Radiation Model for Solar applications (FARMS): Algorithm and performance evaluation", *Solar Energy*, **135**, pp. 435–445, 2016. doi: https://doi.org/10.1016/j.solener.2016.06.003

183. Yang Q., Liu X., Wu W., Kizer S., and Baize R. R., "Fast and accurate hybrid stream PCRTM-SOLAR radiative transfer model for reflected solar spectrum simulation in the cloudy atmosphere", *Optics Express*, **24** (26), pp. A1514-A1527, 2016. doi: https://doi.org/10.1364/OE.24.0A1514

184. Yang Y., Marshak A., Mao J., Lyapustin A., and Herman J., "A method of retrieving cloud top height and cloud geometrical thickness with oxygen A and B bands for the Deep Space Climate Observatory (DSCOVR) mission: Radiative transfer simulations", *Journal of Quantitative Spectroscopy and Radiative Transfer*, **122**, pp. 141–149, 2013. doi: https://doi.org/10.1016/j.jqsrt.2012.09.017

185. Zhou Y., Wang C., Ren T., and Zhao C., "A machine learning based full-spectrum correlated k-distribution model for nonhomogeneous gas-soot mixtures", *Journal of Quantitative Spectroscopy and Radiative Transfer*, 268: 107628, 2021. doi: https://doi.org/10.1016/j.jqsrt.2021.107628

186. Zhu M., Zhang F., Li W., Wu Y, and Xu N., "The impact of various HITRAN molecular spectroscopic databases on infrared radiative transfer simulation", *Journal of Quantitative Spectroscopy and Radiative Transfer*, 234, pp.55-63, 2019. doi: https://doi.org/10.1016/j.jqsrt.2019.04.031

Conflict of Interest

Authors of this manuscript declare no conflicts of interests.